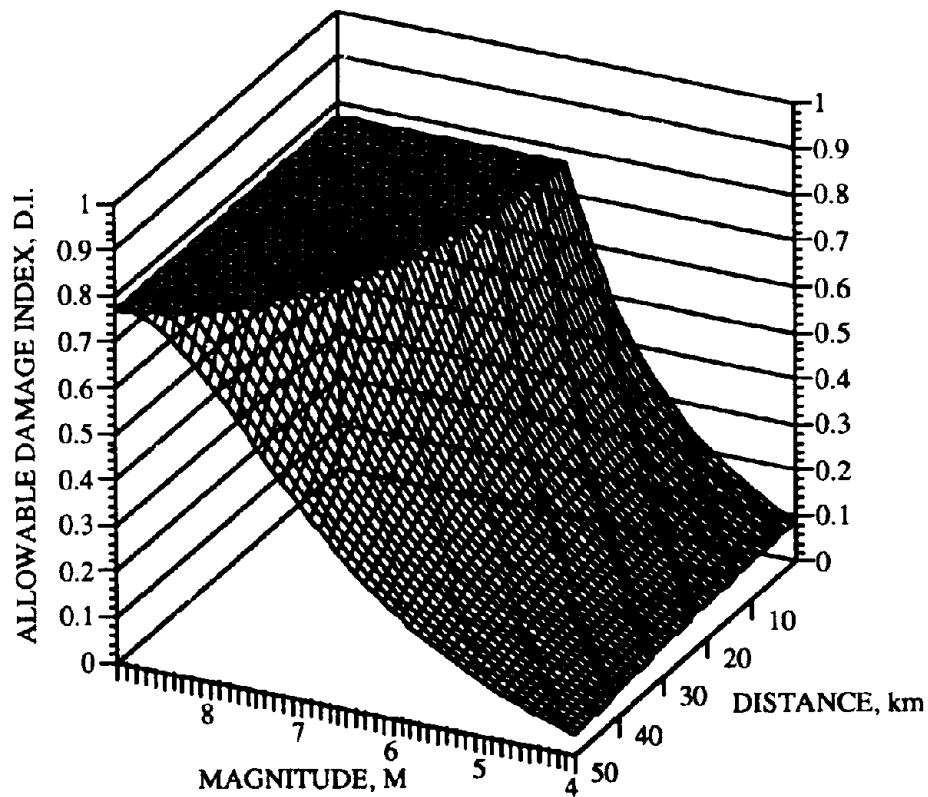NIST BUILDING SCIENCE SERIES 170

Seismic Performance of Circular Bridge Columns Designed in Accordance With AASHTO/CALTRANS Standards

U.S. DEPARTMENT OF COMMERCE • TECHNOLOGY ADMINISTRATION
NATIONAL INSTITUTE OF STANDARDS AND TECHNOLOGY

*T*he National Institute of Standards and Technology was established in 1988 by Congress to "assist industry in the development of technology . . . needed to improve product quality, to modernize manufacturing processes, to ensure product reliability . . . and to facilitate rapid commercialization . . . of products based on new scientific discoveries."

NIST, originally founded as the National Bureau of Standards in 1901, works to strengthen U.S. industry's competitiveness; advance science and engineering; and improve public health, safety, and the environment. One of the agency's basic functions is to develop, maintain, and retain custody of the national standards of measurement, and provide the means and methods for comparing standards used in science, engineering, manufacturing, commerce, industry, and education with the standards adopted or recognized by the Federal Government.

As an agency of the U.S. Commerce Department's Technology Administration, NIST conducts basic and applied research in the physical sciences and engineering and performs related services. The Institute does generic and precompetitive work on new and advanced technologies. NIST's research facilities are located at Gaithersburg, MD 20899, and at Boulder, CO 80303. Major technical operating units and their principal activities are listed below. For more information contact the Public Inquiries Desk, 301-975-3058.

Technology Services
- Manufacturing Technology Centers Program
- Standards Services
- Technology Commercialization
- Measurement Services
- Technology Evaluation and Assessment
- Information Services

Electronics and Electrical Engineering Laboratory
- Microelectronics
- Law Enforcement Standards
- Electricity
- Semiconductor Electronics
- Electromagnetic Fields[1]
- Electromagnetic Technology[1]

Chemical Science and Technology Laboratory
- Biotechnology
- Chemical Engineering[1]
- Chemical Kinetics and Thermodynamics
- Inorganic Analytical Research
- Organic Analytical Research
- Process Measurements
- Surface and Microanalysis Science
- Thermophysics[2]

Physics Laboratory
- Electron and Optical Physics
- Atomic Physics
- Molecular Physics
- Radiometric Physics
- Quantum Metrology
- Ionizing Radiation
- Time and Frequency[1]
- Quantum Physics[1]

Manufacturing Engineering Laboratory
- Precision Engineering
- Automated Production Technology
- Robot Systems
- Factory Automation
- Fabrication Technology

Materials Science and Engineering Laboratory
- Intelligent Processing of Materials
- Ceramics
- Materials Reliability[1]
- Polymers
- Metallurgy
- Reactor Radiation

Building and Fire Research Laboratory
- Structures
- Building Materials
- Building Environment
- Fire Science and Engineering
- Fire Measurement and Research

Computer Systems Laboratory
- Information Systems Engineering
- Systems and Software Technology
- Computer Security
- Systems and Network Architecture
- Advanced Systems

Computing and Applied Mathematics Laboratory
- Applied and Computational Mathematics[2]
- Statistical Engineering[2]
- Scientific Computing Environments[2]
- Computer Services[2]
- Computer Systems and Communications[2]
- Information Systems

---

[1] At Boulder, CO 80303.
[2] Some elements at Boulder, CO 80303.

NIST BUILDING SCIENCE SERIES 170

Seismic Performance of Circular Bridge Columns Designed in Accordance With AASHTO/CALTRANS Standards

William C. Stone
Andrew W. Taylor

Structures Division
Building and Fire Research Laboratory
National Institute of Standards and Technology
Gaithersburg, MD 20899

National Institute of Standards and Technology Building Science Series 170
Natl. Inst. Stand. Technol. Bldg. Sci. Ser. 170, 129 pages (Feb. 1993)
CODEN: NBSSES

ABSTRACT

Limitations of present procedures for the design of bridge columns to withstand seismic loads are discussed. An integrated seismic design procedure is developed which 1) allows the automatic selection and scaling of design earthquakes given the earthquake magnitude, the distance from the site to the fault, and the type of overlying soil strata; 2) predicts the inelastic behavior of reinforced concrete bridge columns when subjected to random lateral loads up to and including failure; and 3) calculates cumulative damage which can be directly correlated to observed states of damage in laboratory tests of bridge columns. Techniques for achieving the above capabilities are described and new design criteria, based on acceptable damage indices as functions of earthquake magnitude, distance, and structural importance, are proposed. Using the proposed procedure and criteria the performance of 72 representative bridge columns designed in accordance with 1992 CALTRANS specifications is analyzed. Analysis parameters included earthquake magnitude, distance from epicenter, subsurface soil characteristics, column aspect ratio, and normalized column axial load. Design charts, based on allowable damage index versus earthquake magnitude, are developed and retrofit strategies are discussed for those designs which do not meet the proposed design criteria.

Key words: circular bridge columns; damage index; design; dynamic analysis; earthquakes; hysteretic damage model; inelastic modeling; reinforced concrete; seismic loads; site specific response; soil amplification; spiral reinforcement.

On the cover: Proposed envelope for acceptable damage index, as a function of earthquake magnitude and distance, for bridge piers deemed moderately important to seismic lifelines. See Chapter 6.

ACKNOWLEDGMENT

List of Symbols

a	=	Peak ground acceleration, g's
a_s	=	Cross section area of spiral bar, cm^2
A_c	=	Spiral core cross section area, cm^2
A_g	=	Gross cross section area, cm^2
ARS	=	Response spectrum factor in CALTRANS design procedure, dimensionless
d_b	=	Diameter of longitudinal bar, cm
d_s	=	Diameter of spiral bar, cm
D	=	Overall diameter of pier, cm
D_c	=	Diameter of spiral core (out to out), cm
D.I.	=	Damage index
f'_c	=	Concrete cylinder strength, MPa
f_{ya}	=	Longitudinal reinforcement yield stress, MPa
f_{ys}	=	Spiral reinforcement yield stress, MPa
F	=	Cumulative error between predicted and experimentally observed differential energy absorption for each point in an experimental record
L	=	Length of pier, from base to first point of contraflexure, cm
M	=	Earthquake moment magnitude
N	=	Number of longitudinal bars in cross section
P	=	$\dfrac{2a_s f_{ys} D_c}{S}$
P_{cr}	=	Lateral load which causes first cracking of the column
P_{fail}	=	Lateral load which causes complete collapse of the column
P_{ult}	=	Maximum lateral load carried by the column
P_y	=	Lateral load which causes observable yielding of the longitudinal column reinforcement
P_e	=	Axial load applied to pier, kN
Q	=	$4\rho_a \sqrt{f'_c} \sqrt{\sigma_o - 0.1}$ $\left[Q = 0 \text{ if } \sigma_o \leq 0.1 \right]$
R_a	=	$\dfrac{A_g}{A_c}$
R_D	=	$\dfrac{S}{D}$

$$R_f \quad = \frac{f_c'}{f_{ya}}$$

$$R_L \quad = \frac{L}{D}$$

$$R_s \quad = \frac{d_s}{S}$$

$$R_t \quad = \frac{f_c'}{f_{ys}}$$

$$R_y \quad = \frac{f_{ys}}{f_{ya}}$$

$$R_\rho \quad = \frac{\rho_s}{\rho_a}$$

S   = Spacing (pitch) of spiral hoops, cm

S_a = Response spectral acceleration, g's

t   = Thickness of steel retrofit shell, mm

$T \quad = \dfrac{\sigma_o}{P+Q}$ (in regressions equations for α, β and γ)

T   = Fundamental period of structure (in CALTRANS design procedure)

W   = Superstructure dead weight in CALTRANS design procedure, kilo pounds

Z   = Risk and ductility factor in CALTRANS design procedure, dimensionless

α = Stiffness degradation parameter for hysteretic failure rules, dimensionless

β = Strength degradation parameter for hysteretic failure rules, dimensionless

γ = Pinching behavior parameter for hysteretic failure rules, dimensionless

ρ_a = Axial reinforcement content, areal %

ρ_s = Spiral reinforcement content, volumetric %

σ = Standard deviation of spectral acceleration for target response spectrum

$\sigma_o \quad = \dfrac{10P_e}{f_c' A_g}$ $\left(kN, MPa \text{ and } cm^2\right)$ Normalized applied axial load

List of Acronymns

AASHTO = American Association of State Highway and
Transportation Officials

CALTRANS = State of California Department of Transportation

EARTHGEN = NIST interactive graphics program for selection and
scaling of design earthquake records

IDARC = Program for Inelastic Damage Analysis of Reinforced
Concrete Frame-Shearwall Structures (Park et al., 1987)

ISDP = NIST Integrated Seismic Design Procedure

NIDENT = NIST interactive graphics program for system identification
of cyclic behavior of reinforced concrete elements

NIST = National Institute of Standards and Technology

SAS/STAT = Commercial statitistical analysis package (SAS/STAT, 1987)

Table of Contents

SEISMIC PERFORMANCE OF CIRCULAR BRIDGE COLUMNS DESIGNED IN ACCORDANCE WITH AASHTO/CALTRANS STANDARDS

1.0 Introduction

Research on the design of bridge structures to resist seismic loadings has traditionally been driven by the inadequate performance of constructed facilities under actual earthquakes. The catastrophic collapse of the I-880 Cypress Freeway, and the significant damage sustained by other elevated highway structures in the Oakland-San Francisco region during the Loma Prieta earthquake of 1989 [Lew 1990] initiated a research project at the National Institute of Standards and Technology (NIST) to develop a rational procedure for the design of ductile bridge columns. Strong emphasis was placed on the creation of an integrated design tool which followed from fundamental physics and took advantage of advanced computational tools developed over the past decade to study various aspects of transient response prediction.

Of particular interest to practicing bridge designers is the state of existing infrastructure immediately following an earthquake: Has the structure been damaged, and if so, how badly? Should it be repaired? Can it be repaired? Even more pressing is the question whether existing bridges should be retrofitted now, before the next, more severe earthquake arrives. What should a "design" earthquake be for the purposes of retrofit analysis? What level of damage should be considered "acceptable" for a given structure in light of its importance and the energy content of a particular earthquake? How is damage to be quantified? All of these questions have been heretofore answered only subjectively by committees of consultants from various fields. As a result, no standard procedure exists for site-specific design.

This paper describes the fundamental concepts used in an integrated seismic design procedure (ISDP) being developed at NIST for bridge columns. The procedure is then employed to investigate the performance of a series of 72 representative bridge columns designed in accordance with 1990 California Department of Transportation [CALTRANS 1990] seismic provisions. Since these represent a more rigorous implementation of the American Association of State Highway and Transportation Officials (AASHTO) design specifications for highway bridges [AASHTO 1989] they can be considered the current state-of-the-art for the seismic design of bridge columns in the United States.

It must be recognized that the vast majority of bridges in use in the United States were constructed more than 40 years ago. Given the enormous capital invested in this existing infrastructure there is strong interest, both at the federal

and state levels, to improve the survivability of these bridges during earthquakes. While it is not possible to address the entire field of bridge retrofitting techniques in this paper the potential power and utility of an integrated seismic design procedure (ISDP) in this field is demonstrated by means of a case study.

1.1 Background (Current CALTRANS Design Procedure)

Before discussing what constitutes a "rational" design procedure, it will be useful to summarize the current generally accepted design procedure for single, cantilevered bridge columns employed by the California Department of Transportation [CALTRANS 1990]. The CALTRANS procedure, summarized in fig. 1.1, requires the selection of a maximum expected bedrock acceleration at the bridge site from a seismicity contour map; the calculation of the anticipated fundamental period of the structure; and the selection of an appropriate response spectrum (the so-called ARS spectrum) based on generic soil conditions. The designer then reads a static equivalent lateral design acceleration from the ARS response spectrum, from which a design base shear, which accounts for presumed ductility based on a generic structural classification, can be calculated. This procedure, while lending itself to a codified standard, suffers from several drawbacks:

• A single peak acceleration value for a regional area ignores important localized phenomena associated with distances from active faults, variations in earthquake magnitudes and their effects on frequency content, and attenuation and frequency shifting with distance from the active faults (or in the case of the Eastern and Central United States, where active fault locations are often unknown, the estimated probable distances, measured in any direction, from earthquake epicenters).

• A sample of representative response spectra for homogeneous soil conditions for a few depth ranges will not necessarily yield a realistic measure of the lateral surface excitation force as experienced by the structure, particularly if a) the frequency content of the earthquake rock motion is other than assumed in the generation of the generic design charts, and b) if there are multi-layered sedimentary deposits.

• There is no basis for the prediction of the post-earthquake damage status for the structure. Thus, the design codes for lifeline structures presently include arbitrary modifiers to the static equivalent lateral design load based on the level of "importance" and the presumed post-elastic ductility capacity of a particular structure. Because of this, there is no ability to perform an effective

2

optimization study which would result in the least-cost design solution to meet a particular survival requirement.

• Current retrofit assessment procedures [e.g., FHWA 1983, and FHWA 1987] rely on a capacity/demand approach which involves the use of single mode or multi-mode linear spectral analyses, again followed by modifications to account for presumed ductility capacity. As with the design of new bridges, there is no means for assessing the effectiveness of the proposed retrofit nor to predict the state of damage that might exist following any particular seismic event.
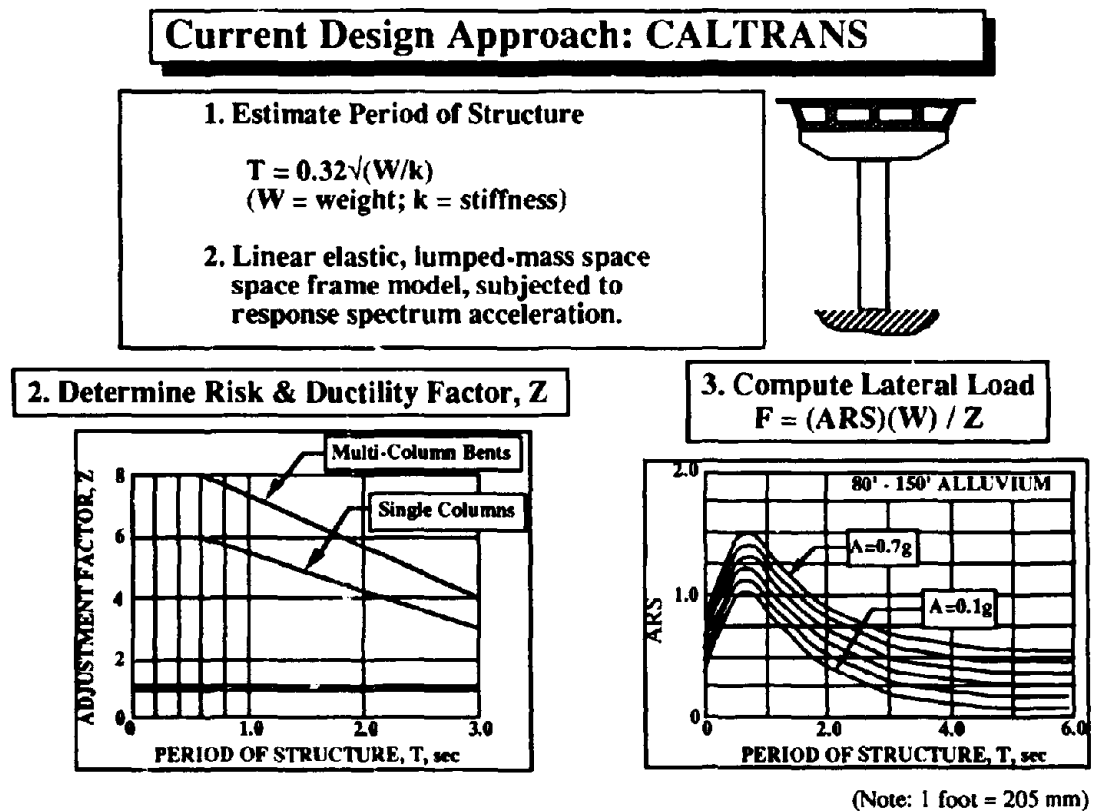
Figure 1.1. Schematic of current CALTRANS seismic design approach.

3

1.2 Integrated Seismic Design Procedure (ISDP)

Rational structural design requires 1) the definition of functional requirements for the structure, and 2) the use of appropriate analysis techniques to determine if a proposed design meets the functional requirements. When considering the seismic design of a highway bridge the functional requirements are most concisely stated by defining the design loads and the acceptable structural behavior in response to those loads. In this paper the design loads are defined by "suites" of likely events (acceleration time histories) which cover a broad range of energy contents (as defined by magnitude and distance from the earthquake epicenter). The specific procedures by which such design suites are selected and/or created are described in Chapter 3. There are several reasons for using this approach, the most important of which is that it explicitly accounts for the transient nature of earthquake loading, rather than reducing it to a simplified static force. The reason for employing a suite is that no single earthquake record can characterize the randomness that will be exhibited in nature at a particular construction site. Thus, given a particular energy content (as defined by magnitude and distance) a group of distinctly different (from a frequency content viewpoint) time histories has a higher likelihood of capturing the worst case response for any given structure at a particular job site.

For any given time history a performance standard is required to determine if the structural response is acceptable. In this paper a significant departure is made from traditional load and resistance factor design procedures by introducing the concept of acceptable damage. It is generally recognized in seismic design (as opposed to design for live loads) that economical construction excludes designs based on elastic response to the anticipated maximum design earthquake. One can envision that elastic response is both desirable, and feasible, for relatively low energy events. Between this condition and total collapse in a high energy event will be a sliding relationship between energy content and acceptable behavior, which necessarily will involve inelastic performance.

Only recently [e.g., Park, Reinhorn, and Kunnath, 1987] have researchers begun to develop practical quantitative analytical models for cumulative damage to reinforced concrete structures under reversed cyclic loading. Research is active in this area and models are being refined. The eventual utility of such models is clearly evident. Since there are no existing quantitative standards for acceptable seismic damage an initial model is proposed by the authors in Chapter 6, that will hopefully be the nucleus of a more refined AASHTO Specification.

4

To determine if the functional requirements described above are met, the designer must employ models that traditionally have belonged to the fields of structural engineering, seismology, and geotechnical engineering. These are structural analysis models, attenuation relationships, and wave propagation models, respectively. Transient seismic analysis begins with the definition of an anticipated attenuation relationship based on historic bedrock motion data, which for a geographic region relates frequency content and amplitude to magnitude and distance. Using this relationship, suites of design bedrock motions can be developed either by scaling recorded time histories or through synthetic generation techniques. Given a knowledge of the soil profile at a particular construction site wave propagation models may be used to determine the altered time history that would be perceived by the structure at the surface. Given a realistic time history, the inelastic response of the structure must be determined. Inherent in the structural analysis phase is the need to realistically model the hysteretic, inelastic behavior of the concrete; to determine a cumulative damage "index"; and to account for any nonlinearities and damping imposed by soil-structure interaction. Each of the above tools is predicated on the existence of certain knowledge bases which include, for example, laboratory tests of bridge substructures and elements; strong motion instrument records made at bedrock sites; strong motion records made at soft soil sites; and boring logs which describe the soil column properties at a particular site.

If properly integrated the above tools and requirements (each of which will be described below) can lead to a rational seismic design, retrofit, and repair procedure which is far more general, effective, and economical than the current AASHTO and CALTRANS approaches (see fig. 1.2).

```
Structural                 Bedrock              Soft Soil
Experimental               Earthquake           Earthquake
Data                       Records              Records
From laboratory tests      Strong-motion        Strong-motion
on reinforced concrete     instrument records   instrument records
elements, bridge           made at bedrock      made at soft soil
subassemblies,             sites.               sites.
and foundations.
```

Knowledge Bases

```
Structural                 Attenuation          Wave
Analysis                   Models               Propagation
Models                     Attenuation relationships   Models
Experimental data is       for acceleration response   Methods for
used to calibrate          spectra as a function of    propagating bedrock
inelastic dynamic          magnitude, distance and     motions to the
analysis codes.            geology.                    ground surface.
(e.g., Park et al. 1987)   (e.g., Joyner and Boore     (e.g., SHAKE91 1992)
                           1988)
```

Analytical Models

Rational Seismic Design, Retrofit and Repair Procedure

Reinforced concrete bridges which meet specific seismic functional requirements, designed using the best available analytical tools.

```
Design                     Acceptable
Earthquakes                Damage Levels
Suite of likely events in  Degree of damage
region over design life    deemed acceptable, as a
of structure: distances    function of earthquake
and earthquake             magnitude, distance to
magnitudes                 fault, and importance of
(geological                bridge
considerations)            (building code-related
                           considerations)
```
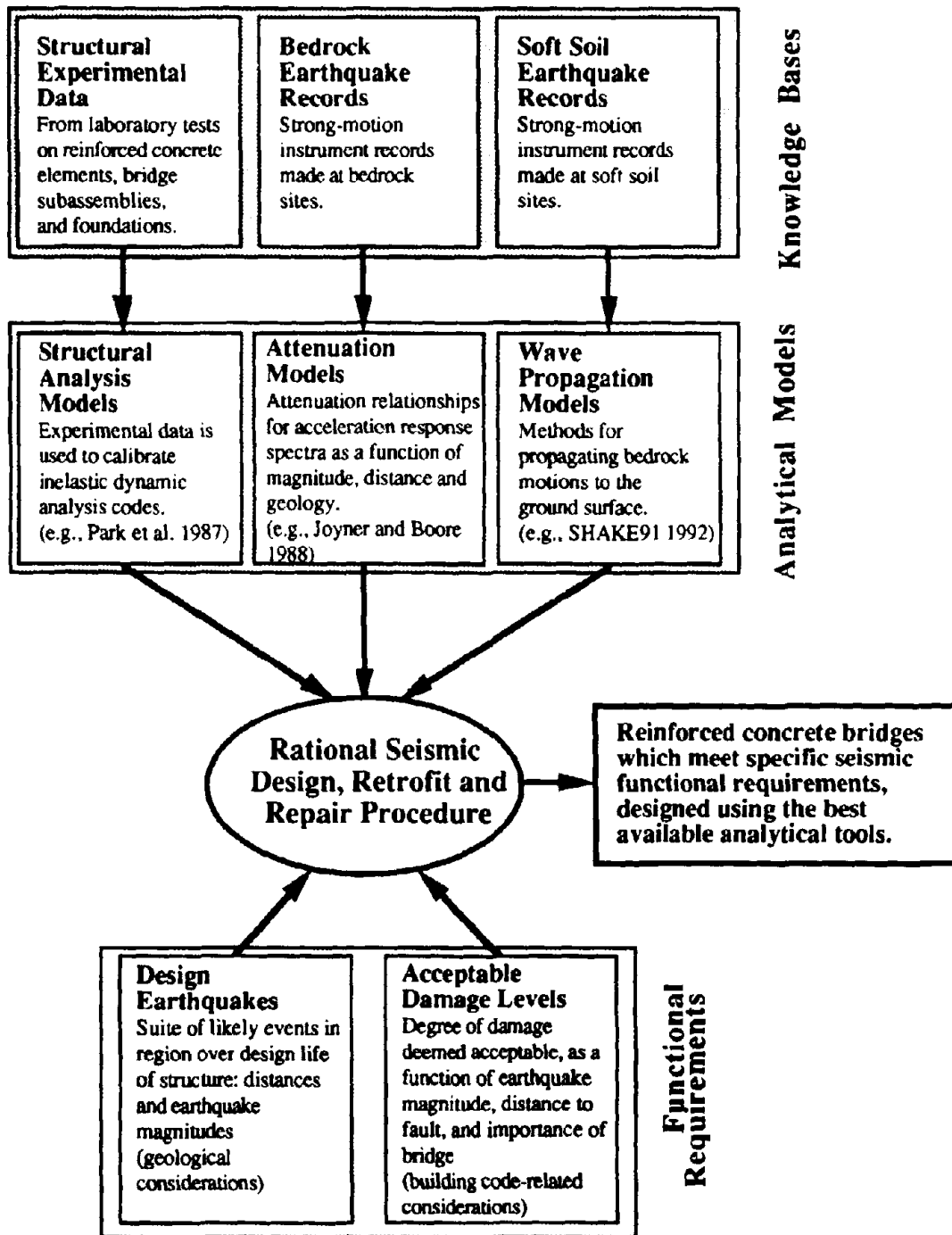
Functional Requirements

Figure 1.2. Overview of development of integrated procedures for the seismic design, retrofit, and repair of concrete bridges.

Figure 1.3 shows a computer program flow chart for the integrated seismic analysis procedure. The approach is modular. It is based on recent advances in methods for acquiring data on appropriate design earthquakes, and on the development of reliable models for the prediction of hysteretic behavior in reinforced concrete structures. Because the concept requires the integration of seismological, subsurface soil, and structural analysis components, the input data upon which the analyses are based are necessarily site- and structure-specific.

Presently there is no national data base from which one might, for example, obtain a set of representative acceleration-time histories for a particular region which might then be used for design. To limit the scope of the required data base generation a demonstration project is presented, using the State of California as an example. Similarly, because there are many possible variations to superstructure architecture, the initial scope of the project is limited to the performance and design of circular, spirally reinforced, single cantilevered columns which are monolithically cast with continuous longitudinal reinforcement through the potential plastic hinge regions. These criteria are applicable to a large number of elevated highway systems presently in use in California and elsewhere in the United States.

There are eight separate, but interrelated, elements governing the design of a bridge column with specified performance under given levels of seismic excitation. These are as follows:

• Structural System and Performance Definition
• Subsurface (Soil Column) Definition
• Bedrock Motion Definition
• Site (Surface) Motion Calculation
• Hysteretic Failure Model Selection
• Soil-Structure Interaction Modeling
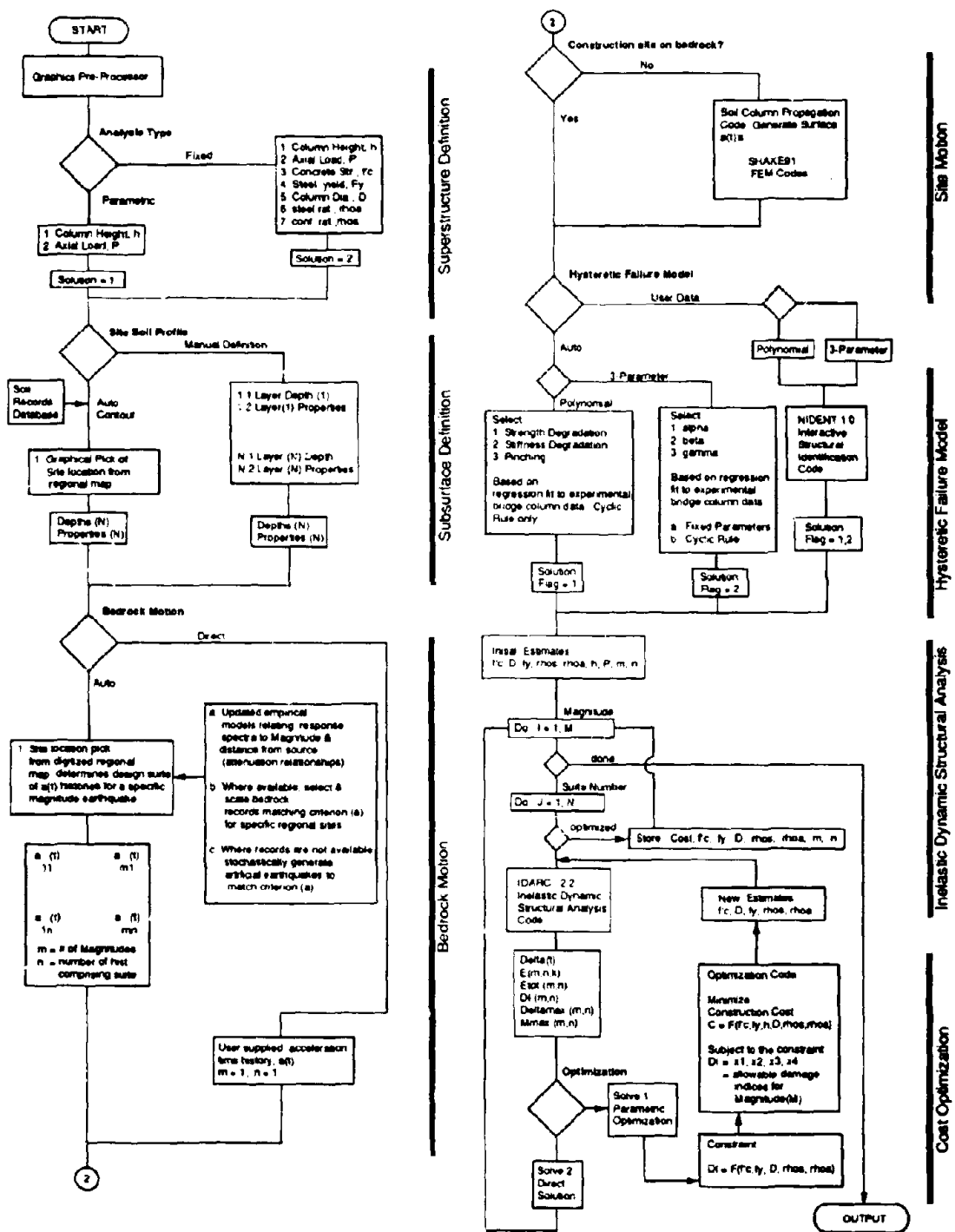• Inelastic Dynamic Analysis
• Cost Optimization

Figure 1.3. Flow chart of seismic design procedure.

8

In considering the first element, Structural System and Performance Definition, the engineer would prefer to enter as few pieces of information into a design procedure as necessary. In the case of geometry and loads, the minimum data required are the height of the column, L, and the effective axial load, P_e, from the superstructure. In addition the engineer would also like to specify the level of acceptable damage following an earthquake of a given magnitude. A bridge column which is required to be totally functional, with no damage at all, following a Magnitude 6.5 earthquake, may demand a more robust design than the same column which would be required to remain marginally standing (and require subsequent demolition) following a Magnitude 7.5 earthquake. Since these criteria will depend on site-specific characteristics, the engineer would also want to provide the computer program with a geographical location (longitude and latitude) of the construction site, from which, ultimately, design loadings would be automatically generated. Obviously, this design approach represents a significant departure from current design practices, particularly in the explicit inclusion of performance based on earthquake magnitude (energy content). Its implementation is predicated upon a number of developments taking place and on the integration of what are presently disparate research software packages into an automated system.

The issue of structural input loadings is addressed in the second, third, and fourth elements listed above. The seismic excitation function (acceleration-time history) is dependent upon the following parameters, among others:

1. The magnitude of the earthquake.
2. The local tectonics which affect the generation and propagation of seismic waves.
3. The distance from the earthquake source to the structure.
4. The underlying soil conditions between the foundation of the structure and bedrock.

Given these parameters the development of an appropriate "design" earthquake loading is a complicated process which is presently the subject of considerable research. The authors envision, ultimately, a national database which would permit the user, by specifying a geographic location for the construction site, to automatically develop a best estimate for the soil column profile from surface to bedrock level; and automatically generate a suite of design bedrock acceleration-time histories, with varying magnitudes and frequency contents which would be representative of that site. Existing wave propagation software [e.g., SHAKE91, 1992] can then be used to automatically generate surface-level acceleration-time histories which would serve as the input loading for the structural design. Initially, it is clear that the scarcity of available boring logs to

bedrock will relegate such automated soil selection procedures to preliminary analyses, pending availability of specific construction site logs. However, with required filing of boring logs to bedrock at all construction sites in seismic regions with a national organization, such as the United States Geological Survey, the completeness of such a soils database would gradually improve.

Procedures are currently available [e.g., Joyner and Boore 1988, Idriss 1985, and Taylor and Stone 1991] for the selection and scaling of earthquake records at a given site, provided information on local geology and tectonics are available. For any given site, and any given structure, a single acceleration-time history is nearly as insufficient for proper analysis as a single equivalent static lateral load. Because some structures may respond more strongly to a particular segment of a response spectrum, it is important to develop, for each site, a suite of acceleration-time histories which, taken together, span the entire target response spectrum, and taken individually, span discrete portions of the target response spectrum. Likewise, because different magnitude earthquakes may occur from different sources, a separate suite of design acceleration-time histories for each magnitude under consideration must be generated. Given these data, one may then develop a suite of surface-level time histories suitable for subsequent structural analysis. An interactive graphics-driven system which employs the above principles has been developed at NIST and will be the subject of a forthcoming paper. Portions of this system are used for the analyses reported in the present paper. The details of design earthquake suite generation are presented in Chapter 3.

The techniques used for inelastic dynamic analysis (steps 5 through 7 in the proposed design procedure) are described in detail in Chapters 2 and 4. Briefly, the approach subjects a column with known geometry and material properties to a suite of independent earthquakes and for each time step in the earthquake record, tracks the top of column lateral displacement as a function of lateral load. These load-displacement (or moment-curvature) histories may then be analyzed to determine a damage index at any point in time. The damage index is a composite, dimensionless number which is a function of both maximum displacement (curvature) ductility and normalized absorbed hysteretic energy. As will be shown in Chapter 4, these damage indices can be correlated to physical states of damage observed in laboratory tests of bridge columns. This then completes the analysis cycle which starts with the definition of a design earthquake based on magnitude and proximity to the earthquake origin, and ends with an assessment of probable damage caused by a given seismic event.

There is thus a means for directly assessing the cumulative damage to a column subjected to a series of events, since any given analysis of a column could simply be extended in time by attaching a subsequent earthquake record to the

input time history. This leads naturally into the subject of retrofit analysis which is discussed in Chapter 6.

In the present study no attempt was made to address the issue of optimized structural design other than to say that it is a logical and straightforward extension of the analytical package (ISDP) presently under development at NIST. As described in figure 1.3 and graphically in fig. 1.4, automated design is possible using the ISDP approach. figure 1.4 shows one possibility in which there are two optimization constraints. The damage constraint is provided by means of a closed form equation which relates acceptable structural damage to earthquake energy and structural importance (see Chapter 6). The second constraint is the construction cost of the column. Using this approach the practicing designer will ultimately be able automatically to determine the lowest cost design which meets the acceptable damage criteria.

1.3 Scope of Present Study

Chapters 2-4 describe the analysis tools used to assess bridge column performance. Beginning in Chapter 5 these techniques are used to study the specific question of how bridge columns designed in accordance with current CALTRANS specifications would perform when subjected to various design earthquakes. In all, three column geometries (L/D = 3,6, and 9), three axial load levels (P_c/f_cA_g = 0.05, 0.10, and 0.15); and four epicentral (fault) distances (D = 10, 20, 30, and 40 kilometers) were investigated, comprising 36 separate design scenarios. Each design scenario was subjected to a suite of four automatically generated earthquakes for four earthquake magnitudes (M= 5,6,7,8) for a total of 16 inelastic transient analyses per scenario or a total of 576 analyses for each subsurface condition investigated.

In order to assess the importance of soil amplification two subsurface conditions were considered: a) column founded on bedrock; b) column founded on 37 m (120 foot) layer of alluvium (sand) underlain by bedrock. For each of these cases (representing a total of 1152 analyses) design charts are constructed relating cumulative column damage as a function of earthquake magnitude. These charts also include, based on the work presented in Chapter 4, 90th percentile probability limits representing damage states corresponding to three discrete conditions: a) yield of axial reinforcement; b) ultimate load capacity; and c) complete column failure.

11
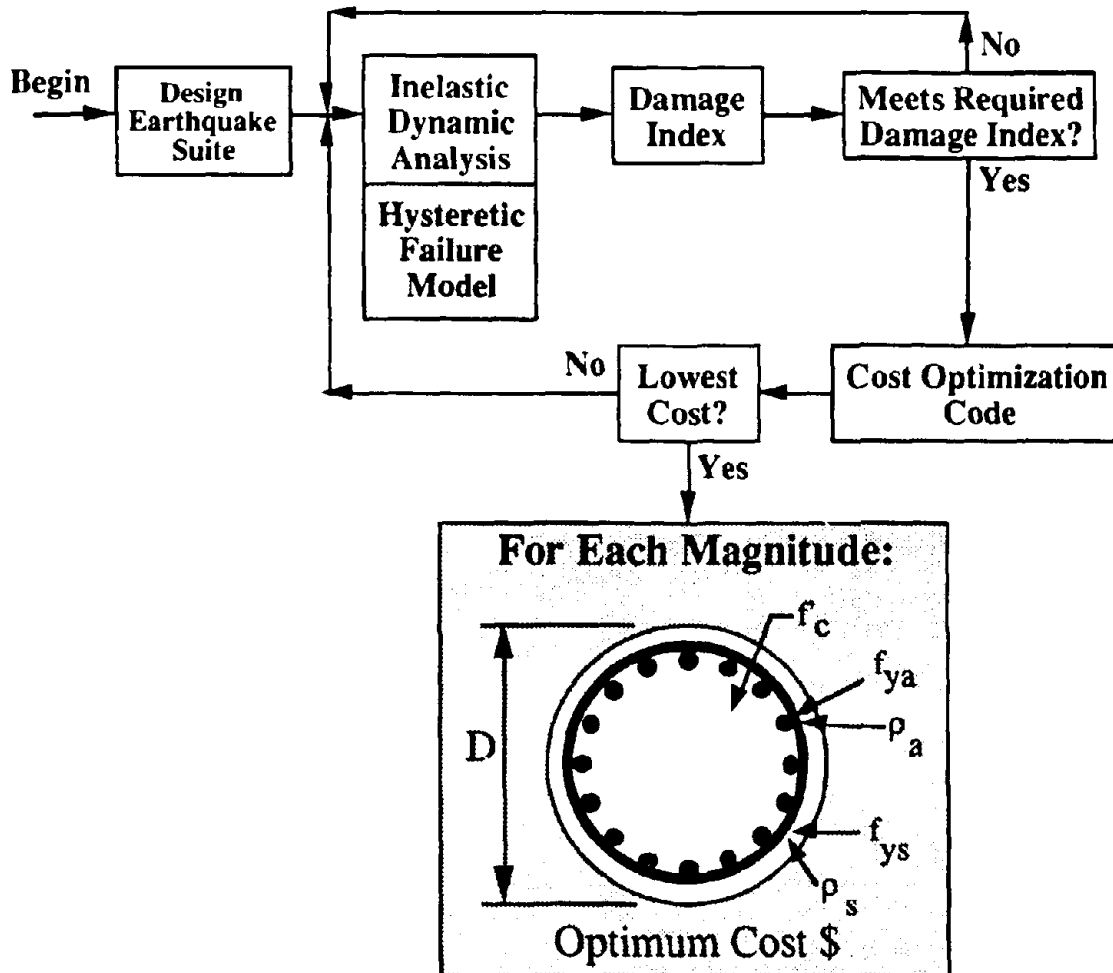
Figure 1.4. Schematic of automated inelastic design algorithm.

The design and analysis procedures used to investigate the CALTRANS columns are described in Chapter 5. Chapter 6 presents first a brief treatise on the subject of acceptable damage and then reduces the concept to a closed form equation suitable for inclusion into the integrated seismic design procedure. The performance of the CALTRANS columns analyzed using the procedures identified in Chapter 5 is then discussed. Two types of design charts are presented, each of which has specific practical application. The first chart series relates the total damage that would occur to a particular column at a particular construction site (located a specified distance from a likely fault or earthquake source) as a function of earthquake magnitude. This is a highly useful tool for examining the effect of column axial load and aspect ratio (L/D = height/diameter) on damage avoidance. The second series of charts allows for

12

quick assessment of the anticipated performance of a column whose geometric properties and axial loading are known but the variance of damage is desired as a function of both magnitude and location.

On the basis of the material presented through Chapter 6 a column retrofit design example is solved for a specific case in which the predicted performance of a column designed to current CALTRANS specifications is unacceptable. The procedure described is general and can be used to analyze a broad class of existing circular bridge columns in any area of the United States. Chapter 7 summarizes the implementation of the damage index design procedure for retrofit problems and discusses the effectiveness and limitations of steel jacketing procedures presently in use by CALTRANS.

1.4 Limitations and Assumptions

Because of the reliance of the NIST method on direct calibration of analytical tools to empirical test data the results described in this paper are limited in scope to the design of circular, spirally reinforced bridge columns, for which a substantial digital database has been established at NIST. It is anticipated in the future that the method will be extended to handle other cross section geometries, as well as multiple column bents.

Although the present ISDP package can handle any soil profile (including clays), the analyses presented were limited to those for which direct comparisons could be made with the existing simplified CALTRANS column design procedures, as defined by the available ARS spectra charts. The intent was to demonstrate the potential of the ISDP procedure and to call attention to certain shortcomings in existing simplified design approaches.

In an effort to limit the scope of the present study, the influence of soil-structure interaction was neglected. Generally, bridge foundations will fall into three categories: piles, battered piles, and spread footings. Each of these substructure systems will react inelastically with surrounding soil media during an earthquake with the general effect of damping, to varying degrees, the superstructure response. The results presented in the present paper can therefore be considered conservative for bridge foundations constructed on deep soil deposits. There is significant active research in the area of soil-structure interaction. Those analytical models which have thus far been developed, and those likely to be developed to characterize this phenomenon, reduce the effects of soil interaction to a series of frequency-dependent nonlinear springs which are, in essence, boundary conditions that can be directly assimilated at some future date into the structural analysis models presently used in the ISDP package.

Finally, in Chapter 7, the retrofit analysis example is solved by considering, for various seismic loadings, the effects on damage of changing design parameters, specifically the confining reinforcement ratio (as determined by the thickness of a steel jacket). Retrofitting is a global process and once the column retrofit has been determined to be acceptable, a revised analysis must be performed on both the foundation as well as the superstructure systems to ensure that the point of failure has not merely been displaced from the column plastic hinge zone to some other point in the bridge.

2.0 Modeling Inelastic Reversed Lateral Response of Circular Bridge Columns

2.1 Inelastic Dynamic Analysis Codes

Several computer programs presently exist including SAKE [Otani 1974], SARCF-II [Rodriguez-Gomez, Chung, and Meyer 1990], DRAIN-2DX [Allahabadi 1987], and IDARC [Park, Reinhorn, and Kunnath 1987], among others, which have achieved some measure of success in analytically predicting the dynamic response of reinforced concrete structures, not just to their elastic limits, but to complete failure. All are "research codes" and to date are limited to the analysis of two dimensional structural systems. At the heart of these programs are hysteretic rules to idealize the inelastic behavior of reinforced concrete under dynamic or quasi-static loading. Such models attempt to capture overall behavior of the structural element based on load-displacement (or moment-curvature) predictive algorithms calibrated to experimental data. The output of these programs lends itself to the computation of absorbed hysteretic energy and displacement ductility, both of which have been shown to be correlated to a quantifiable measure of the state of damage sustained by the structure following a seismic event [Park, Ang, and Wen 1984]. In the present study a multi-linear hysteretic model, known as a "Three Parameter Model," was employed. This same algorithm is presently used in the program IDARC [Park, Reinhorn, and Kunnath 1987].

2.2 Development of Hysteretic Failure Models

It is common practice to describe the envelope curve of the force-deformation relation of reinforced concrete components by a multi-linear function with three turning points, e.g., cracking, yield, and ultimate strength. The tri-linear approximation to the envelope curve is known as the "skeleton" curve. Procedures have been developed to extract this curve from an equivalent monotonic load-displacement envelope curve that has been fitted to experimental data for columns tested under reversed cyclic loading [Park, Reinhorn, and Kunnath 1987]. A variety of hysteretic properties can be obtained through the combination of the tri-linear skeleton curve and three characteristic parameters, α, β and γ. Complete definitions of these variables may be found in Stone and Taylor [1991]. Briefly, the parameter α controls the degradation (softening) in the unloading stiffness that is generally observed in reinforced concrete members as they degrade under reversed cyclic loading. The parameter β determines the rate of strength deterioration, and is commonly a function of cumulative absorbed energy and maximum displacement. Pinching behavior is controlled by the parameter γ. The introduction of such a

pinching parameter causes constriction of the hysteresis loops, and an overall reduction in the cyclic energy absorbed by the structural element.

These three parameters, together with the skeleton curve information described above, are the variables required for implementation of the hysteretic rule described in Park, Reinhorn, and Kunnath [1987]. El-Borgi, White, and Gergely [1991] warn that proper implementation of this type of model requires calibration of the variables to a specific type of structural element if reliable results are to be obtained. It was for this reason that the initial project scope was restricted to circular, spirally reinforced, single bridge columns. The first task was thus to assemble a suitable digital database of tests of spirally reinforced, circular concrete bridge columns subjected to reverse cyclic loading combined with axial load. The process of determining the relationship between the hysteretic parameters α, β, and γ and the column geometry and materials is known as "system identification."

2.3 Digital Database

An extensive literature search identified several sources of bridge column test data. Digitized records were available from Stone and Cheok [1989]; Cheok and Stone [1990]; Lim and McLean [1991]; and McLean and Lim [1990]. Additional records, generally in the form of lateral load-displacement plots, were obtained from Ang, Priestley, and Park [1981]; Mander [1984]; Munro, Park, and Priestley [1976]; Priestley and Park [1984]; Zahn, Park and Priestley [1986]; Petrovski and Ristic [1984]; Wong, Paulay, and Priestley [1990]; Ang, Priestley and Paulay [1985, 1989]; Davey [1975]; Ng, Priestley and Park [1978]; Kenchiku Kenkyu Siryo [1975, 1978]; and Watson [1989]. All of the analog data were digitized from large scale precision photo enlargements of the analog records.

2.4 System Identification Procedures (NIDENT)

The term "System Identification" is generally associated with the experimental acquisition of such dynamic characteristics of a structure as its mode shapes, frequencies, and damping coefficients. In this report we use the term to refer to the determination of the three parameters α, β, and γ, which best characterize the hysteretic behavior of a given test specimen. The system identification procedure used in this study consists of a three dimensional trial and error search with bounded limits on α, β, and γ subject to the constraint of minimizing the cumulative error between predicted and experimentally observed differential energy absorption for each point in the experimental

16

database. In equation form, we seek to minimize the function F, where F is defined as follows:

$$F = \sqrt{\frac{\sum\limits_{i=1}^{n} 0.5|\delta_{i+1} - \delta_{i-1}|\left(P_{exp}(i) - P_{theo}(i)\right)^2}{n}}$$

where:

∂_{i+1}	= displacement of next point in load-displacement record
∂_{i-1}	= displacement of previous point in load-displacement record
$P_{exp}(i)$	= experimentally observed load at current point
$P_{theo}(i)$	= predicted load at current displacement, calculated using the multi-linear hysteretic rule and the currently selected values of α, β, and γ.
n	= number of data points in the experimental record

Following the initial identification of the parameters α, β, and γ, the predicted load-displacement record was superimposed graphically, in a different color, on top of the experimental record. Using a high performance graphics workstation it was then possible to interactively adjust any of the three model parameters by means of a dial-box while viewing the results in real time on the graphics screen. This visual-feedback approach proved effective in arriving at a "best fit." As a final check, the absorbed energy was calculated for the experimental and predicted data for each cycle and compared in a histogram plot. When the error between the theoretical and experimental sums of the cyclic absorbed energies was reduced to a level of a few percent, the final values of α, β, and γ were recorded. The above tasks were carried out using NIDENT 3.0, the NIST graphics-based system identification package, running on a Silicon Graphics 4D-420 workstation.

Examples of the fit between the analytical model and experimental data are shown in figures 2.1 and 2.2. Several details of these figures bear discussion. The first, as evidenced, for example, in figure 2.1, is that as the column begins to fail, there is a tendency for the predicted loads to overshoot the experimentally observed load at the maximum observed displacements for each cycle. This is an expected consequence of using a tri-linear skeleton curve where the post-yielding stiffness for such a model is defined to be positive for reasons of numeric stability. Second, as evidenced in the associated cyclic absorbed energy histograms (see figures 2.1-2.2), there is a tendency for the predicted absorbed energy to overestimate the experimental data for low values of lateral displacement and to underestimate the experimental data for high displacement ductility. Despite these shortcomings, the Three Parameter model is able to generally predict both overall absorbed cyclic energy and displacement ductility to within a few percent error, which was considered acceptable for the purposes of dynamic behavior studies involving reinforced concrete.

90
70
50
30
10
-10
-30
-50
-70
-90

Lateral Load (kN)

— Experimental
...... Theoretical

Alpha	12.01
Beta	0.005
Gamma	1.00
Energy Error	-1.2 %

-70 -60 -50 -40 -30 -20 -10 0 10 20 30 40 50 60 70

Lateral Displacement (mm)

8.00 10^3
7.00 10^3
6.00 10^3
5.00 10^3
4.00 10^3
3.00 10^3
2.00 10^3
1.00 10^3
0.00 10^0

Absorbed Energy Per Cycle (kN·mm)

■ Experimental
▨ Theoretical

$$\text{Cumulative Error} = \sum_{i=1}^{N \text{ cycles}} \left(\frac{E_{theor} - E_{exp}}{E_{exp}} \right) \times 100 = -1.2\%$$

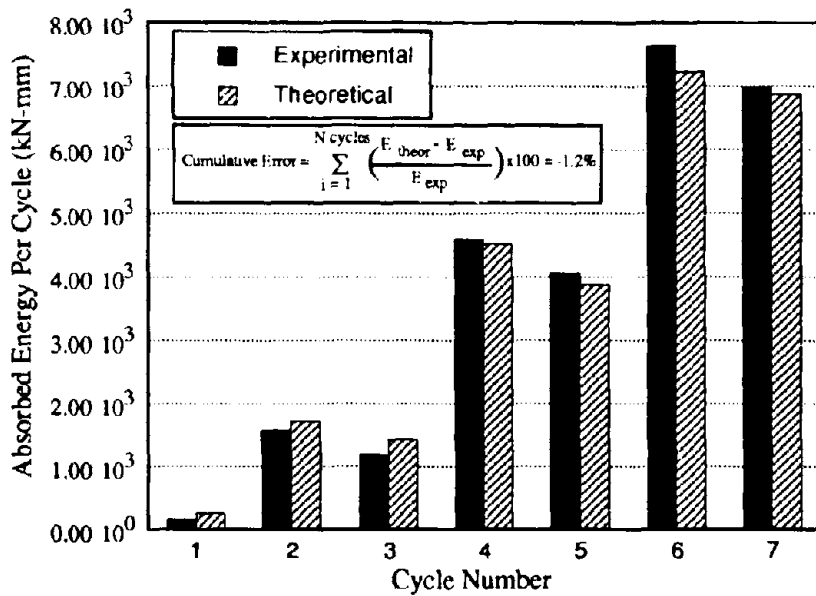1 2 3 4 5 6 7

Cycle Number

Figure 2.1. Experimental and analytical results for specimen N1 of Cheok and Stone [1990].

Alpha	5.00
Beta	0.120
Gamma	0.95
Energy Error	-0.5 %

$$\text{Cumulative Error} = \sum_{i=1}^{N \text{ cycles}} \left(\frac{E_{theor} - E_{exp}}{E_{exp}} \right) \times 100 = -0.5\%$$
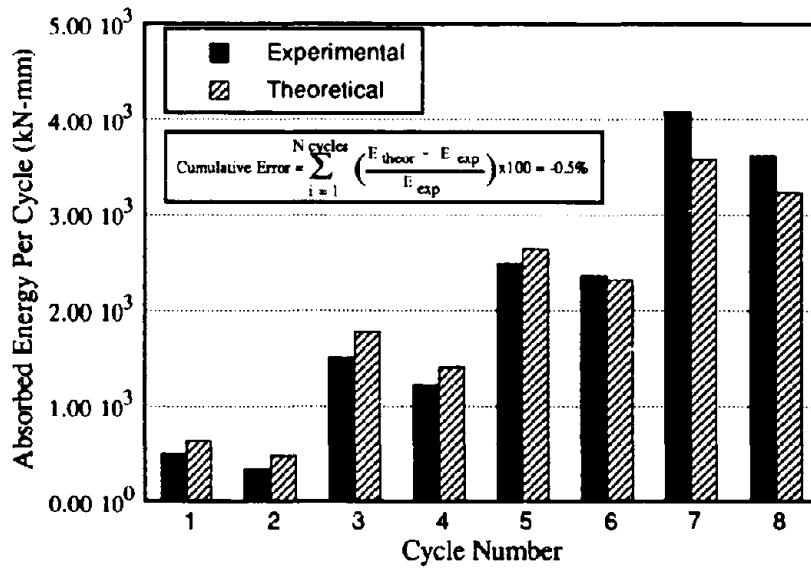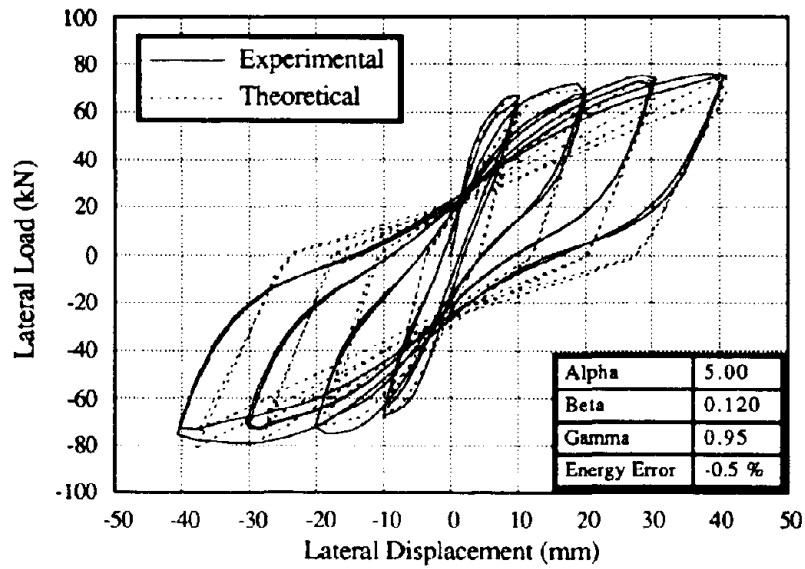
Figure 2.2. Experimental and analytical results for specimen 3 of Ng.

2.5 Closed-Form Equations for Hysteretic Parameters

Given best-fit values of the parameters α, β, and γ for many different column tests, the next objective is to ascertain if there is any correlation between these parameters and the physical properties and dimensions of the test specimens which were modeled. A stepwise linear regression analysis was conducted using 65 digital test records. The regression analysis was carried out using the commercial software package SAS/STAT [SAS/STAT, 1987]. R^2 (square of the regression correlation coefficient) values of 0.79, 0.85, and 0.80 were obtained for the estimates of the parameters α, β, and γ. It would be possible to find a model which would explain a larger percentage of the total scatter in the data, but at the expense of a significant number of additional terms. The regression equations associated with the three parameters are given below.

Let

a_s = Cross sectional area of spiral bar, cm^2

A_c = Spiral core cross section area, cm^2

A_g = Gross cross section area, cm^2

d_b = Diameter of longitudinal bar, cm

d_s = Diameter of spiral bar, cm

D = Overall diameter of pier, cm

D_c = Diameter of spiral core (out to out), cm

$f_c^{'}$ = Concrete cylinder strength, MPa

f_{yl} = Longitudinal reinforcement yield stress, MPa

f_{ys} = Spiral reinforcement yield stress, MPa

L = Length of pier, from base to first point of contraflexure, cm

N = Number of longitudinal bars in cross section

P_e = Axial load applied to pier, kN

S = Spacing (pitch) of spiral layers, cm

ρ_a = Axial reinforcement content, %

ρ_s = Spiral reinforcement content (volumetric), %

$$\sigma_o = \frac{10P_e}{f_c^{'}A_g} \quad (kN, \ MPa \ and \ cm^2)$$

$$P = \frac{2a_s f_{ys} D_c}{S}, \qquad Q = 4\rho_s \sqrt{f_c^{'}} \sqrt{\sigma_o - 0.1} \quad [Q = 0 \ if \ \sigma_o \leq 0.1], \qquad T = \frac{\sigma_o}{P+Q}$$

$$R_a = \frac{A_s}{A_c}, \quad R_D = \frac{S}{D}, \quad R_f = \frac{f_c^{'}}{f_{ys}}, \quad R_L = \frac{L}{D}, \quad R_s = \frac{d_s}{S}, \quad R_t = \frac{f_c^{'}}{f_{yl}}, \quad R_y = \frac{f_{ys}}{f_{yl}}, \quad R_\rho = \frac{\rho_s}{\rho_a}$$

then

$$\alpha = 135 - 0.0439\sqrt{f'_c}\left[1000 - 0.0178\frac{L}{R_f} + 6.14R_L - 1.02f_{yn}\right] + 230R_sR_f[1 + 1.09\sigma_o]$$

$$+ \frac{0.0646}{R_s}[1000 - 0.114A_s] - 104.5R_y - 198R_t + \frac{22.0}{p_s} - 28700T + \frac{1}{12700T}$$

$$+683R_f + 2.84S - 62.8R_D - 108(0.1)^{P_s}$$

$$\beta = 2.53 + \frac{\sqrt{f'_c}}{1470}\left[30.1\frac{R_L}{p_s} - f_{yn} + \frac{8.81\times10^6}{f_{yn}L} - \frac{4750p_s}{f_cR_L}\right]$$

$$-\frac{1}{96000T}[1 - 17.0\sigma_o] - \frac{D}{21.9} + \frac{A_c}{3260} + \frac{p_s(0.3)^{P_s}}{2.76} - \frac{307}{f_{yn}} - \frac{603}{P}$$

$$\gamma = 4.29 + 0.204\sqrt{f'_c}\left[\frac{\sigma_o}{R_L} - \frac{4660}{f_{yn}L} + \frac{12.8}{p_sf_c}\right] + 0.219p_s\left[R_s - 1.85(0.3)^{P_s}\right] - 769T - 1.12d_b$$

$$+ \frac{A_s}{7700} + \frac{627}{A_s} - \frac{N}{83.0} + \frac{R_p}{8.13} + \frac{1}{133R_D} - \frac{1}{41.5\sigma_o} - \frac{1}{21.2R_f} - \frac{87.2}{D}$$

The above equations were subsequently used to derive calculated estimates for each hysteretic model parameter given the geometry and material properties for each test specimen. Scatter plots for each parameter (values determined by system identification on the x-axis; values calculated from the regression equations on the y-axis) are shown in figures 2.3-2.5. In the case of the parameter β it should be noted that negative predicted values are not valid (and a zero should be substituted). β values must be positive, and are normally less than 1.0. A practical upper limit on β, based on the experimental data, is 1.75. Predicted γ values greater than 1.0 are not valid (and 1.0 should be substituted).

A perfect model for α, β and γ would cause all of the data in figures 2.3-2.5 to fall on a 45-degree line intersecting the origin. Actually there is moderate, but not unreasonably large, scatter, which is characterized by the R^2 values of 0.79, 0.85, and 0.80. We anticipate that the expansion of the column test database will extend the range of applicability of the regression equations. However, as the limits of scatter are likely controlled by the variability of response that is typical of reinforced concrete, it seems unlikely that the quality of correlation between the parameters derived via system identification and those calculated using closed form equations will improve significantly, and that the scatter cloud will simply become more dense. For the purposes of conservative inelastic dynamic-based design it should be possible to shift α and γ downward and β upward by some multiple of the standard deviation, much as strength

adjustment factors are incorporated in traditional design codes to account for workmanship and material variability.
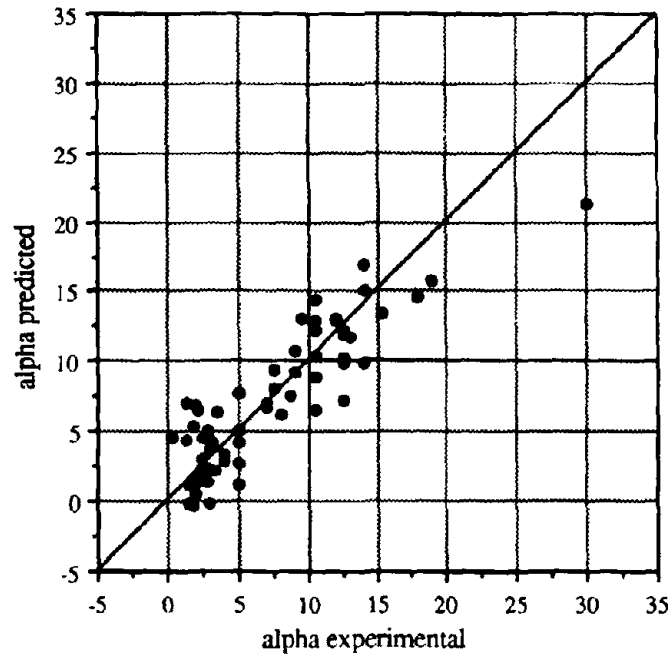
Figure 2.3. Predicted and experimental values of α.
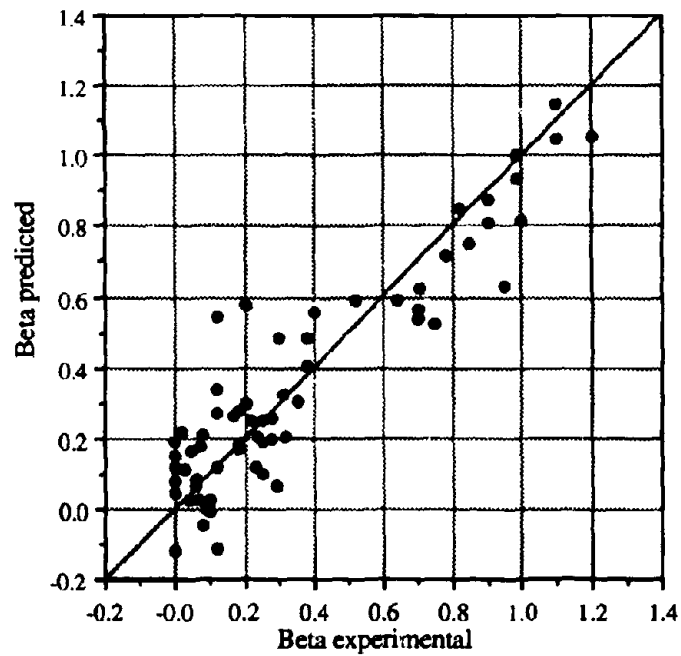
Figure 2.4. Predicted and experimental values of β.
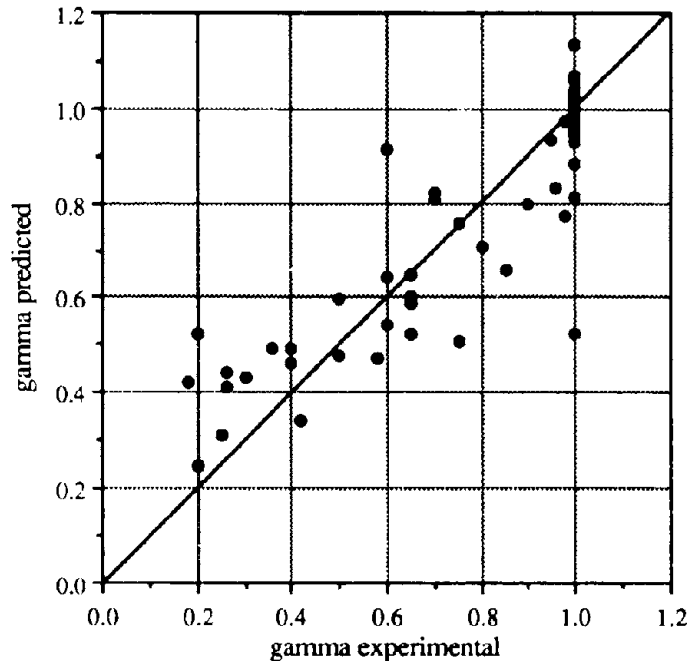
Figure 2.5. Predicted and experimental values of γ.

2.6 Summary

Within the bounds of the available test data for circular, spirally reinforced concrete bridge columns subjected to cyclic lateral loading, it was found that the Three Parameter model was able to generally predict the observed experimental load-deflection histories, and more importantly to produce an estimate of the cumulative absorbed cyclic energy within an error bound of several percent. Preliminary regression equations, which are functions of the physical properties of the bridge columns, were developed for the parameters α, β, and γ. The availability of closed form equations for these failure model parameters permits an *a priori* inelastic dynamic solution for a large class of bridge columns which employ circular cross-sections and spiral confining steel. This was one of three critical factors which needed to be addressed in order to create the integrated seismic design procedure (ISDP) described in Chapter 1. The remaining two factors – damage model correlation to experimental data and the development of a closed-form model for acceptable damage – are described in Chapters 4 and 6, respectively.

23

3.0 Selecting Design Earthquakes

3.1 Introduction

A critical step in the implementation of any time-step analysis is the selection of appropriate earthquake motions to drive the analysis. In order to design a new bridge, evaluate the potential for seismic damage to an existing bridge, or evaluate the effectiveness of earthquake protection systems, it is first necessary to obtain a prediction of the seismic forcing function. In the case of the NIST integrated seismic design procedure (ISDP), the desired earthquake motions are bedrock acceleration-time records: the motions at the ground surface are obtained by employing the shear wave propagation model SHAKE91 [SHAKE91, 1992] to filter the bedrock motions upward through the overlying soil layers. This chapter describes a method for selecting site-specific bedrock motions for the seismic design or evaluation of bridges.

3.2 Earthquake Record Selection and Scaling Method

There are in general two approaches to the generation of site-dependent earthquake bedrock motions. First, synthetic ground motions can be generated. These motions are normally computed on the basis of parameters derived from probabilistic studies of seismicity in the region of interest. The parameters not only account for earthquake magnitude but also distance from the causative fault. In many cases an historically-recorded ground motion, or some "standard" fictitious record, is selected to serve as a basis for the synthetic motion. This record is then altered (sometimes radically) in frequency content, duration and intensity to arrive at a synthetic motion which satisfies the statistical model.

With the second approach, a "design" or "target" acceleration response spectrum is established, and "natural" response spectra, from historically-recorded ground motions, are matched to it. The target spectrum is derived from statistical studies of response spectra, calculated from all available historically-recorded ground motions in the region of interest. Attenuation relationships are derived to adjust the target spectrum for earthquake magnitude and distance from the causative fault. The natural response spectrum, or spectra, which best match the target spectrum are chosen for design purposes. If no natural spectra match the target spectrum closely, the natural spectra can be altered to some degree. Amplitude scaling is accomplished by multiplying the ordinates of the entire natural response spectrum by a constant scale factor.

24

The second approach has been chosen for use in the NIST seismic design procedure for several reasons. First, the NIST study has focused initially on the Northern California region. Since there is a relative abundance of historic earthquake data from the West Coast of the United States it is possible to derive relationships for the target response spectrum and attenuation equations in the region of interest. Second, the method relies mainly on natural earthquake records which are minimally altered to match the target response spectrum. It is preferable to make use of natural earthquake records whenever possible, rather than synthetic records, as the natural records may reflect aspects of the ground motions which are not accounted for in the synthetic record generation procedures. Finally, the use of a suite of three to five natural earthquake records, which together span the target spectrum, provides a more realistic loading history than a single synthetic record, which is forced to match the entire target spectrum. In reality, a structure is subjected to a series of earthquakes over its lifetime. Taken together, these earthquakes tend to cover the entire range of the target response spectrum. A single synthetic earthquake record which covers the entire target response spectrum represents an unrealistic agglomeration of earthquake effects.

3.3 Target Response Spectrum and Attenuation Relationships

A number of methods for computing site-dependent target response spectra have been proposed [e.g., Campbell 1981, Idriss 1985, Joyner and Boore 1988, and Youngs et al. 1988]. In the present study, the spectral equations developed by Idriss [1985] were employed. This is because the development of the equations was based exclusively on seismic data from California (the initial area of interest in this study), and because the equations have been recently updated to reflect the seismic data collected from the 1989 Loma Prieta earthquake. Figure 3.1 illustrates schematically how the target response spectrum is computed, as a function of magnitude and distance. This method is summarized briefly below.

The method begins with a basic normalized spectral shape for a magnitude 6.75 earthquake. The ordinates of this curve, shown in table 3.1 below, were determined from a statistical study of historically-recorded earthquake bedrock motions in California.
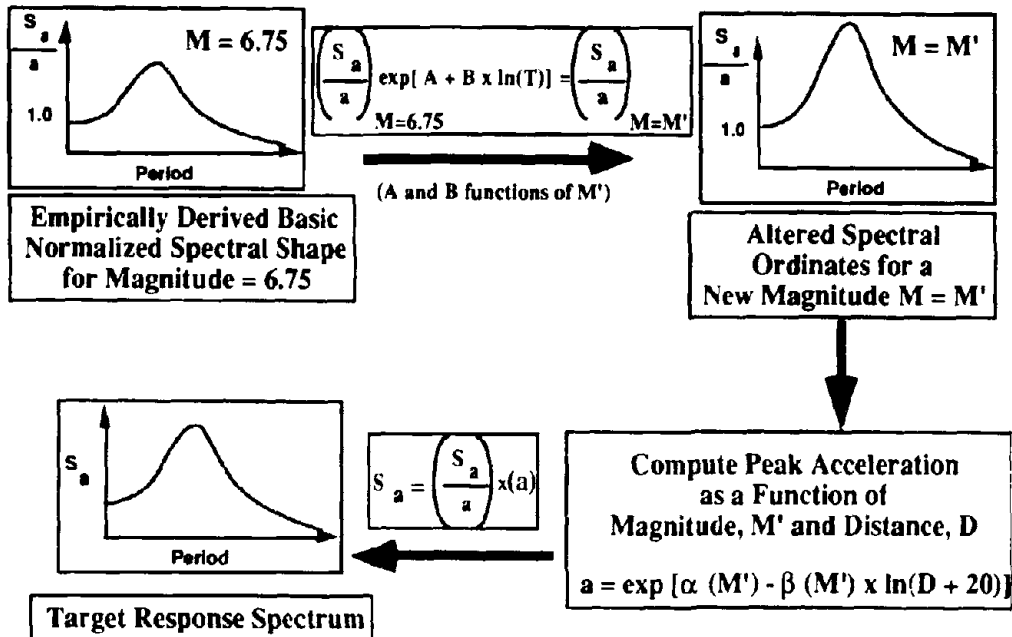
Figure 3.1. Calculation of Target Response Spectrum.

Table 3.1. Bedrock accelerations, normalized spectral ordinates for M=6.75

Period, seconds	Normalized Spectral Ordinates $\frac{S_a}{a}$	Period, seconds	Normalized Spectral Ordinates $\frac{S_a}{a}$
0.03	1.000	0.50	2.170
0.05	1.275	0.55	2.020
0.075	1.635	0.60	1.875
0.10	1.920	0.65	1.724
0.11	2.022	0.70	1.600
0.13	2.210	0.75	1.481
0.15	2.375	0.80	1.375
0.18	2.525	0.85	1.280
0.20	2.610	0.90	1.200
0.22	2.666	1.00	1.065
0.25	2.720	1.50	0.648
0.27	2.769	2.00	0.452
0.30	2.755	3.00	0.266
0.32	2.751	4.00	0.180
0.35	2.690	5.00	0.130
0.37	2.630	6.00	0.1
0.4	2.530	8.00	0.065
0.45	2.340		

The next step is to alter this basic normalized spectrum to account for a magnitude other than 6.75. This is accomplished using equation 1 below, which was derived from a statistical study of earthquakes in California, and accounts for the variation of spectral amplitude as a function of magnitude, M, and period, T, in seconds (Idriss 1985).

$$\left(\frac{S_a}{a}\right)_M = \exp[a(M) + b(M)\ln(T)]\left(\frac{S_a}{a}\right)_{M=6.75} \quad (Eqn.1)$$

where $a(M) = -7.427 + 1.654(M) - 0.082(M^2)$

and $b(M) = -3.224 + 0.718(M) - 0.036(M^2)$

The peak acceleration, "a", is computed using equation 2, which is a function of magnitude, M, and the distance from the earthquake source, d, in kilometers.

$$a = \exp[\alpha(M) - \beta(M)\ln(d + 20)] \quad (Eqn.2)$$

where $\alpha(M) = \exp[2.261 - 0.083M]$ for $M \leq 6.0$

$\alpha(M) = \exp[3.477 - 0.284M]$ for $M > 6.0$

$\beta(M) = \exp[1.602 - 0.142M]$ for $M \leq 6.0$

$\beta(M) = \exp[2.475 - 0.286M]$ for $M > 6.0$

Finally, the normalized spectral ordinates are multiplied by the peak acceleration to obtain the absolute spectral ordinates, as shown by equation 3.

$$S_a = \left(\frac{S_a}{a}\right)_M \times (a) \quad (Eqn.3)$$

3.4 Demonstration Computer Program

The method of selecting and scaling bedrock motions outlined above is well suited for implementation in a computer program on a work station with interactive graphics capabilities. Such a program called EARTHGEN was written at NIST for a Silicon Graphics IRIS 4D/410VGX work station.[*] It is anticipated that EARTHGEN will make up one module of the comprehensive seismic design procedure for bridge piers currently under development at NIST. A block diagram of EARTHGEN is shown in figure 3.2, and the operation of EARTHGEN is summarized below.
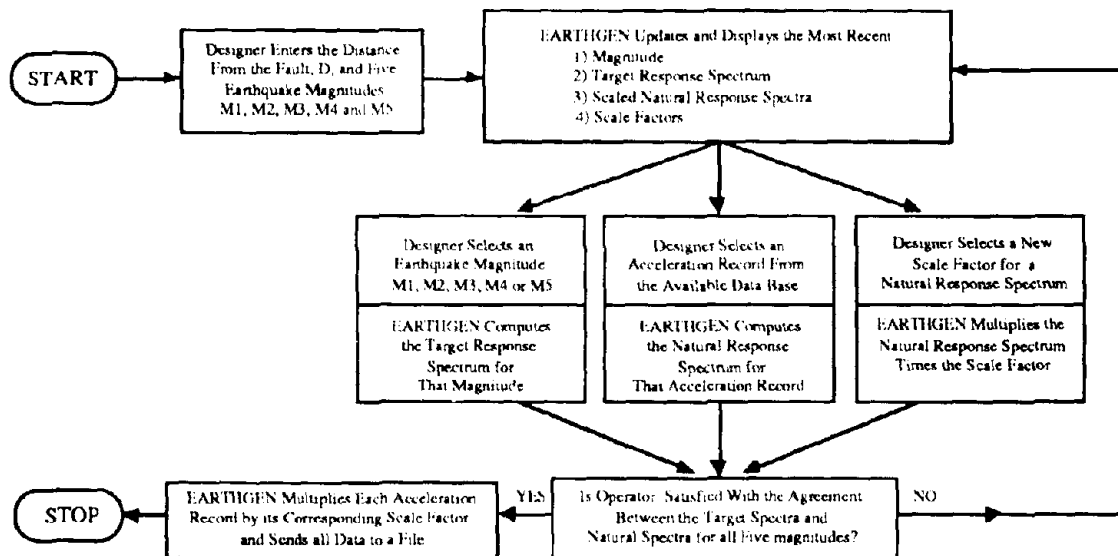
Figure 3.2. Block diagram of the program EARTHGEN.

Initially, EARTHGEN displays a menu and prompts the designer to enter the distance of the bridge site from the fault of interest, and up to five earthquake magnitudes. EARTHGEN then displays the target response spectrum for the first magnitude value. The 84th and 16th percentile limits (the target spectrum plus and minus one standard deviation) are also displayed (fig. 3.3). The designer may then select, from a list, the name of an historically-recorded bedrock motion. EARTHGEN retrieves the corresponding acceleration-time record from a data base, computes the response spectrum, and overlays this natural response spectrum on the target response spectrum already displayed

---

[*] EARTHGEN could have been written for any work station with high resolution graphics capabilities.

28

(fig. 3.4). (As part of this study some 60 recorded bedrock acceleration records for the state of California were compiled and incorporated into the EARTHGEN data base). The designer may then alter the vertical scale of the natural response spectrum by adjusting a valuator dial (fig. 3.5). EARTHGEN continuously updates the display to reflect, in real time, this scaling of the natural response spectrum.

The designer may repeat the record selection and scaling procedure for up to five other historically recorded bedrock motions, all of which are displayed simultaneously on the screen (fig. 3.6). When the designer is satisfied that this suite of scaled natural response spectra adequately covers the target spectrum, a new magnitude value is chosen and the record selection and scaling process is repeated. The designer may re-display and adjust the scaling of the spectra for any of the five magnitudes at any time. An automated scaling option is also incorporated in EARTHGEN. When invoked, this routine determines the scale factor for each natural response spectrum which results in the least total difference between the natural spectra and the target spectrum. The designer may use this feature to provide an objective measure of the agreement of the natural and target spectra.

Finally, when records have been selected and scaled for all five magnitude values, the designer terminates the interactive session, and data are written to an output file. These data include the initial input data (distance and magnitudes), and up to 25 historically recorded bedrock motions and their scale factors (up to five records for each of five magnitudes). The scaled bedrock motions may then be used for later non-linear analyses of the bridge structure subjected to five-earthquake suites of varying magnitude.
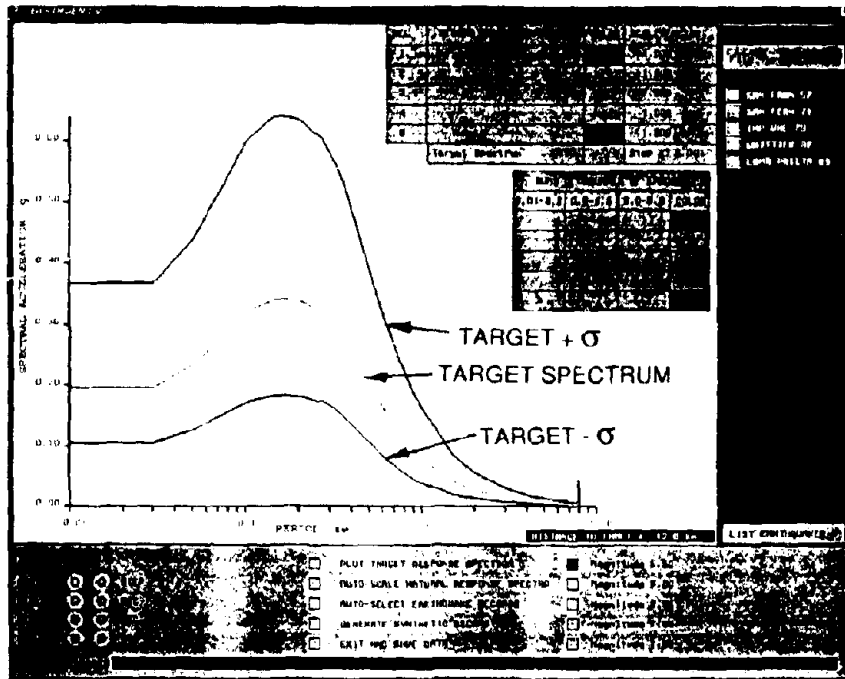
Figure 3.3. EARTHGEN display of target spectrum and 84th and 16th
percentiles.
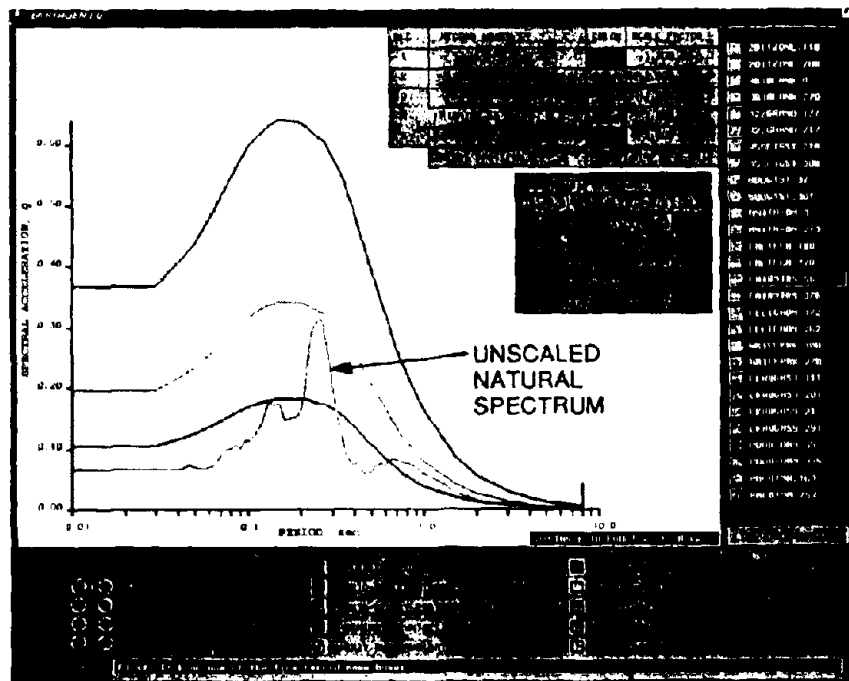
Figure 3.4. EARTHGEN display of natural response spectrum before scaling.
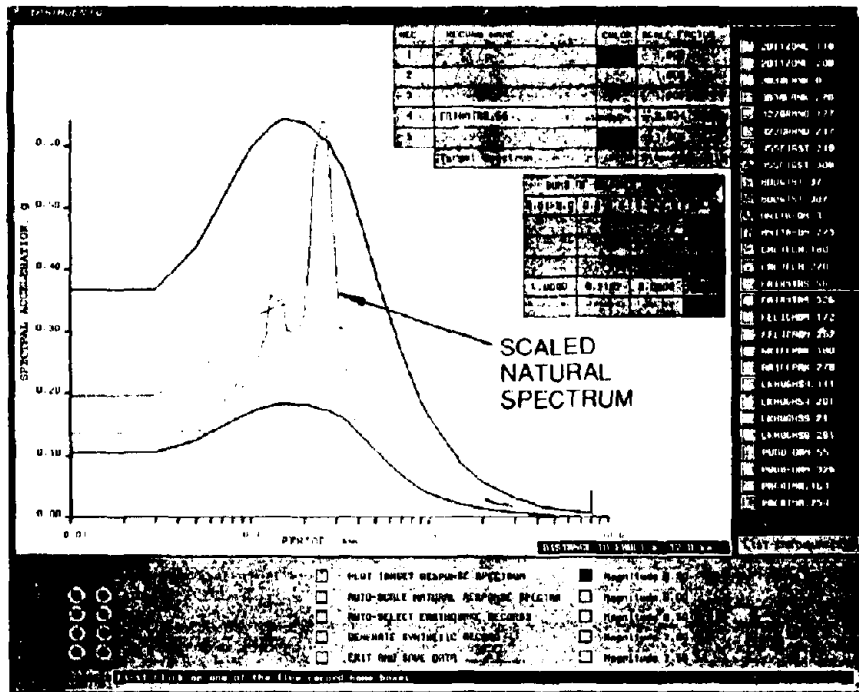
Figure 3.5. EARTHGEN display of scaled natural response spectrum.
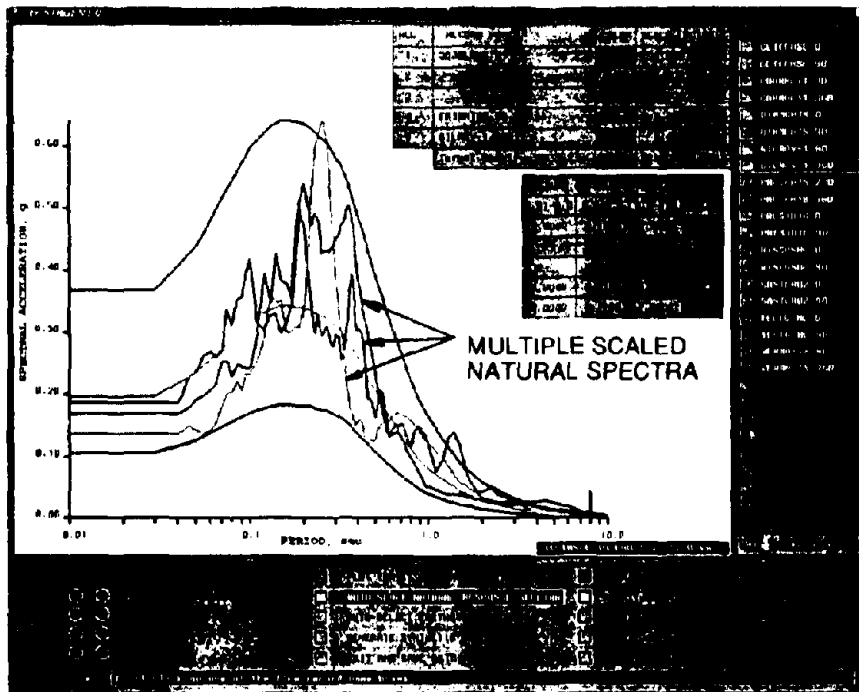
Figure 3.6. EARTHGEN display of multiple scaled natural response spectra.

31

3.5 Discussion

A method has been presented for selecting and scaling bedrock earthquake motions for the seismic design and evaluation of bridges. The method lends itself well to implementation on a computer with interactive graphics capabilities. A demonstration program, EARTHGEN, has been described. EARTHGEN allows a designer to rapidly view response spectra from a large number of historically recorded ground motions, then select and scale the records which are most appropriate for a particular site and structure. EARTHGEN has been initially configured for Northern California region, but could easily be re-configured for other localities. To do so it is only necessary to supply attenuation relationships (such as those developed in the studies of Campbell 1981, Idriss 1985, Joyner and Boore 1988, and Youngs et al. 1988) and specify a data base of bedrock motion records which are appropriate for the geology of the region of interest.

3.6 Bedrock Acceleration Records Selected for Trial Bridge Column Designs

EARTHGEN was used to select and scale suites of bedrock acceleration records for use in the trial bridge column designs of this study. A total of 64 records were selected and scaled: (suite of 4 records) x (magnitudes 5.0, 6.0, 7.0, and 8.0) x (distances 10 km, 20 km, 30 km and 40 km) = 64 records. These records are listed, along with their amplitude scale factors, in Appendix B. In all cases, records were selected which required the minimum amplitude scale factor to match the target response spectrum. However, for some of the high magnitude events at close distances the scale factors were comparatively large, out of necessity, since very few near-field records exist for large magnitude earthquakes.

32

4.0 Damage State Prediction

4.1 Introduction

It was shown in Chapter 2 that the inelastic response of a spiral-reinforced bridge column when subjected to random lateral loading can now be analytically predicted with reasonable accuracy. The present availability of empirical closed-form equations for the hysteretic model parameters α, β, and γ allows the extension of this type of analysis to practical seismic design, where the engineer has available beforehand only the geometry and material properties of a bridge column and a suite of appropriate design earthquakes (the selection of which was described in Chapter 3).

Given that we can predict the response of the bridge to an earthquake characterized by magnitude and distance, the next question is: "would the column be damaged, and if so, how severely?" For practicing engineers who must perform post-earthquake assessments of highway structures, the quantification of damage is a subjective process. The determination of when a column is serviceable; when it is not serviceable but can be economically repaired; or when it must be destroyed, based solely on an external inspection inherently involves a high degree of variability.

In this chapter we discuss an alternative approach to damage assessment. It is a two step process involving first the analytical calculation of a damage index, and second a comparison of this value with a statistical damage state model. The latter, as will be discussed in greater detail below, is based upon extensive empirical correlation studies with existing laboratory data from tests of full-scale and model bridge columns.

Briefly stated, a damage index is a dimensionless quantity generated by a mathematical algorithm during the course of an inelastic dynamic analysis. Many damage algorithms have been proposed over the last two decades. All have the common feature of equating the damage index to parameters believed to be related to the overall state of a structural element, as observed in laboratory tests of beams, columns, bents, multi-story frames, etc. The original models were primarily based upon a ratio of the maximum observed lateral displacement and the calculated ultimate displacement of the structure under monotonic loading. Later improvements recognized that strength degradation also occurred during consecutive cycles at the same displacement ductility. This additional cyclic damage was presumed to be caused by energy absorbed by the structural element, as measured by the area bounded by a hysteresis loop for one cycle of reversed loading.

33

The damage index model employed in the original release of IDARC [Park, Ang, and Wen 1985] is given by:

$$D.I. = \frac{\partial_m}{\partial_u} + \beta\left(\frac{\sum E_{abs}}{\partial_u P_y}\right)$$

where:

∂_m =   Maximum deformation under seismic loading
∂_u =   Ultimate deformation under monotonic loading
P_y =   Yield load under monotonic loading
E_{abs} =   Absorbed cyclic energy under seismic loading
β =   Strength deterioration parameter

This equation may be evaluated at any successive displacement step (if the analysis is simulating a displacement-controlled test) or at any discrete time step in a transient (earthquake) analysis. The first component represents a ductility ratio whereas the second component is a strength deterioration term which is tied to the cumulative normalized energy absorbed by the column. Although damage indices calculated using this equation generally run between 0 and 1.0, values of D.I. can be significantly higher depending on confining reinforcement details.

The 1992 release of IDARC, which was modified extensively for work specific to this report, employs an alternative formulation of the damage index equation which is more versatile. Direct application of the original model to structural systems requires determination of an overall member deformation. Since inelastic behavior is confined within plastic zones near the ends of a member, the relationship between overall member deformation, local plastic rotations, and the damage index is difficult to correlate. The 1992 IDARC damage index equation, based on moment and curvature, rather than loads and deflections, is

34

$$D.I. = \frac{\Phi_m - \Phi_r}{\Phi_u - \Phi_r} + \beta\left(\frac{A_t}{\Phi_u M_y}\right)$$

where:

Φ_m = Maximum curvature attained during seismic loading
Φ_u = Ultimate curvature capacity of section
Φ_r = Recoverable curvature at unloading
M_y = Yield moment of section
A_t = Total area contained in M-Φ loops
β = Strength deterioration parameter

The term A_t does not correspond to the original energy term in Park's model. However, it does represent an implicit measure of energy, and when normalized as indicated above, was found to correlate well with the original strength deterioration parameter, β. As described above, the moment-curvature model is more versatile, particularly where complex indeterminate structures are involved. For the case of a cantilevered bridge column, however, the results are essentially the same as for the load-displacement formulation and either model could be used effectively (the previous model being more intuitive). For the sake of continuity with future, more sophisticated, analyses of indeterminate multiple-pier bridge bents, we have used the moment-curvature formulation for the work presented in this paper. Because the damage index equations are in a non-dimensional format, they permit comparisons between columns of different sizes as well as columns with different loading histories.

4.2 Damage States

Figure 4.1 shows a typical inelastic cyclic test of a bridge column under displacement control through failure of the column. In this figure three discrete conditions relating to the structural integrity of the column are called out: yield, ultimate, and failure. Although cracking and "spalling" might also be useful, these were not considered as limiting states for the following reasons. First, except in special prestressed situations, service load cracking is normal in reinforced concrete and does not always represent a cause for concern, nor does it constitute the sole cause for repair of a structure in the wake of an earthquake.

35

NIST Test Column: Model-N2

$P_{ult} = 74$ kN $P_{fail} = 60$ kN

$P_y = 65$ kN

$P_{cr} = 23$ kN

Lateral Load (kN)

Lateral Displacement (mm)
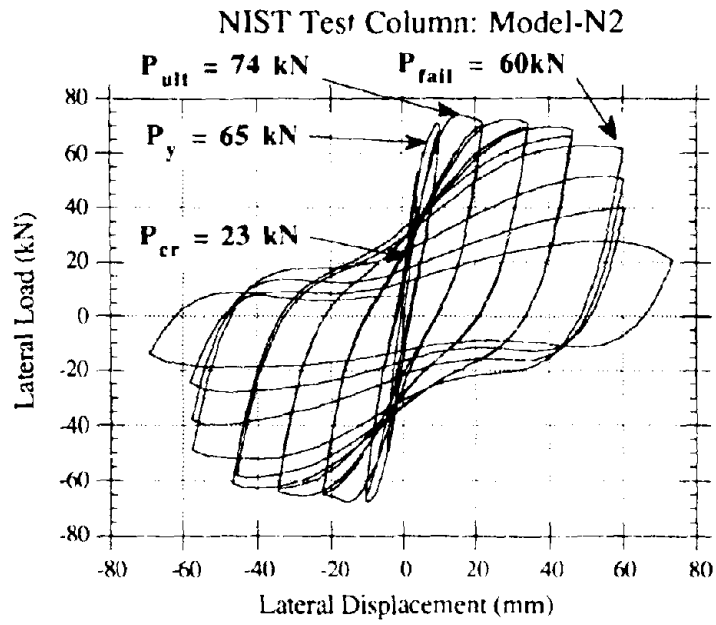
Figure 4.1. Damage states of a laboratory test column.

Damage Index vs. Load Step Number
NIST Test Column Model N2
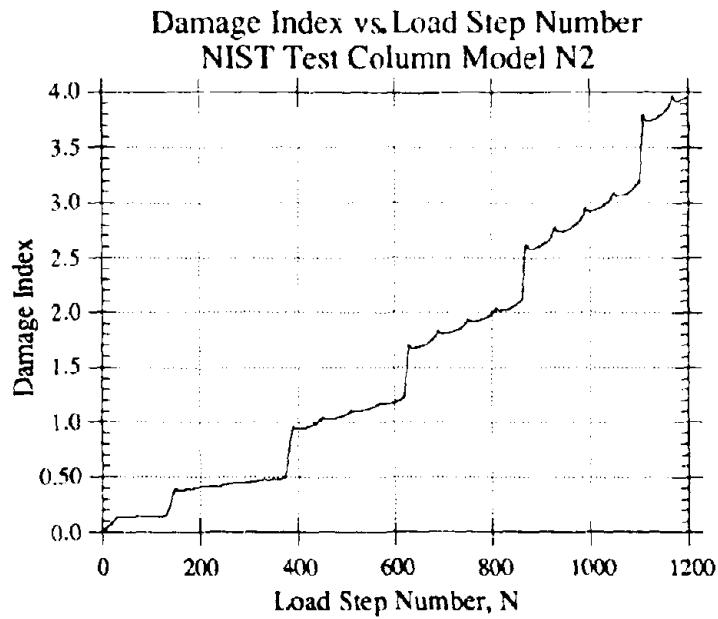
Damage Index

Load Step Number, N

Figure 4.2. Increase of damage index with load step.

Yielding of longitudinal steel, on the other hand, is a signal of the onset of real structural distress. Spalling of cover concrete in the plastic hinge region will generally occur following extensive yielding but prior to reaching the ultimate load (moment) capacity of the section. It is therefore a symptom of extensive yielding, and not the cause. Ultimate load (moment) capacity of the section is simply the maximum observed lateral load (moment) capacity of the column.

Beyond this point the stiffness of the column is negative and continued application of the ultimate load would lead to complete failure of a single, isolated column. However, a bridge column is usually part of a larger structural system, and, depending on the structural configuration, can often be restrained from lateral collapse by other structural elements. In displacement-controlled tests it is possible to track the behavior of the column in this regime. It has generally been accepted that once the lateral load capacity has fallen off to less than 80% of the ultimate load the column will completely fail in an actual earthquake, due to high moments created by its own axial load (P-δ effects). This has been labeled in figure 4.1 as the failure state of the column.

The above three states form useful delimiters for four possible damage conditions that might exist in a bridge column following an earthquake. These are:

1) *No Damage*: the column has not yielded. Although cracking may have occurred it will likely not be extensive and will not compromise the serviceability of the structure.

2) *Repairable*: the column has yielded but has not reached ultimate load. Extensive spalling may have occurred but inherent stiffness remains and economics will likely dictate that the structure should be repaired rather than replaced.

3) *Demolish*: the column has been loaded beyond ultimate load but remains standing. Complete failure is likely pending another severe earthquake and the column, at least, and possibly the entire bridge structure must be replaced.

4) *Collapse*: the column has completely failed and will likely contribute to collapse of the entire bridge.

As described above, the model employed in IDARC produces a quantitative estimate of deterioration under cyclic loading, namely the damage index. As an example of how this index is cumulative throughout the loading history for a particular column figure 4.2 shows the damage index at each displacement load step for the same column depicted in figure 4.1.

While the damage index provides a convenient relative measure of degradation under cyclic loading, in a practical sense the damage index is useless unless it can be calibrated against experimentally observed states of column damage. Therefore, it was necessary to investigate the correlation between the observed states of damage in cyclic lateral load tests of spirally-reinforced bridge piers and the calculated damage indices produced by IDARC. Furthermore, for the purpose of establishing seismic design guidelines, it is advantageous to establish threshold damage indices which indicate the likely occurrence of three damage states: onset of yielding (P_y); attainment of maximum lateral load capacity (P_{ult}); and complete failure (P_{fail}).

4.3 Determination of Threshold Damage Indices

Threshold damage indices for the yield, ultimate and failure damage states were conservatively estimated by examining the statistical distribution of calculated damage indices from laboratory tests of 82 spiral-reinforced bridge piers (a digital database for these tests has been established at NIST). The procedure for the determination of the damage indices is outlined below.

For each of the 82 tests listed in table A.1 and A.2 the points in the experimental loading history at which the yield, ultimate and failure damage states occurred were determined by inspection of the load-displacement histories, as illustrated in figure 4.1. Three separate IDARC analyses were then carried out for each test specimen: the first analysis produced a calculated damage index resulting from the load-displacement history applied up to the observed point of yielding; in the second analysis the damage index was calculated for a virgin column subjected to the load-displacement history from its beginning up to the observed point of ultimate load; and in the third analysis a virgin column was subjected to the load-displacement history from its beginning up to the observed failure point.

Table C.1 presents a summary of the damage analyses, indicating the number of displacement steps ("Number of Data Points") from the laboratory tests used in the analysis, the observed damage state, the deformation (curvature) damage, the energy (M-Φ) damage, and total damage. The yield state could not be determined for one test, the ultimate state did not occur for one test, and the failure state did not occur for 16 tests. Thus, the available populations were 81, 81, and 66 tests for estimating threshold damage indices for yield, ultimate, and failure damage states, respectively.

38

Histograms of calculated damage indices for each of the three damage states are shown in figures 4.3, 4.4, and 4.5. In all three cases the distributions have a pronounced mode (peak value) and are skewed strongly to the left. An estimate of the most frequently occurring threshold damage index would be the mode of the distribution, and a conservative estimate of the threshold damage index would lie somewhat to the left of the mode. After close examination of the data it was determined that the tenth percentile of each of the three distributions provides threshold damage index estimates which are close to the mode, but are fairly conservative. That is, in all three cases the tenth percentile threshold lies close to the most frequently observed value of the threshold damage index, and at the same time 90% of the calculated damage indices lie above the tenth percentile. The tenth percentile threshold damage indices for the three damage states are discussed in Section 4.4, and shown in table 4.1.

Yield State Damage Indices (Closeup of Range 0.0 to 2.5)

Histogram category size	0.1
Minimum recorded damage index	0.05
Maximum recorded damage index	12.66
Tenth percentile	0.11
Tenth percentile 90% confidence interval	(0.08,0.17)

81 Observations

Tenth Percentile

Frequency of Occurrence

Computed Damage Index
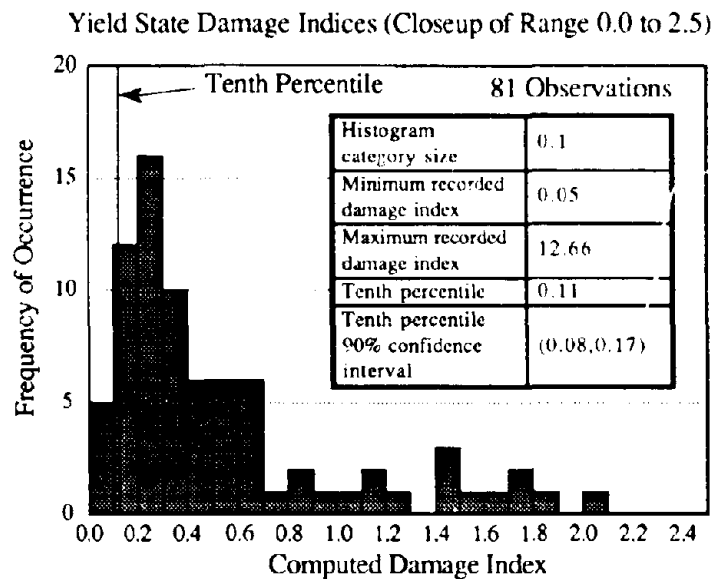
Figure 4.3. Histogram of observed yield state damage indices.

39

Ultimate State Damage Indices (Closeup of Range 0.0 to 5.0)

Tenth Percentile 81 observations

Histogram category size	0.1
Minimum computed damage index	0.19
Maximum computed damage index	54.12
Tenth percentile	0.40
Tenth percentile 90% confidence interval	(0.32,0.43)

Frequency of Occurrence

16 12 8 4 0

0.0   0.5   1.0   1.5   2.0   2.5   3.0   3.5   4.0   4.5   5.0

Computed Damage Index
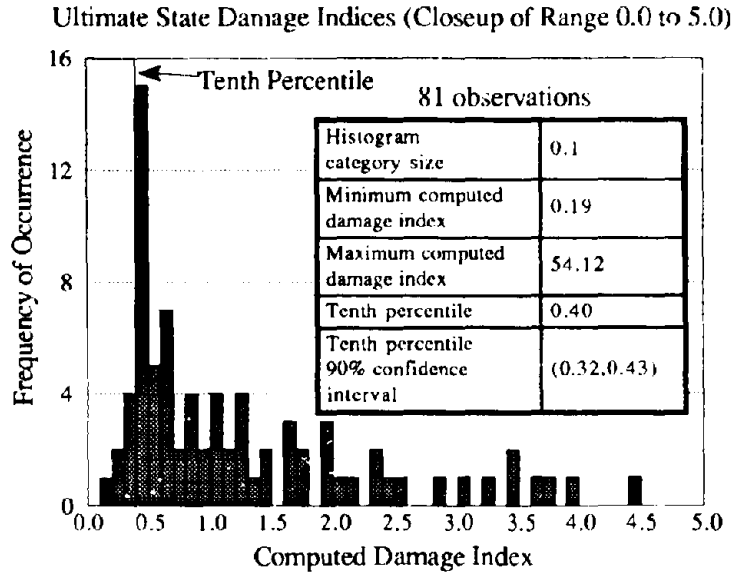
Figure 4.4. Histogram of observed ultimate state damage indices.

Failure State Damage Indices (Closeup of Range 0.0 to 5.0)

Tenth Percentile 66 observations

Histogram category size	0.1
Minimum computed damage index	0.18
Maximum computed damage index	62.43
Tenth percentile	0.77
Tenth percentile 90% conf. inter.	(0.71,0.86)

Frequency of Occurrence

6 5 4 3 2 1 0

0.0   0.5   1.0   1.5   2.0   2.5   3.0   3.5   4.0   4.5   5.0

Computed Damage Index

Figure 4.5. Histogram of observed failure state damage indices.

4.4 Variability of Threshold Damage Indices

The proposed threshold damage indices discussed above were derived from a diverse experimental database. Thus, in a qualitative sense one could be fairly confident that the proposed tenth percentile threshold values will not change dramatically in light of future experimental results. However, it is desirable to have a quantitative measure of the variability of the tenth percentile values. In other words, one would like to know how precisely the tenth percentile values have been determined. If there is wide variability in the tenth percentile values, then further experimentation might be required to establish reliable damage index thresholds. If there is narrow variability, then the proposed values could be used with reasonable confidence.

4.4.1 The Bootstrap Method

As described in section 4.3 above, estimates of the threshold damage indices were made, using as a database of all the known experimental results from cyclic lateral load tests on spirally-reinforced bridge piers. Since this database is of finite size, it would appear that an estimate of the variability of any single statistical parameter (such as the tenth percentile) coul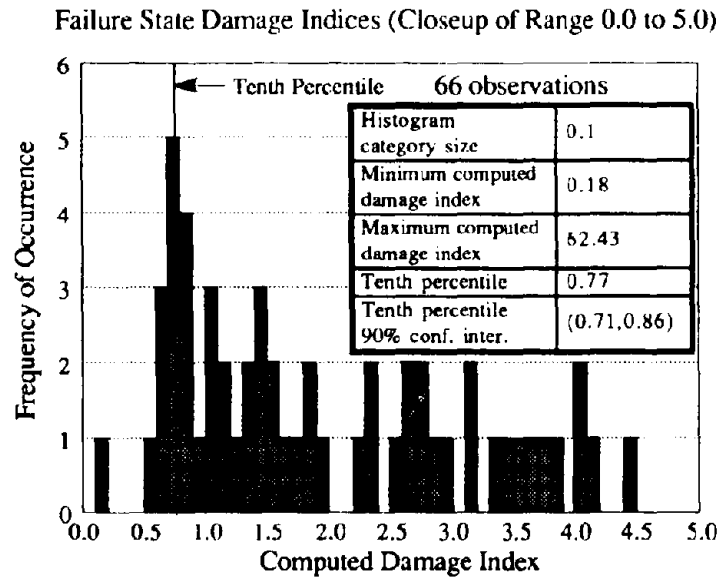d only be made if a large number of additional databases of similar size became available. Specifically, in order to determine the variability of the tenth percentile estimates made above, one would need to collect a large number, say 500, additional sets of tests on 82 bridge piers, compute the tenth percentile of each set of 82 tests, then find the mean and standard error terms of the 500 resulting tenth percentile values. Clearly, it is very unlikely that such a large number of tests on spirally-reinforced bridge piers will ever be carried out. However, using a statistical technique known as "resampling" or "the bootstrap method," one can simulate a very large data set and obtain estimates of the variability of the statistical parameters that characterize the original, smaller, data set.

Overviews of the bootstrap method, its theory and applicability are presented by Efron and Gong (1983), Diaconis and Efron (1983), and Efron and Tibshirani (1986). The fundamental requirement for valid application of the bootstrap method is that the available data set be a representative subset of a much larger population. In the case at hand, it is reasonable to assume that the 82 column tests, performed by a number of different researchers working in separate laboratories, and employing a variety of experimental methods, is a representative random sample of the very large number of column tests which could be (but probably will not be) performed in the future.

41

The steps of the bootstrap method may be described conceptually as follows. First, the original data set of size n is randomly sampled, with replacement of each value after sampling, to obtain a new set of n variables. Because sampling is done with replacement, the probability of sampling any one value from the original data set is always 1/n, and there may be multiple occurrences of the same value in the new data set. Once the new data set is obtained, the statistical parameter of interest (mean, variance, percentile, etc.) is computed. Sampling of new data sets with n values is carried out a sufficient number of times (on the order of several hundred to several thousand) to obtain a histogram which shows the variability of the parameter of interest. Once this histogram has been constructed, indicators of the variability of the parameter, such as the standard error term and confidence intervals, can be computed.

4.4.2 Application of the Bootstrap Method to Threshold Damage Indices

The bootstrap method was applied to the tenth percentile threshold damage indices, derived earlier, by carrying out sampling with replacement of data sets with 81 values (or 66 values in the case of the failure damage index) 10,000 times. Tenth percentile damage indices were computed for each of these 10,000 data sets. Subsequent analyses of the 10,000 damage indices resulted in standard error terms and 90% confidence intervals for each of the three threshold damage indices (yield, ultimate and failure damage states). Table 4.1 summarizes the estimates of the threshold damage indices obtained from the original data sets, and the standard error terms and 90% confidence intervals obtained from the bootstrap method. The threshold damage indices in the table can be interpreted as the best available empirical estimates of the tenth percentile thresholds, and the 90% confidence intervals can be interpreted as the estimated variability in the threshold damage indices, based on a large bootstrapped data set.

Table 4.1. Threshold Damage Indices for Spiral-Reinforced Bridge Piers, and Estimates of Their Variability

Damage State	Threshold Damage Indices	Standard Error Term	90% Confidence Interval
Yield	0.11	0.03	(0.08, 0.17)
Ultimate	0.40	0.03	(0.32, 0.43)
Failure	0.77	0.05	(0.71, 0.86)

5.0 Analysis of CALTRANS Columns

5.1. Selection Criteria

To demonstrate the seismic design approach described in this report, a series of representative spiral-reinforced single column bridge bents was selected for analysis. These columns were designed according to the seismic design procedures currently published by CALTRANS [CALTRANS 1990], which are an extension of AASHTO standards [AASHTO 1989], and are generally considered to be the most stringent seismic design standards for bridges in the United States. This series of CALTRANS-designed columns was then analyzed using the procedures outlined above in Chapters 1 through 4, and the performance of the columns was evaluated. The series of columns chosen for analysis had geometries, material strengths and axial loads typical of those found in practice. However, due to the limited scope of this study, it was not possible to perform a comprehensive set of analyses encompassing all common design parameters. That is, the series of analyses addresses a sampling of columns, and further study is required to fully evaluate the adequacy of the CALTRANS approach to seismic design.

The general characteristics of the series of columns analyzed in this study are summarized in table 5.1 below.

Table 5.1. General characteristics of CALTRANS columns analyzed in this study

Column Characteristic	Values Investigated
Diameter, D	122 cm
Length/Diameter ratio, L/D	3, 6, 9
Concrete cylinder strength, f'c	27.6 MPa
Axial reinforcement yield, ultimate stress	414, 724 MPa
Spiral reinforcement yield, ultimate stress	414, 724 MPa
Axial load level = Pe/(f'c*Ag)	0.05, 0.10, 0.15
Clear cover to spiral bars	5.1 cm
Diameter of spiral reinforcing bar	1.59 cm
Soil overburden	none (bedrock), 37 m sand
Distance from causative fault	10, 20, 30 and 40 km

The column diameter in all cases was fixed at 122 cm, and the length was varied to obtain length-to-diameter ratios of 3, 6, and 9. Concrete and steel material properties were assigned the typical values shown in table 5.1. The

axial load levels of 0.05, 0.10, and 0.15 cover the range of values commonly found in practice. The spiral bar diameter and concrete clear cover dimensions also have typical values. Two soil overburden conditions were selected for analysis: no soil overburden (construction on bedrock, or less than 3 m of alluvial deposits), and 37 m of sand. Distances of 10, 20, 30, and 40 km from the causative fault were investigated, in order to explore the effects of distance attenuation effects on column behavior. A total of 72 columns were designed by the CALTRANS procedures [(3 L/D ratios) x (3 axial load levels) x (2 soil conditions) x (4 distances to causative fault) = 72 cases].

5.2. Design of Columns

The currently published CALTRANS seismic design procedures permit an equivalent static lateral load analysis for most ordinary bridge structures. This procedure is summarized in figure 1.1, and its essential features are outlined below

The first step of the procedure is to estimate the fundamental period of the elastic, undamaged structure by means of a simple function:

$$T = 0.32\sqrt{W/k}$$

where W is the axial dead load of the bridge, and k is the lateral stiffness of the substructure, in compatible units. An empirical factor, Z, is then read from a graph. Z accounts for the approximate ductility of the member being analyzed, and the risk associated with failure of that member. Next, knowing the geographic location of the proposed bridge, a value of peak bedrock acceleration is read from a series of acceleration isoclines plotted on a map of California. This map accounts for the locations of known active faults in California, the maximum credible earthquakes associated with those faults, and the attenuating characteristics of the subsurface geology. Once the period of the structure and the peak bedrock acceleration have been determined, an "ARS factor" is read from a curve which corresponds to one of four soil overburden conditions: 0-3 m alluvium, 3-24 m alluvium, 24-46 m alluvium, or over 46 m alluvium. These ARS curves are pseudo-acceleration response spectra, which have been adjusted for peak bedrock acceleration and soil amplification effects. Finally, the equivalent static lateral load, F, for which the structure is to be designed is found from the equation

$$F = \frac{(ARS)(W)}{Z}$$

Sizing and detailing of the pier then proceeds as it would for a static design, with certain additional constraints imposed on reinforcement contents to insure adequate ductility under cyclic loading.

The distance of the bridge from the causative fault is not an explicit factor in the CALTRANS design procedure; rather, distance is considered implicitly by means of the peak bedrock acceleration map for California. Since the design method described in this report accounts explicitly for distance, a means of explicitly entering distance in the CALTRANS designs procedure was required. This was accomplished by surveying the California peak acceleration map and extracting peak acceleration values from the map for distances of 10, 20, 30, and 40 km from major active faults. A total of 15 locations were examined near major faults throughout the state. The maximum peak acceleration values from any of these 15 locations (conservatively rounded up to the nearest 0.1g) are shown in table 5.2 below. These acceleration values represent the worst possible peak ground accelerations required under the CALTRANS design procedure, and should result in conservative, or at least acceptable, designs at any location in the state.

Table 5.2. Maximum CALTRANS bedrock accelerations for various distances from fault

Distance of bridge from causative fault km	Maximum peak bedrock acceleration from CALTRANS design map, g's
10	0.6
20	0.4
30	0.4
40	0.3

It was found that for all 72 designs the spiral reinforcement content was controlled by the CALTRANS requirement for minimum confining steel, so #5 spirals spaced at 12.1 cm are used in all cases. The calculated longitudinal reinforcement contents for the 72 designs are shown in tables 5.3 and 5.4 below.

Table 5.3. Longitudinal reinforcement contents for CALTRANS designs on bedrock

L/D	Pe/(f'c*Ag) = 0.05	Pe/(f'c*Ag) = 0.10	Pe/(f'c*Ag) = 0.15
	Distance = 10 km, amax = 0.6 g		
3.0	18 - #9 bars	18 - #9 bars	18 - #10 bars
6.0	18 - #9 bars	18 - #9 bars	18 - #10 bars
9.0	18 - #9 bars	18 - #9 bars	25 - #10 bars
	Distance = 20 km, amax = 0.4 g		
3.0	18 - #9 bars	18 - #9 bars	18 - #9 bars
6.0	18 - #9 bars	18 - #9 bars	18 - #9 bars
9.0	18 - #9 bars	18 - #9 bars	21 - #10 bars
	Distance = 30 km, amax = 0.4 g		
3.0	18 - #9 bars	18 - #9 bars	18 - #9 bars
6.0	18 - #9 bars	18 - #9 bars	18 - #9 bars
9.0	18 - #9 bars	18 - #9 bars	21 - #10 bars
	Distance = 40 km, amax = 0.3 g		
3.0	18 - #9 bars	18 - #9 bars	18 - #9 bars
6.0	18 - #9 bars	18 - #9 bars	18 - #9 bars
9.0	18 - #9 bars	18 - #9 bars	21 - #10 bars

Table 5.4. Longitudinal reinforcement contents for CALTRANS designs on 37 m sand

L/D	Pe/(f'c*Ag) = 0.05	Pe/(f'c*Ag) = 0.10	Pe/(f'c*Ag) = 0.15
	Distance = 10 km, amax = 0.6 g		
3.0	18 - #9 bars	18 - #9 bars	18 - #9 bars
6.0	18 - #9 bars	21 - #11 bars	22 - #14 bars
9.0	18 - #10 bars	20 - #14 bars	31 - #14 bars
	Distance = 20 km, amax = 0.4 g		
3.0	18 - #9 bars	18 - #9 bars	18 - #9 bars
6.0	18 - #9 bars	18 - #10 bars	25 - #10 bars
9.0	18 - #9 bars	21 - #10 bars	20 - #14 bars
	Distance = 30 km, amax = 0.4 g		
3.0	18 - #9 bars	18 - #9 bars	18 - #9 bars
6.0	18 - #9 bars	18 - #10 bars	25 - #10 bars
9.0	18 - #9 bars	21 - #10 bars	20 - #14 bars
	Distance = 40 km, amax = 0.3 g		
3.0	18 - #9 bars	18 - #9 bars	18 - #9 bars
6.0	18 - #9 bars	18 - #9 bars	20 - #10 bars
9.0	18 - #9 bars	18 - #9 bars	19 - #11 bars

5.3. Inelastic Dynamic Analyses of CALTRANS Designs

5.3.1. Overview

In Chapter 3 the selection and scaling of bedrock acceleration records for seismic design of bridges was discussed. This method is briefly summarized below.

The approach taken in this report is to utilize, to the greatest extent possible, suites of three to five natural bedrock acceleration records which were recorded under conditions similar to the specified design conditions for the bridge. Suites of records, rather than a single record, are used to account for the natural variability in frequency content of seismic events. If the design requirements for the bridge call for a certain minimum level of performance when the bridge

is subjected to a magnitude 7.0 event at a distance of 20 km, then the preferred
suite of bedrock motions for input to the inelastic analyses procedure would be,
of course, bedrock motions recorded under similar geological conditions, from
magnitude 7.0 events at a distance of 20 km. However, lacking such a suite of
recorded bedrock acceleration records, minimal amplitude (but not frequency)
scaling is carried out on records obtained from events which are as close as
possible to the desired event. The amplitude scaling factor for each record in
the suite is determined by comparing the acceleration response spectrum of
each record to a "target" response spectrum, which is calculated for the desired
event.

Experience has shown that a sufficient number of recorded bedrock motions are
currently available to make this approach within the realm of possibility for
California, and possibly for much of the West Coast region of the United States.
However, for the Central and Eastern regions of the United States, it may be
necessary to make use of synthetic acceleration records. While the validity of
using synthetic records is open to debate, they may be the only available option
in some cases.

Once a suite of design bedrock motions is determined whether the suite is
natural, amplitude scaled or synthetic, the bridge design under consideration is
subjected to each record in the suite individually (not sequentially). The single
record which causes the greatest damage to the structure determines the worst-
case damage index expected for the bridge under the design-level earthquake at
the design distance. This worst-case damage index is then compared with
acceptable levels of damage, discussed in Chapter 6, to determine whether or
not the design is adequate.

The suites of design-level earthquakes derived for use in this study are listed in
Appendix B. A suite of four records was developed for each of magnitudes 5.0,
6.0, 7.0, and 8.0, at distances of 10 km, 20 km, 30 km, and 40 km, making a
total of 64 records.

5.3.2. Analyses on Bedrock Substrate

A schematic of the analysis of a single spiral column bridge bent situated on
bedrock is shown in figure 5.1. Each inelastic dynamic analysis of a column
results in a plot of damage index vs. time for the column. Examples of such
plots (for the same column with three different L/D ratios) are shown at the top
of figure 5.1. It can be seen that for each analysis the damage index rises to a
certain value, then levels off as the ground shaking subsides. This terminal
value of damage index is used to characterize the performance of the column
design, when subjected to the given seismic event.

48

As discussed in Section 5.2 above, 36 sample columns were designed using CALTRANS procedures, assuming the columns were situated on bedrock (table 5.2). Each of these designs was subjected to 16 bedrock acceleration records: four suites consisting of four records, each suite containing four earthquakes of the same magnitude and distance. The highest of the four terminal damage index values obtained from each suite was used to characterize the performance of the column when subjected to the given magnitude earthquake at the given distance. The numerical results of these analyses are presented in Section 6.2.

5.3.3. Analyses on 37 m Sand Substrate

A schematic of the analysis of a single spiral column bridge bent situated on an alluvium substrate is shown in figure 5.2. The process of computing the damage index is exactly the same as describe above, except for the intermediate step of propagating the bedrock acceleration record to the ground surface. As explained in Section 1.2, this was accomplished in the present study using the program SHAKE91.

Thirty-six sample columns were designed assuming they were situated on a 37 m thick layer of sand overlying bedrock (table 5.4). The results of these analyses are presented in Section 6.2.
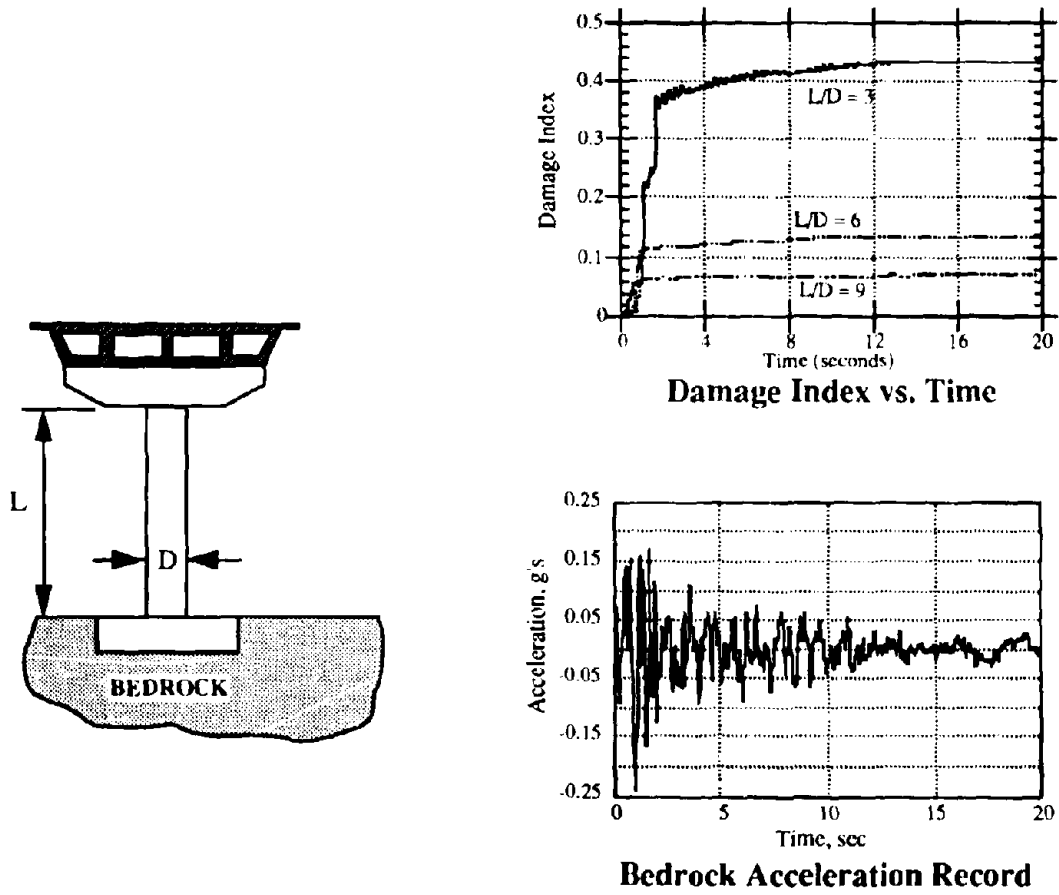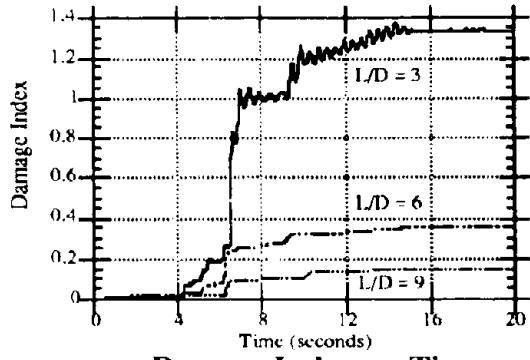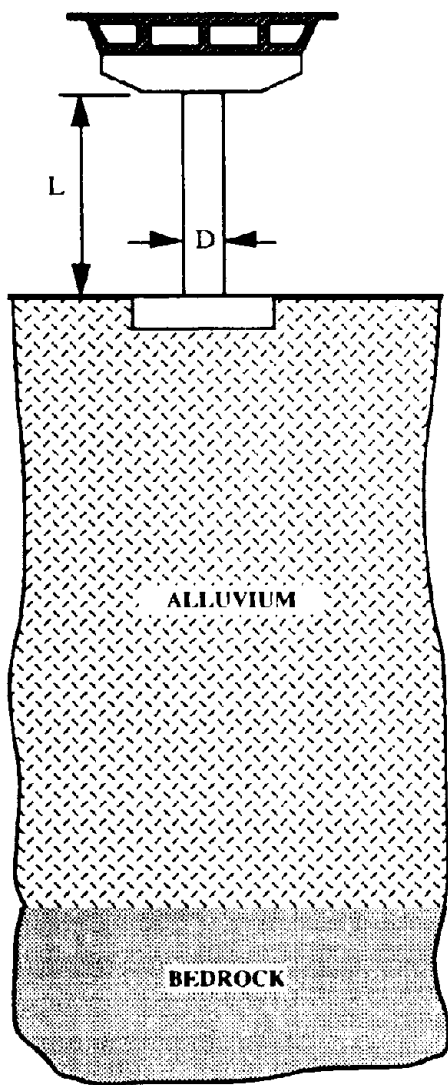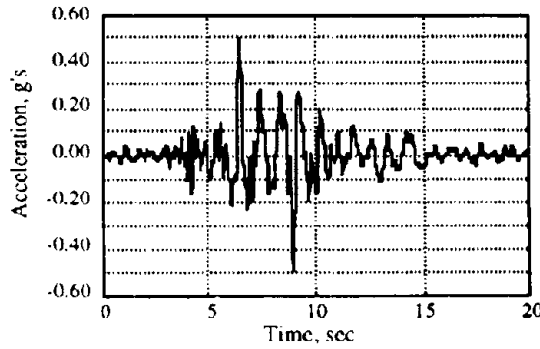
49

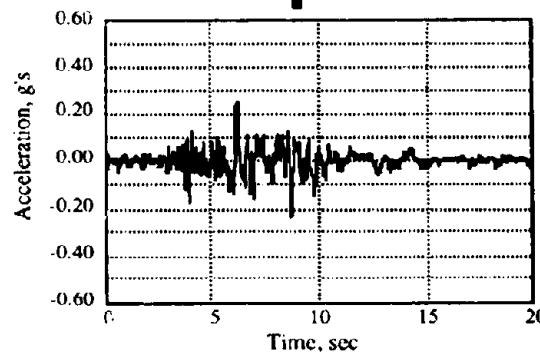Figure 5.1. Calculation of damage index for bridges on bedrock substrate.

Figure 5.2. Calculation of damage index for bridges on alluvium substrate.

6.0 Performance of CALTRANS-Designed Columns

6.1. Development of Relationships for Acceptable Damage

In this section relationships are proposed for acceptable levels of seismic damage to spiral reinforced bridge piers. In this study damage is quantified in terms of the damage index, and acceptable values of the damage index are expressed in terms of earthquake magnitude, distance of the structure from the causative fault, and the importance of the structure.

Acceptable levels of structural performance (e.g., minimum strength, allowable deflections) are normally determined by code writing organizations, and local, state and national government agencies. However, no guidelines for acceptable levels of seismic damage currently exist. Because the notion of employing a "damage index" to gage the seismic performance of reinforced concrete structures is relatively new, code writing bodies have not yet addressed the issue of determining an "acceptable" damage index for a given structure subjected to a given seismic event. Therefore, a proposed model for acceptable damage level was derived in this study, and is described below. While the model was developed specifically for spiral-reinforced concrete bridge piers, with minor modifications the model could be applied to other types of reinforced concrete members and structures.

The level of seismic damage deemed "acceptable" for a given structure is mainly a function of two conditions: the severity of the seismic event, and the importance of the structure. In turn, the severity of the seismic event depends on a number of subsidiary factors, including the magnitude of the event, the distance of the causative fault from the structure, and the ground motion attenuation characteristics of the local geology. Likewise, the importance of the structure depends on several subsidiary factors, such as the threat to life-safety posed by the structure, the role of the structure in maintaining essential lifeline services (transportation, communication, utilities delivery, medical care, and governance) following a major earthquake, and the potential cost of repair or replacement of the structure. (For further discussions of evaluating the structural importance of bridges, see Maroney 1990, FHWA 1983, and FHWA 1987).

Thus, many factors figure into the determination of an acceptable level of damage for a specific structure at a specific location subjected to a specific seismic event. For example, extensive damage of an unimportant and inexpensive structure in a minor seismic event might be tolerated, but a highly important structure might be required to remain fully operational following a

52

severe earthquake. Along these lines, a number of guiding principles can be stated which shape the development of a model of acceptable damage. First, regardless of the characteristics of the seismic event or the importance of the structure, total collapse of the structure must be avoided, as total collapse would likely result in loss of life. Second, for small events at large distances from causative faults the damage suffered by any structure should be minor. Depending on the importance of the structure, this minor level of damage should lie somewhere between the state of no perceptible damage and the state of first yield. Third, for very large, extraordinary, seismic events (on the order of magnitude 8) extensive damage is unavoidable even at moderate distances from the causative fault (say 40 km). Therefore damage indices approaching (but less than) the failure damage state must be allowed in some cases. Finally, allowable damage levels should in general be lower for important structures than for unimportant structures.

Using the guiding principles outlined above, matrices of acceptable damage indices could be constructed, which are functions of earthquake magnitude, distance to fault and structural importance. Although the precise level of acceptable damage at a given magnitude, distance and structural importance level is somewhat open to interpretation, the approximate levels of acceptable damage are generally evident. In this study, three damage index thresholds have been defined: yield, ultimate, and failure, as discussed in Chapter 4. Acceptable damage index matrices are constructed in terms of those threshold values.

An example of a matrix of acceptable damage indices is illustrated by the bar chart in figure 6.1. The proposed values shown are for bridge piers which are deemed moderately important to seismic lifelines, that is, for piers in bridges which are judged to have a secondary role in sustaining transportation routes and emergency services following an earthquake. Notice that for earthquakes near magnitude 8.0 a high level of allowable damage is proposed for all distances up to about 50 km. This reflects the difficulty and impracticality of limiting damage of moderately important bridges subject to massive, extremely rare events, even at considerable distances from causative faults. Similarly, a fairly high level of damage is allowed for moderate magnitude earthquakes at small distances, up to about 30 km. Very low levels of damage are permitted for low magnitude earthquakes at moderate-to-large distances.
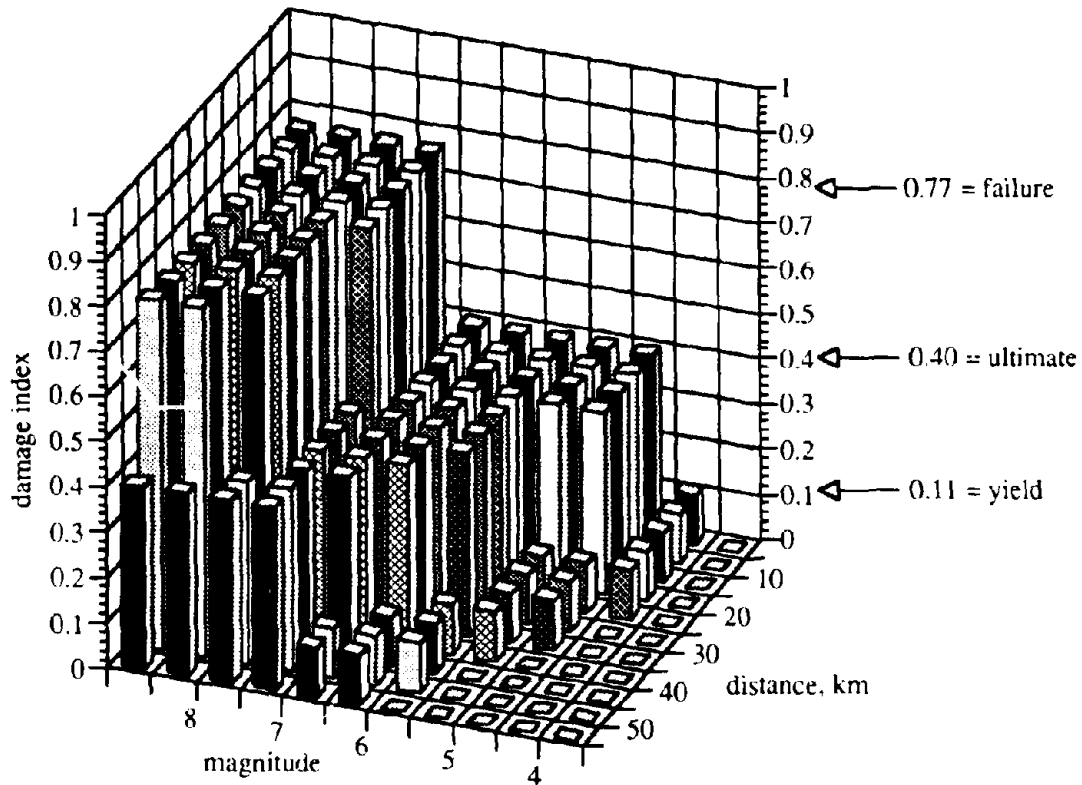
Figure 6.1. Estimated acceptable damage indices, as functions of magnitude and distance, for bridge piers deemed moderately important to seismic lifelines.

Figure 6.2 shows a matrix of proposed allowable damage indices for piers in bridges which are highly important to seismic lifelines. High levels of damage are acceptable only for very large events at small distances, and the allowable damage index decreases rapidly as distance increases and magnitude decreases. This would permit most important lifeline bridges – except those very close to the causative fault – to remain in limited operation following a major earthquake. At moderate-to-small magnitudes and moderate-to-large distances little or no damage is allowed. since under those conditions important lifeline bridges should remain completely serviceable.

Figure 6.2. Estimated acceptable damage indices, as functions of magnitude and distance, for bridge piers deemed highly important to seismic lifelines.

The process outlined above can be extended another step by fitting smooth, three-dimensional surfaces to the discrete values shown in the bar charts of figures 6.1 and 6.2. In this way acceptable damage levels for moderately important and highly important bridge piers can be expressed as simple, continuous functions of magnitude and distance. Continuous functions have the advantage of being easily usable by design engineers, and, unlike tables of discrete values, continuous functions provide unambiguous values of acceptable damage at any magnitude and distance. A simple surface with a shape appropriate to the data of figures 6.1 and 6.2 is a hyperbolic trumpet, which has an equation of the form

$$D.I. = \frac{1}{\dfrac{D^2}{a} + \dfrac{(9-M)^2}{b}} - c$$

where
    D.I. =   damage index
    D =   distance, km
    M =   earthquake moment magnitude
    a,b,c =   coefficients

and
$$0 \leq D.I. \leq 0.77$$
$$5 \leq D \leq 50$$
$$5.0 \leq M \leq 8.0$$

The valid range of the surface is limited by the three conditions on damage index, distance, and magnitude, as shown above. The first condition reflects the fact that damage indices greater than the failure damage index, determined in this study as 0.77 for spirally reinforced bridge piers, are not possible. The second and third conditions are imposed by limitations on the ranges of distance and magnitude investigated in this study.

Figures 6.3 and 6.4 show surfaces which, in general, fit conservatively (that is, generally provide a lower bound to) the bar graphs of figures 6.1 and 6.2. These surfaces have equations of the form shown above. The equations of the curves in figures 6.3 and 6.4 were found by selecting three mathematical control points for each curve, which in turn were used to solve for the coefficients a, b and c. The control points used in this study are shown in table 6.1 below. Although some of the control point values are outside the normal ranges considered in design, they do serve to mathematically constrain the smoothed curves of figures 6.3 and 6.4 so that they generally form lower bounds to the bar graphs of figures 6.1 and 6.2, over practical ranges of magnitude and distance (5 km ≤ distance ≤ 50 km and 5.0 ≤ magnitude ≤ 8.0).

Table 6.1. Control points used to solve for curves of figures 6.3 and 6.4

	Magnitude	Distance	Damage Index
Structures of Moderate Importance to Seismic Lifelines (figure 6.1)			
Control Point 1	6.5	0	0.77
Control Point 2	9.0	65	0.40
Control Point 3	9.0	50	0.77
Structures of High Importance to Seismic Lifelines (figure 6.2)			
Control Point 1	7.0	0	0.4
Control Point 2	9.0	50	0.0
Control Point 3	4.0	0	0.0

The equation of the surface in figure 6.3, for moderately important bridge piers, is

$$D.I. = \frac{1}{\dfrac{D^2}{2300} + \dfrac{(9-M)^2}{5.7}} - 0.14$$

where   D.I. =   damage index
         D =   distance, km
         M =   earthquake moment magnitude
         a,b,c =   coefficients

and $0 \leq D.I. \leq 0.77$
         $5 \leq D \leq 50$
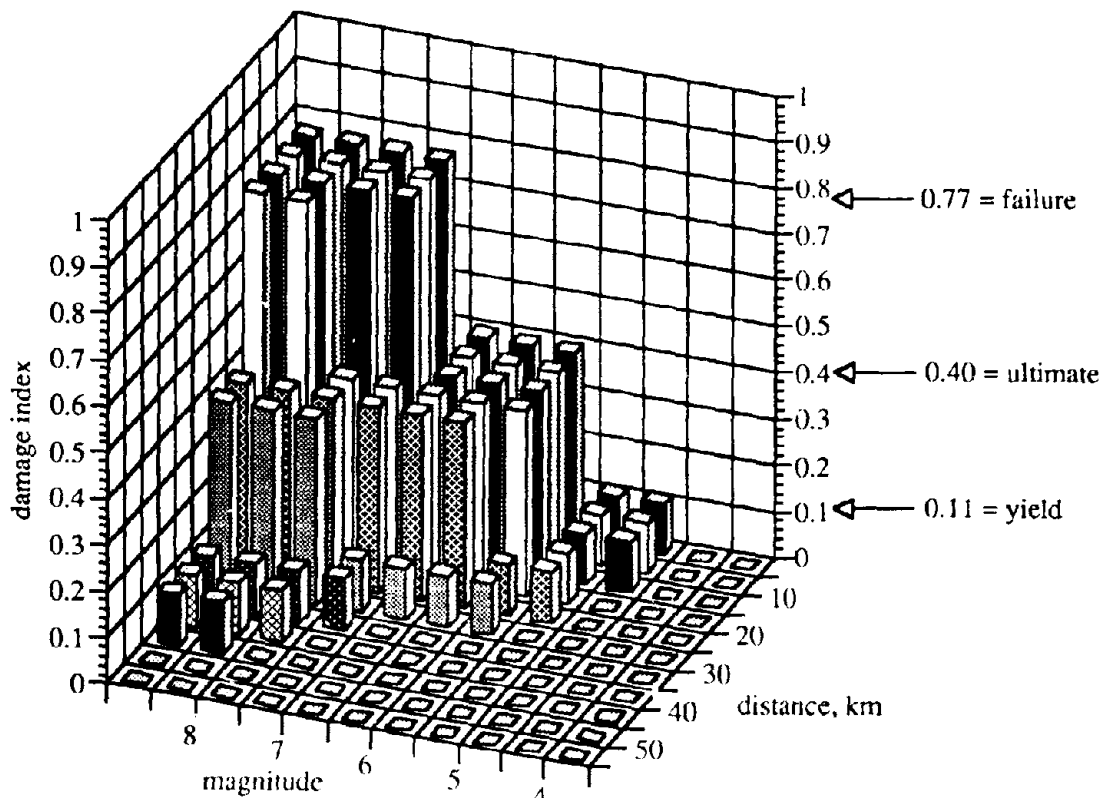 $5.0 \leq M \leq 8.0$
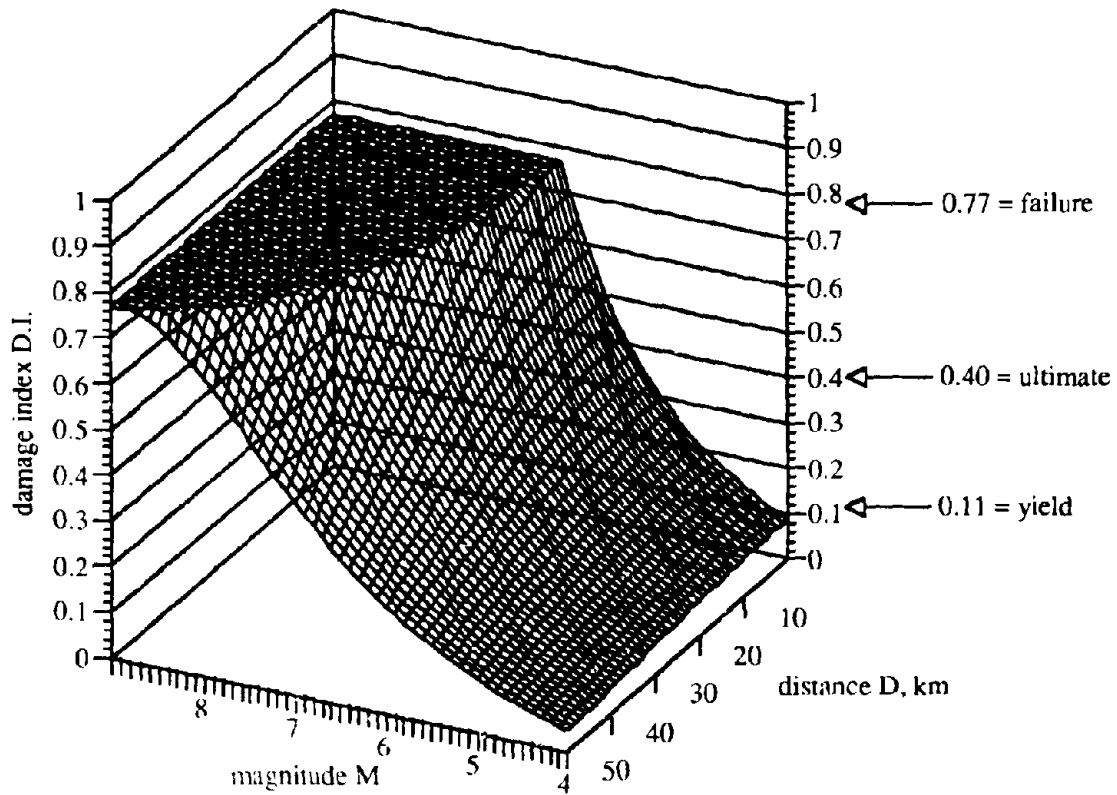
Figure 6.3. Proposed envelope for acceptable damage index, as a function of magnitude and distance, for bridge piers deemed moderately important to seismic lifelines.

The equation for the surface in figure 6.4, for highly important bridge piers, is

$$D.I. = \frac{1}{\dfrac{D^2}{190} + \dfrac{(9-M)^2}{1.9}} - 0.08$$

$0 \le D.I. \le 0.77$
$5 \le D \le 50$
$5.0 \le M \le 8.0$
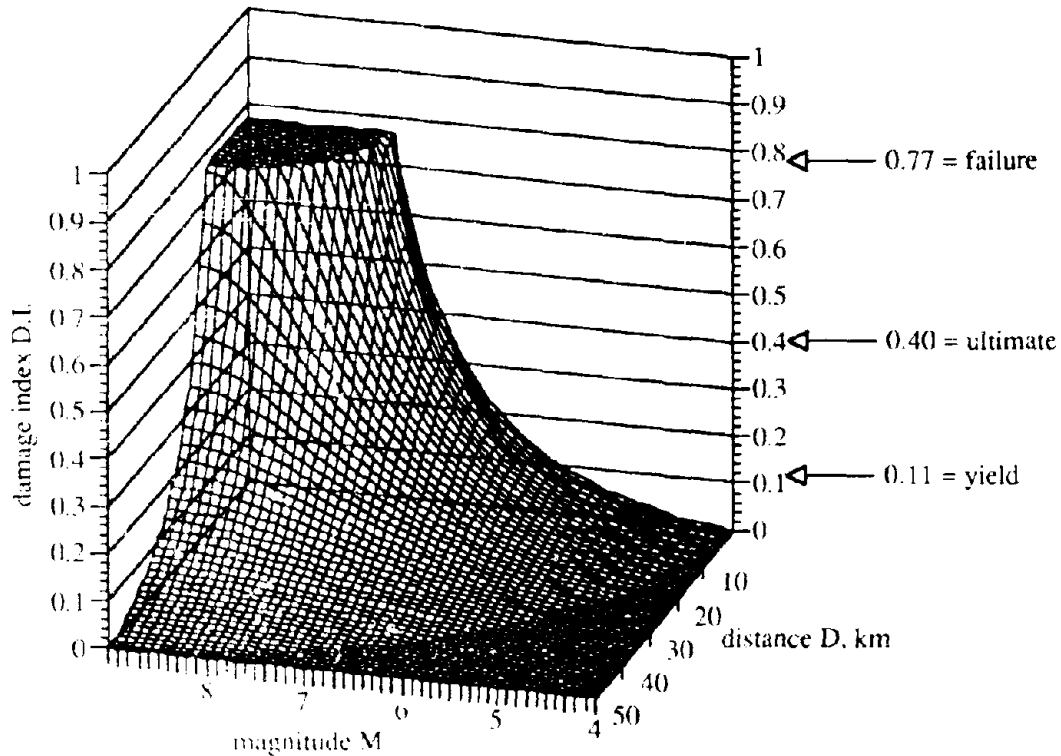
Figure 6.4. Proposed envelope for acceptable damage index, as a function of magnitude and distance, for bridge piers deemed highly important to seismic lifelines.

Further refinement of these acceptable damage level surfaces is possible, and other surfaces could be constructed for other types of members and structures and other levels of structural importance. The presentation here of the steps followed in deriving these surfaces is intended as a demonstration of a rational procedure. Such a procedure could be followed by code-writing bodies, and by government agencies, to derive similar curves for the types of structures under their jurisdiction.

6.2. Summary of Critical State Failures for CALTRANS Columns

In Chapter 5 a series of example analyses of CALTRANS-designed 122 cm diameter spiral-reinforced bridge columns was described. In this section the results of those analyses are presented, and the performance of the CALTRANS designs, as compared with the proposed acceptable damage index functions derived in Section 6.1, is discussed.

59

6.2.1. Damage Index as a Function of Magnitude and Epicentral Distance

Below, 24 plots are presented showing calculated damage indices for the example CALTRANS-designed columns as a function of magnitude and distance. Twelve plots are for the example CALTRANS designs situated on bedrock, and twelve are for the example CALTRANS design situated on 37 m of sand overlying bedrock. Also shown, by heavy lines on each plot, are the proposed acceptable damage level curves for bridges which are moderately (upper curve) and highly important (lower curve) to seismic lifelines. (These curves may be visualized as "slices" through the three-dimensional plots of figures 6.3 and 6.4, parallel to the Magnitude axis). Horizontal shaded bands on each plot show stages of degradation of the column, determined from analyses of experimental data, as described in Chapter 4. Each plot presents results for a single soil condition (bedrock or 37 m sand overburden), a single distance from the causative fault (10 km, 20 km, 30 km, or 40 km), a single axial load level (5%, 10%, or 15%) and three L/D ratios (3.0, 6.0, and 9.0).

Due to limitations on the scope of this study, the plots shown are only representative of a much larger set of design charts which could in principle be derived. Such a set of charts would allow the design engineer to estimate, in advance of or following an earthquake, the level of damage a particular column design suffers when subjected to a specific magnitude earthquake at a specific distance. This estimate of damage could then be compared with specified acceptable damage levels, such as the suggested curves shown by heavy lines in each plot.

It is important to note that only those column performance curves that fall entirely beneath a particular acceptable damage curve, up to the maximum credible earthquake magnitude for the region, are considered to have met the requirements of the proposed acceptable damage provisions. If the actual column performance curve rises above the acceptable damage curve at a magnitude less than the maximum credible earthquake for the region, then retrofitting should be considered. For example, referring to figure 6.9, the design with L/D = 9.0 would be unacceptable in much of the Western U.S., but might be acceptable in parts of the Central United States and Eastern United States, where in many localities maximum credible earthquake magnitudes are less than 7.0.
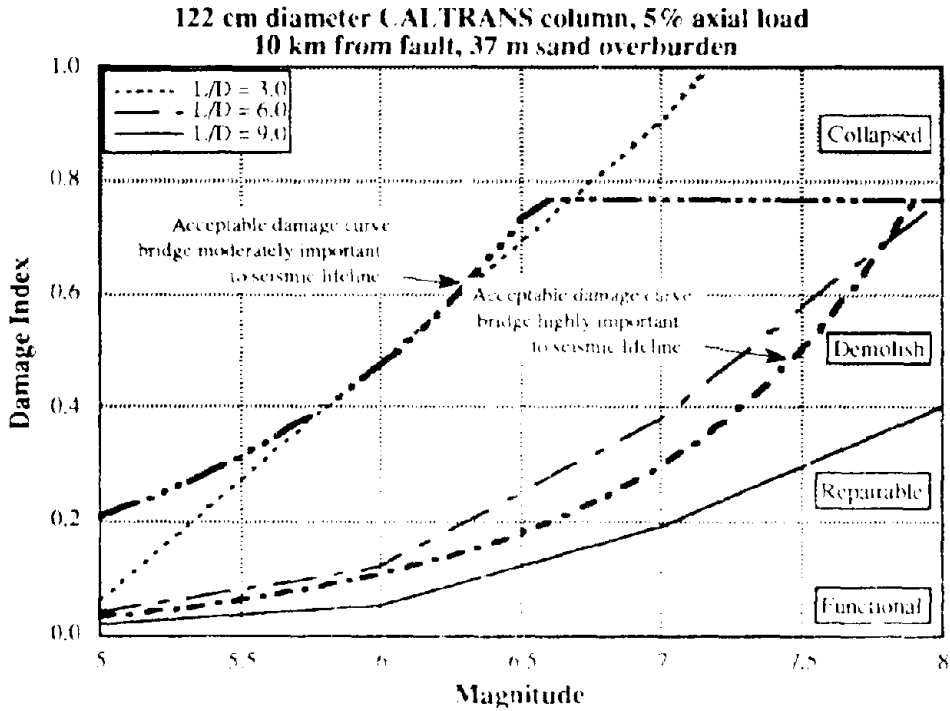
Figure 6.5. Damage index 122 cm dia., 10 km, 37 m sand, 5% axial load.
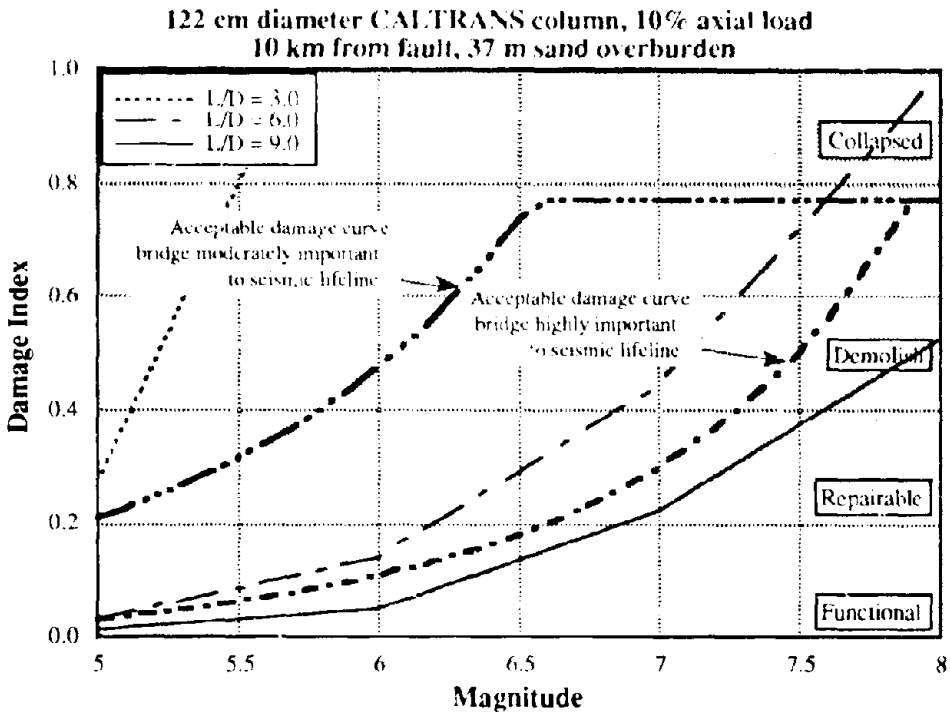
Figure 6.6. Damage index 122 cm dia., 10 km, 37 m sand, 10% axial load.

122 cm diameter CALTRANS column, 15% axial load
10 km from fault, 37 m sand overburden

Figure 6.7. Damage index 122 cm dia., 10 km, 37 m sand

122 cm diameter CALTRANS column, 5% axial load
20 km from fault, 37 m sand overburden, 0

Figure 6.8. Damage index 122 cm dia., 20 km, 37 m sand

122 cm diameter CALTRANS column, 10% axial load
20 km from fault, 37 m sand overburden

Figure 6.9. Damage index 122 cm dia., 20 km, 37 m sand, 10% axial load.

122 cm diameter CALTRANS column, 15% axial load
20 km from fault, 37 m sand overburden

Figure 6.10. Damage index 122 cm dia., 20 km, 37 m sand, 15% axial load.

122 cm diameter CALTRANS column, 5% axial load
30 km from fault, 37 m sand overburden

Figure 6.11. Damage index 122 cm dia., 30 km, 37 m sand, 5% axial load.

122 cm diameter CALTRANS column, 10% axial load
30 km from fault, 37 m sand overburden

Figure 6.12. Damage index 122 cm dia., 30 km, 37 m sand, 10% axial load.

122 cm diameter CALTRANS column, 15% axial load
30 km from fault, 37 m sand overburden

Figure 6.13. Damage index 122 cm dia., 30 km, 37 m sand, 15% axial load.

122 cm diameter CALTRANS column, 5% axial load
40 km from fault, 37 m sand overburden

Figure 6.14. Damage index 122 cm dia., 40 km, 37 m sand, 5% axial load.

**122 cm diameter CALTRANS column, 10% axial load
40 km from fault, 37 m sand overburden**
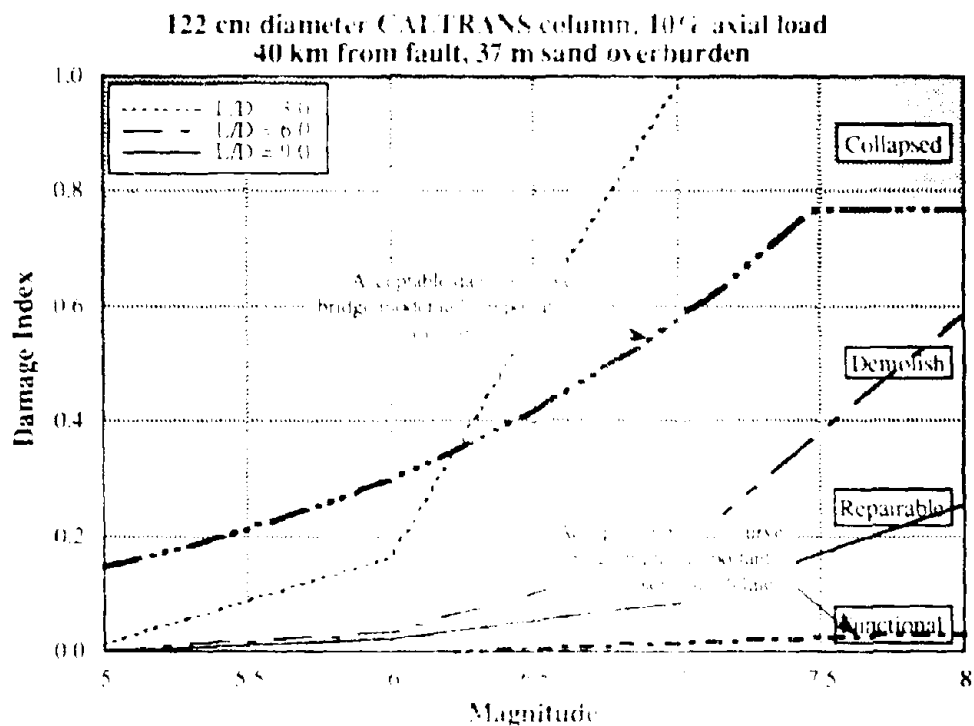
Figure 6.15. Damage index 122 cm dia., 40 km, 37 m sand, 10% axial load.

**122 cm diameter CALTRANS column, 15% axial load
40 km from fault, 37 m sand overburden**
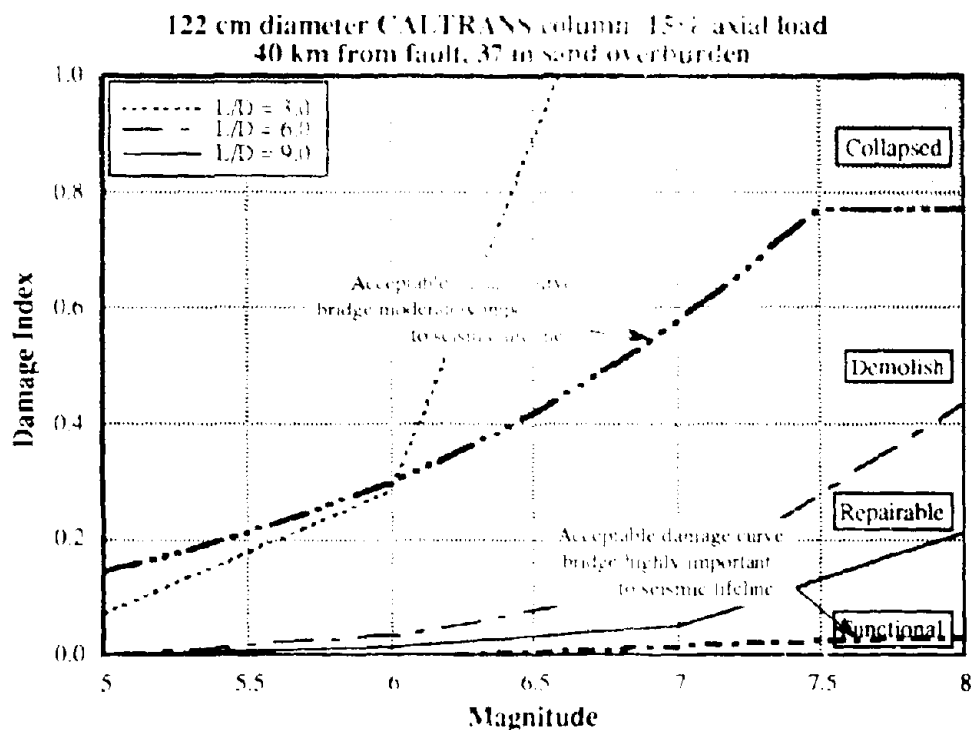
Figure 6.16. Damage index 122 cm dia., 40 km, 37 m sand, 15% axial load.

122 cm diameter CALTRANS column, 5% axial load
10 km from fault, on bedrock

Figure 6.17. Damage index 122 cm dia., 10 km, bedrock, 5% axial load.

122 cm diameter CALTRANS column, 10% axial load
10 km from fault, on bedrock

Figure 6.18. Damage index 122 cm dia., 10 km, bedrock, 10% axial load.
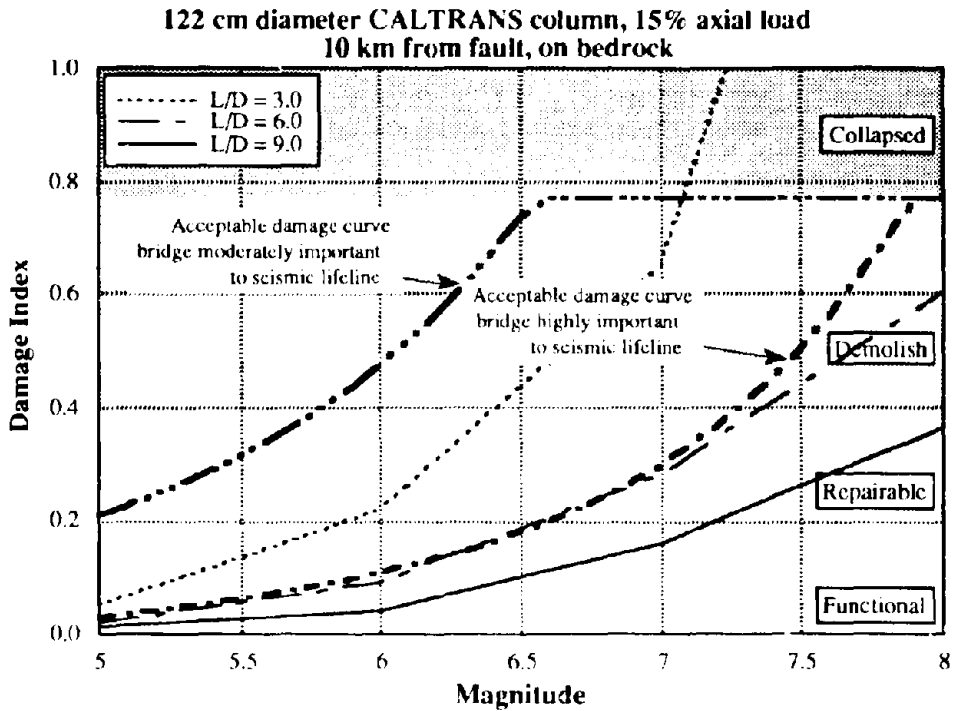
Figure 6.19. Damage index 122 cm dia.. 10 km, bedrock, 15% axial load.
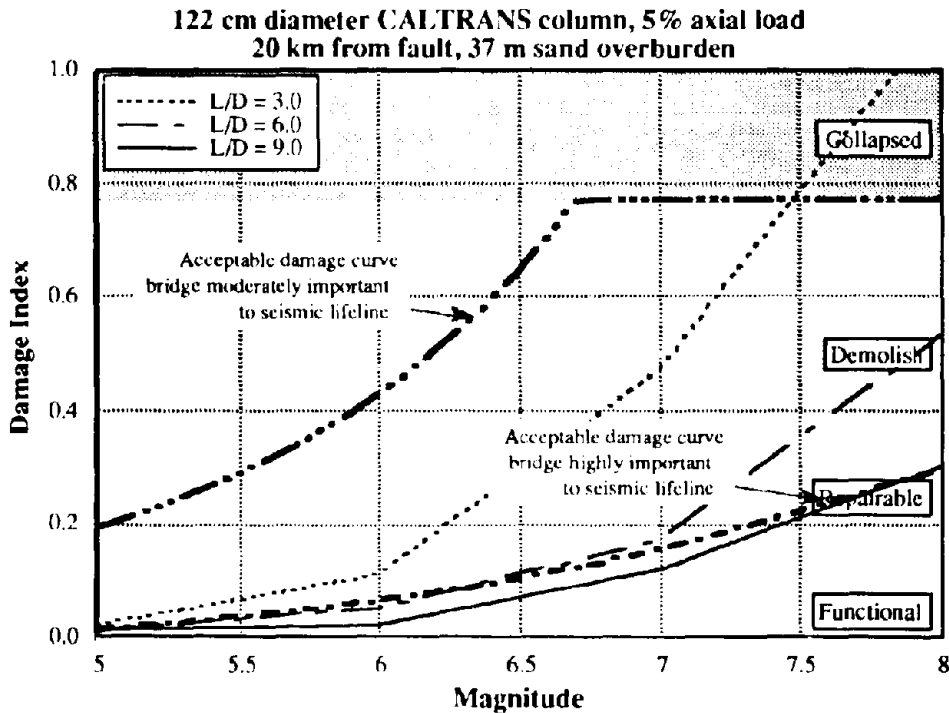
Figure 6.20. Damage index 122 cm dia.. 20 km, bedrock, 5% axial load.

122 cm diameter CALTRANS column, 10% axial load
20 km from fault, on bedrock
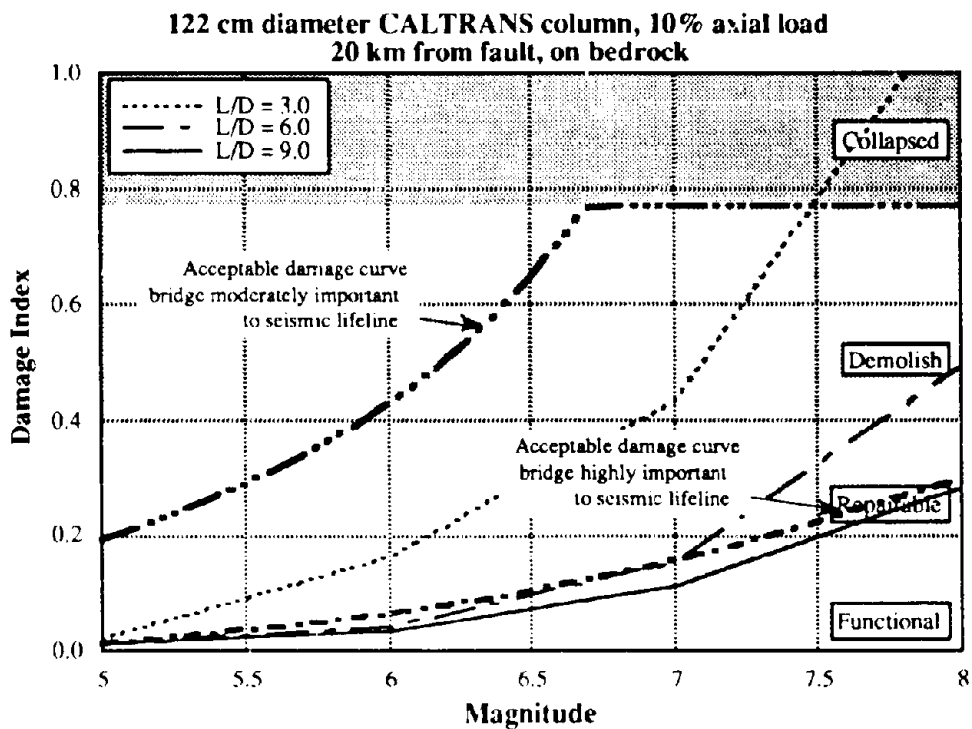
Figure 6.21. Damage index 122 cm dia., 20 km, bedrock, 10% axial load.

122 cm diameter CALTRANS column, 15% axial load
20 km from fault, on bedrock
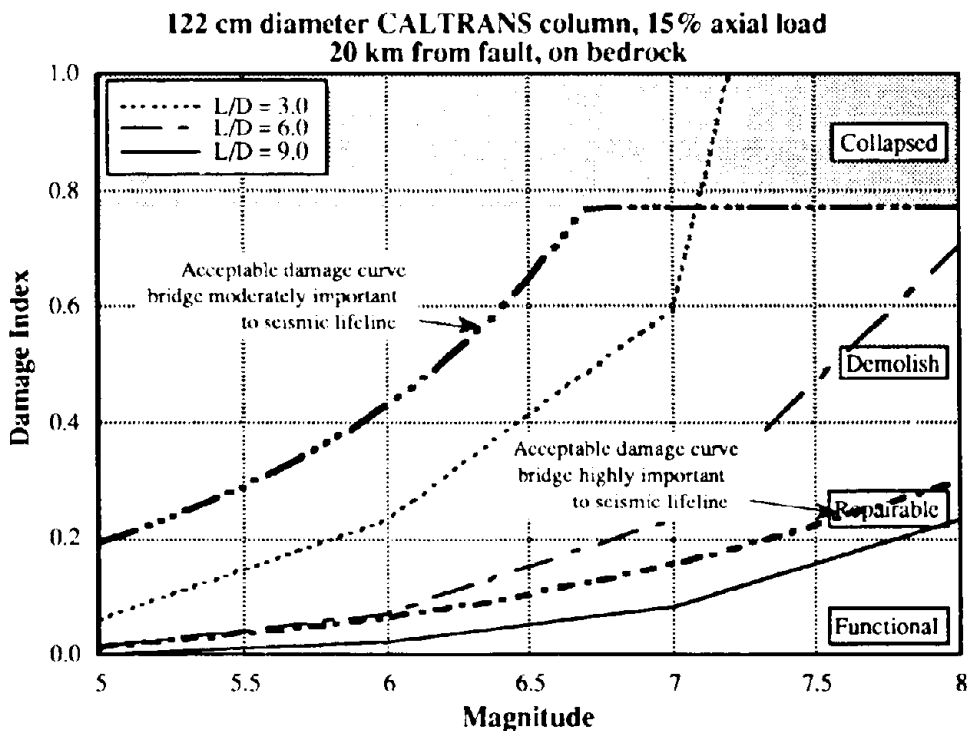
Figure 6.22. Damage index 122 cm dia., 20 km, bedrock, 15% axial load.

122 cm diameter CALTRANS column, 5% axial load
30 km from fault, on bedrock

L/D = 3.0
L/D = 6.0
L/D = 9.0

Collapsed

Acceptable damage curve
bridge moderately important
to seismic lifeline

Demolish

Repairable

Acceptable damage curve
bridge highly important
to seismic lifeline

Functional
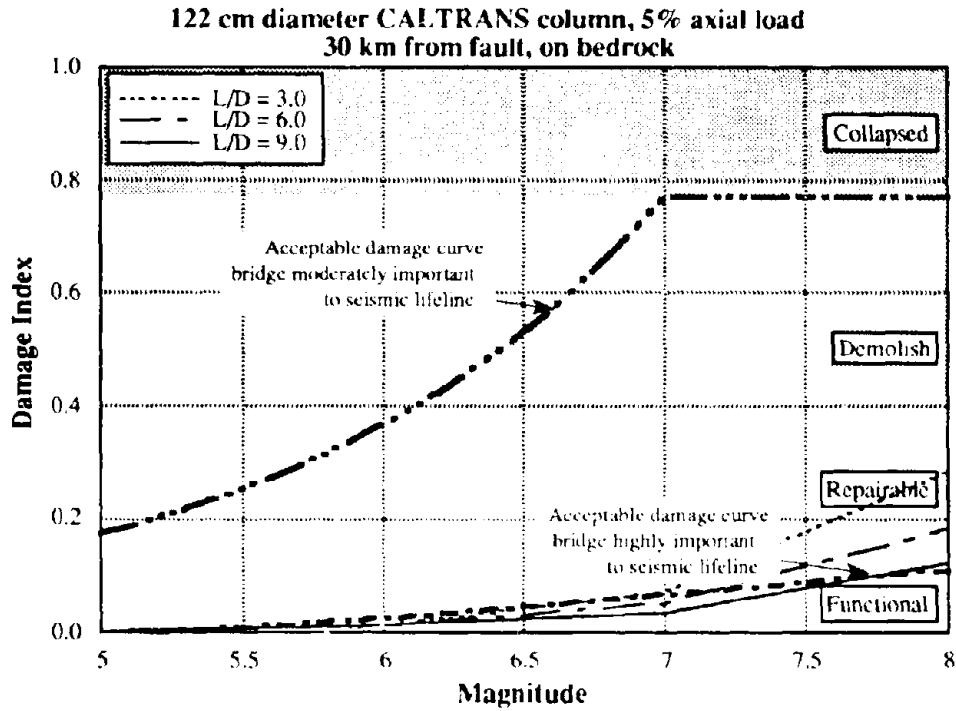
Figure 6.23. Damage index 122 cm dia., 30 km, bedrock, 5% axial load.

122 cm diameter CALTRANS column, 10% axial load
30 km from fault, on bedrock

L/D = 3.0
L/D = 6.0
L/D = 9.0

Collapsed

Acceptable damage curve
bridge moderately important
to seismic lifeline

Demolish

Repairable

Acceptable damage curve
bridge highly important
to seismic lifeline
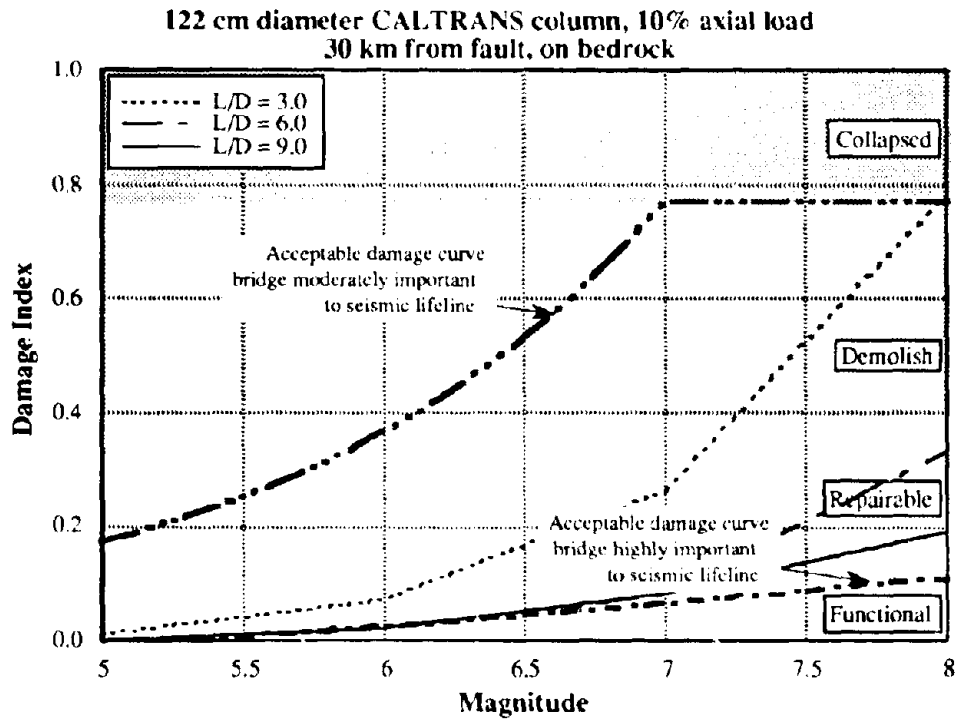
Functional

Figure 6.24. Damage index 122 cm dia., 30 km, bedrock, 10% axial load.

70

122 cm diameter CALTRANS column, 15% axial load
30 km from fault, on bedrock

Figure 6.25. Damage index 122 cm dia., 30 km, bedrock, 15% axial load.

122 cm diameter CALTRANS column, 5% axial load
40 km from fault, on bedrock
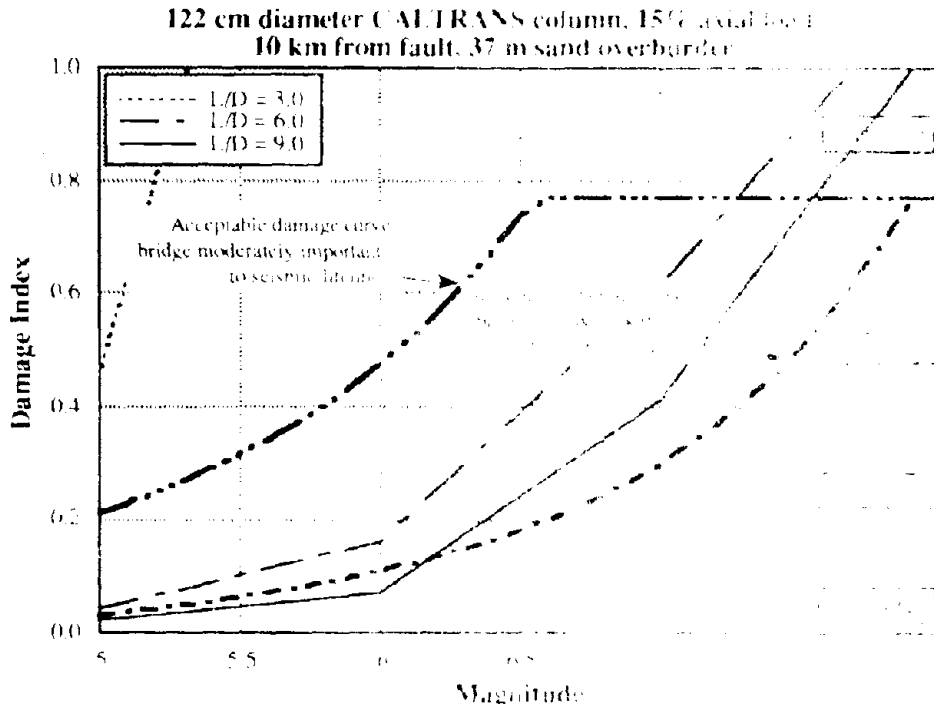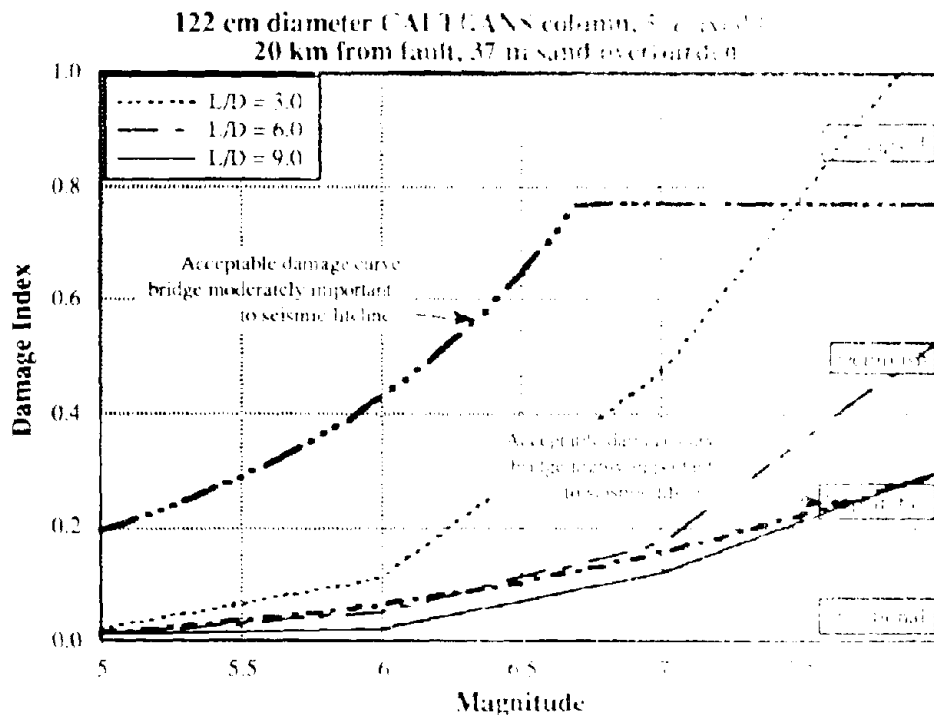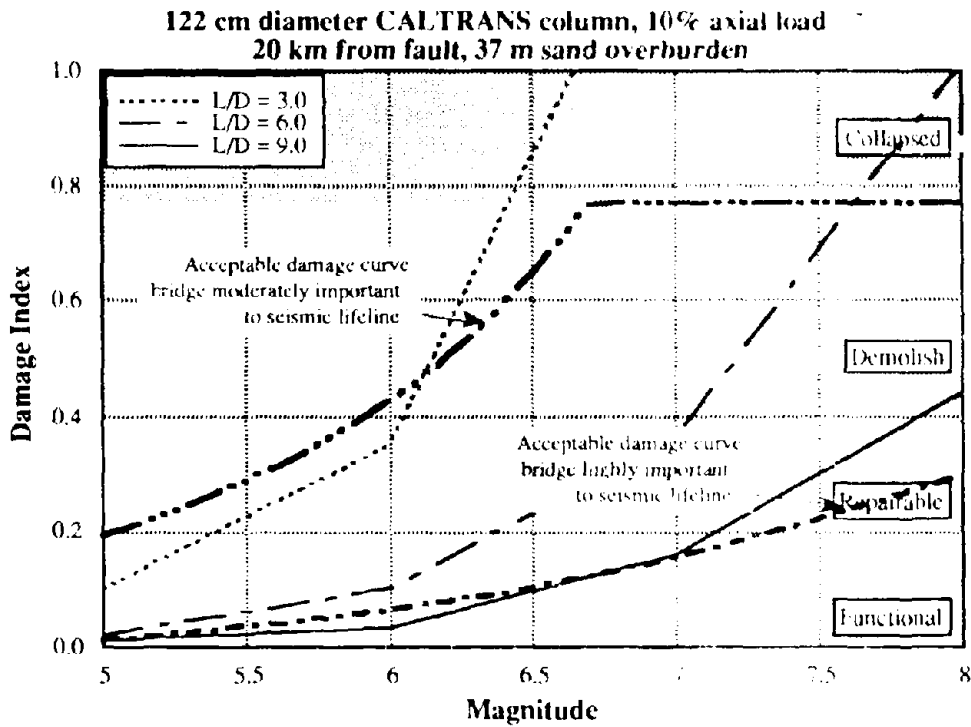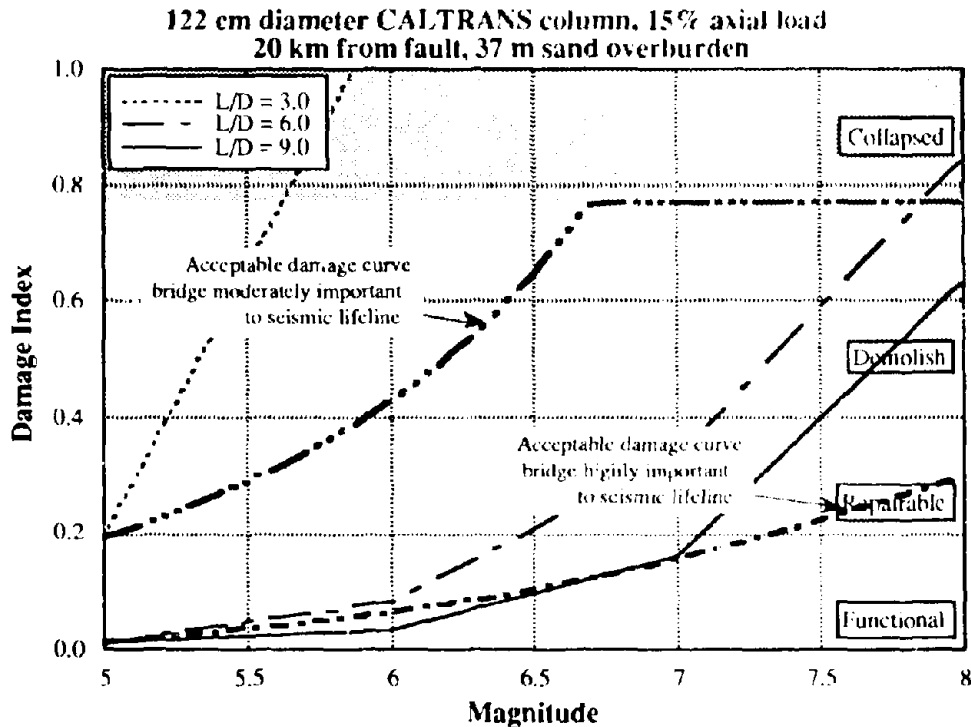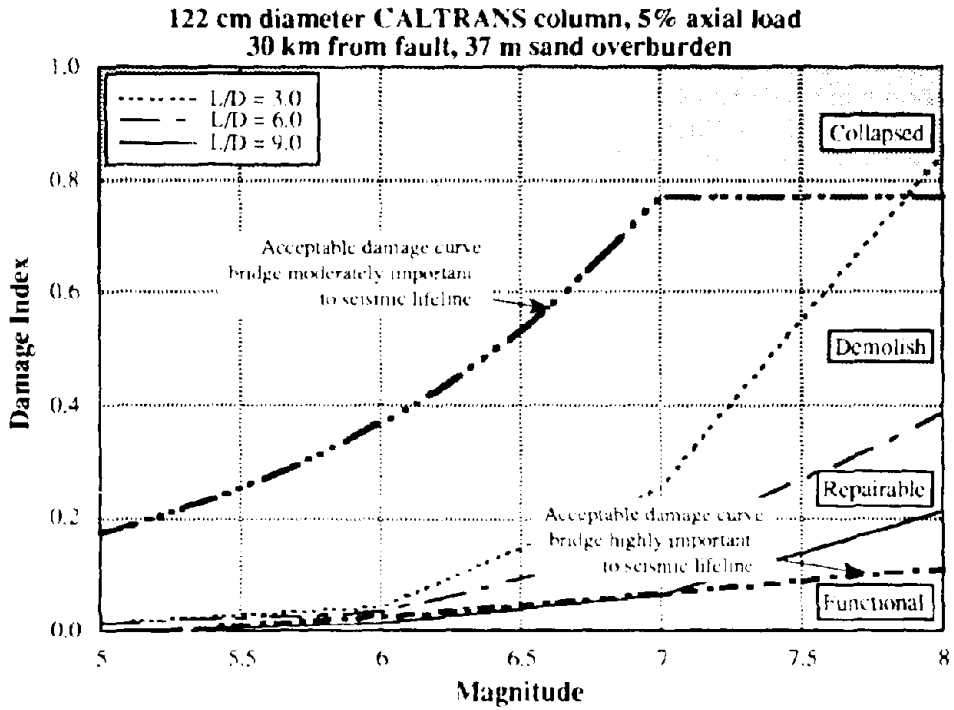
Figure 6.26. Damage index 122 cm dia., 40 km, bedrock, 5% axial load.

Figure 6.27. Damage index 122 cm dia., 40 km, bedrock, 10% axial load.

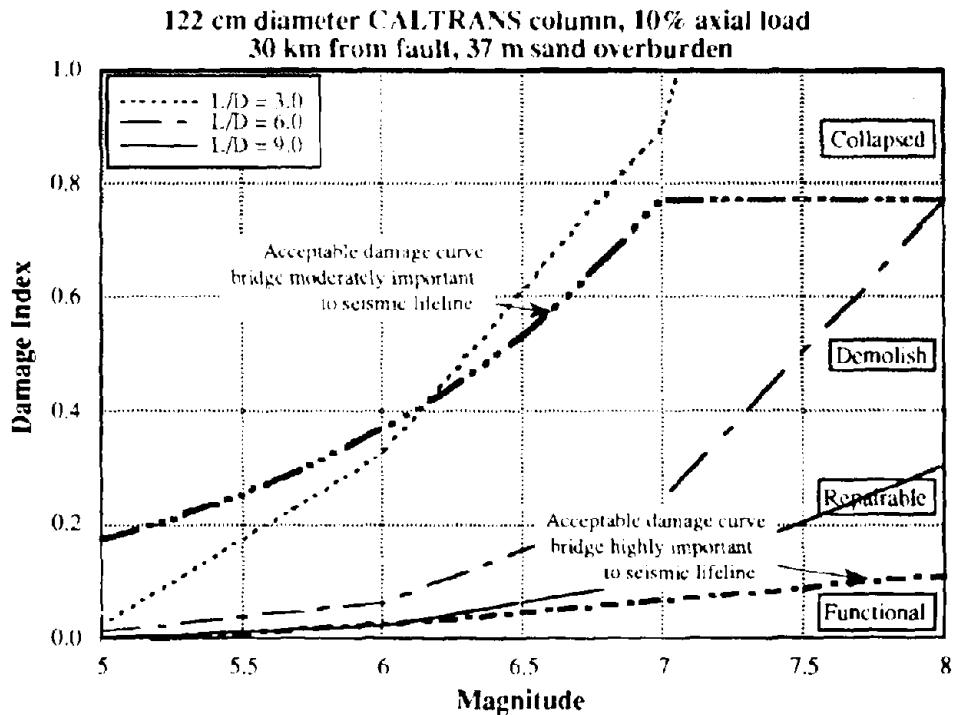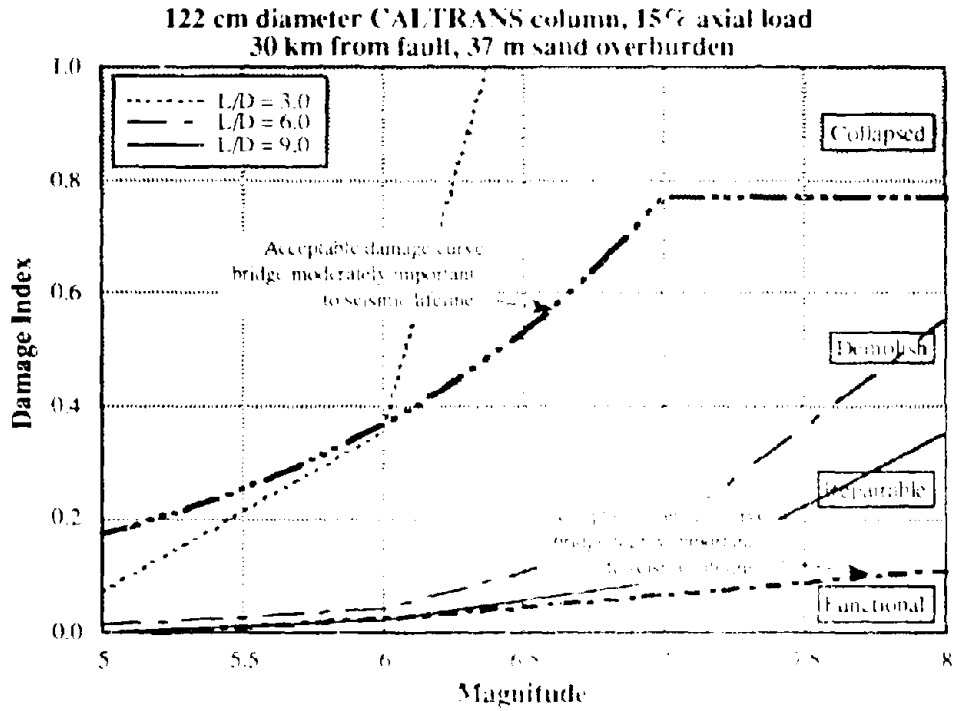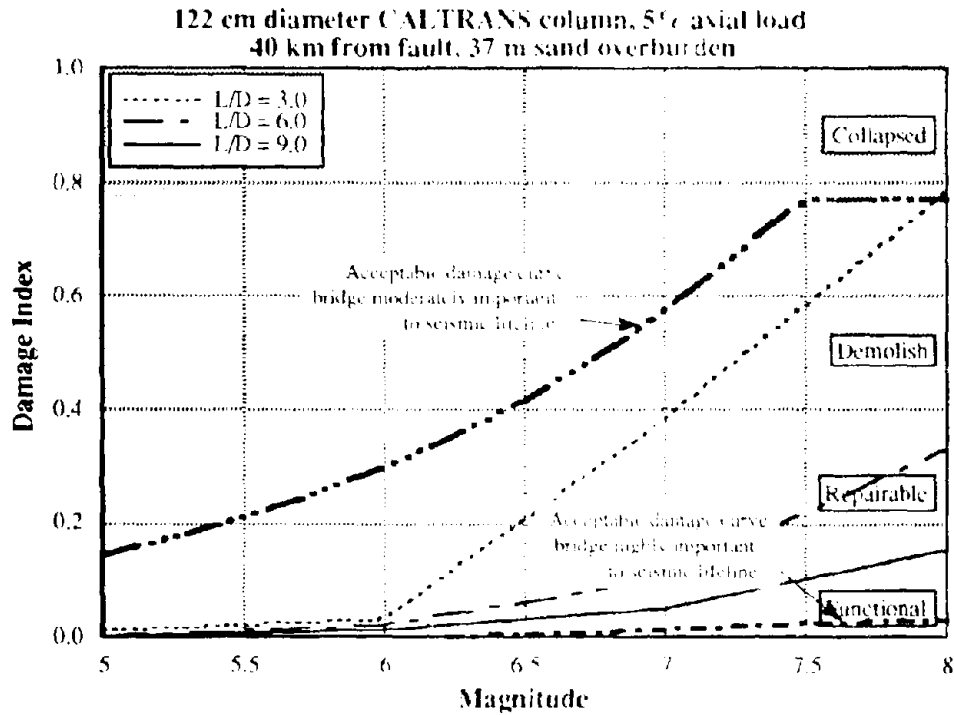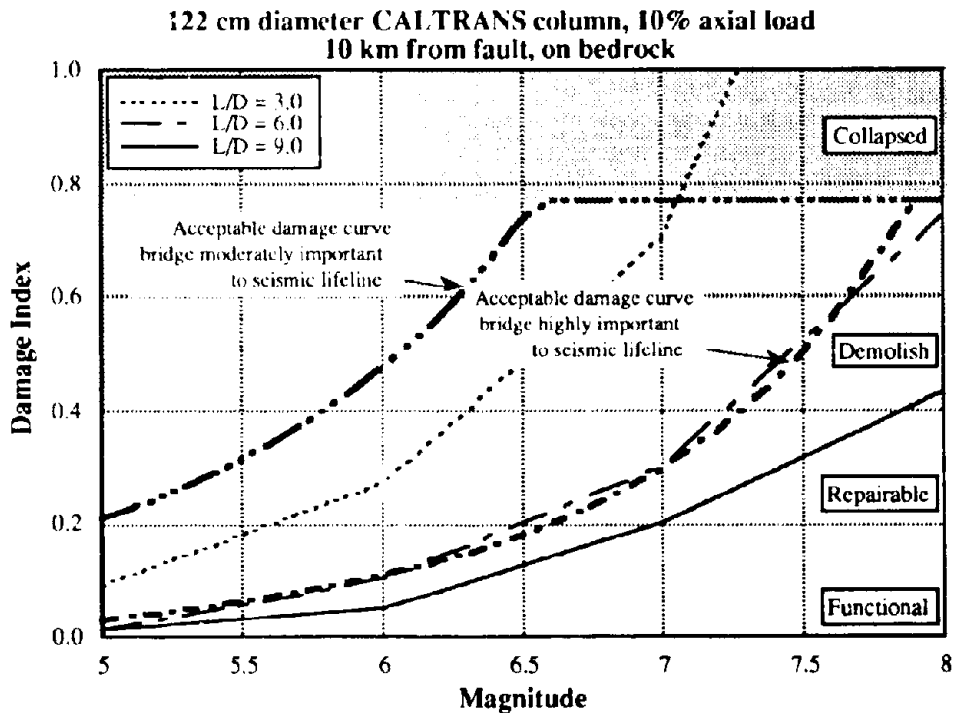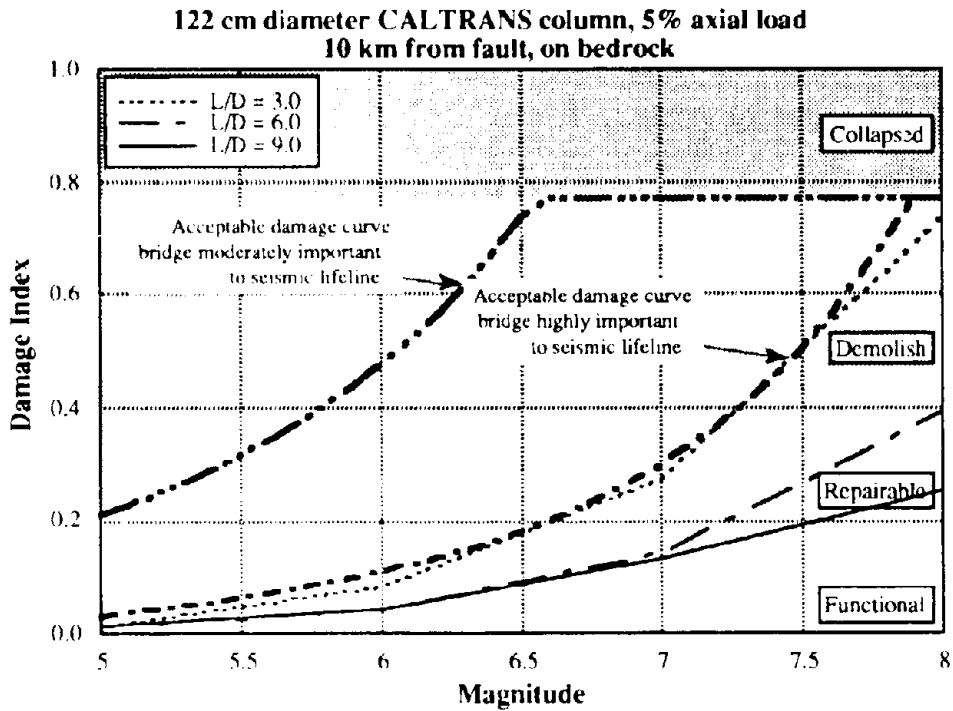Figure 6.28. Damage index 122 cm dia., 40 km, bedrock, 15% axial load.

6.2.2. Column Performance Charts

Below, 18 plots are presented which show three damage states for a particular column as a function of earthquake magnitude and distance. The three damage states shown are the onset of significant yielding of longitudinal reinforcement, the attainment of ultimate lateral load (moment) capacity, and the overall failure (collapse) of the column. The data for these plots was extracted from the figures of Section 6.2.1: each of the curves shown in Section 6.2.1 crosses the yield, ultimate and failure damage threshold states at certain values of earthquake magnitude, and these three values form one vertical row of data points in the figures below. Nine of the plots below are for the example CALTRANS-designed columns situated on bedrock, and the remaining nine are for the CALTRANS-designed columns situated on 37 m of sand overlying bedrock. Each plot shows data for a single axial load level (5%, 10%, or 15%) and a single L/D ratio (3.0, 6.0, or 9.0).

As with the plots in Section 6.2.1, the plots below are useful for evaluating the future performance of proposed designs, or for estimating the need for repair or retrofit of a particular column after a particular seismic event at a specific distance. While the plots below do not indicate specific values of damage index, they do illustrate clearly how a column is expected to perform in terms of laboratory-calibrated damage states. This type of plot is useful to the design engineer in giving an overall sense of the performance of a class of columns, and for suggesting changes in design parameters which will improve seismic performance. Examination of these plots leads to a number of observations, which are outlined below.

General Observations:

For a given magnitude, distance, σ_0 [where $\sigma_0 = P_e/(f'_c * A_g)$], and soil condition, **lower values of L/D result in greater damage.**

For a given magnitude, L/D ratio, σ_0, and soil condition, **smaller values of distance result in greater damage** (obviously).

For a given L/D ratio, σ_0, soil condition, and distance, **greater values of magnitude result in greater damage** (obviously).

For a given L/D ratio, distance, σ_0, and magnitude, **37 m of granular soil overburden results in greater damage than bedrock alone.** This supports the generally accepted hypothesis, as demonstrated by the performance of engineered structures during the 1985 Mexico City and the

1989 Loma Prieta Earthquakes, that soil amplification can occur in thick overburden deposits and will result in higher forces imparted to the structure.

For a given L/D ratio, distance, magnitude, and soil condition, **greater values of σ_0 result in greater damage.**

Specific Observations for Columns Founded on Bedrock:

a) At axial load levels of 5%, all columns analyzed performed acceptably, regardless of aspect ratio.

b) At axial load levels greater than 10% but less than 15%, columns with aspect ratios of three or less can be expected to suffer total failure under a magnitude 7.0 earthquake at 10 kilometers from the epicenter and for a magnitude 8.0 earthquake at 30 kilometers from the epicenter. Although results are not available in this study for axial load levels greater than 15% it seems clear that increases in this variable would lead to deteriorated column performance.

Specific Observations for Columns Founded on 37 m of Alluvium:

c) At axial load levels as low as 5%, failure of columns with aspect ratios of less than 3 is indicated for a magnitude 6.6 event at 10 kilometers and for a magnitude 8.0 event at 40 kilometers.

d) At axial load levels of 10%, total failure of columns with aspect ratios of less than 3 is indicated for a magnitude 5.5 event at 10 kilometers and for a magnitude 6.7 event at 40 kilometers. Total failure of columns with L/D ratios of 6 are indicated for a magnitude 7.5 event at less than 20 kilometers.

e) At axial load levels of 15%, total failure of columns with aspect ratios of less than 3 is indicated for a magnitude 5.3 event at 10 kilometers and for a magnitude 6.4 event at 40 kilometers. Total failure of columns with L/D = 6 is indicated for a magnitude 7.2 earthquake at 10 kilometers.

It may be gathered from the above discussion that short, stubby CALTRANS columns as well as columns carrying high axial loads are particularly susceptible to failure, despite what might be considered to be a significant amount of confining reinforcement (as compared with pre-1971 standards). In most cases only columns with axial loads of less than 10% and L/D ratios of at least 9 the acceptable damage criteria for important structures presented earlier in this chapter.

122 cm diameter CALTRANS column
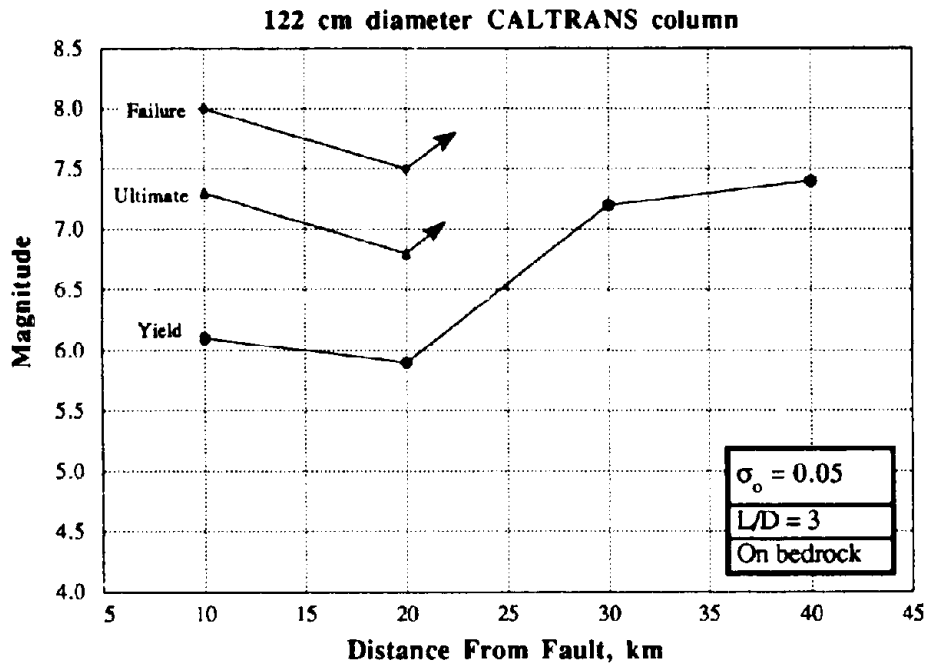
Figure 6.29. Damage states for 122 cm dia. column, $\sigma_o = 0.05$, L/D = 3, on bedrock.

122 cm diameter CALTRANS column
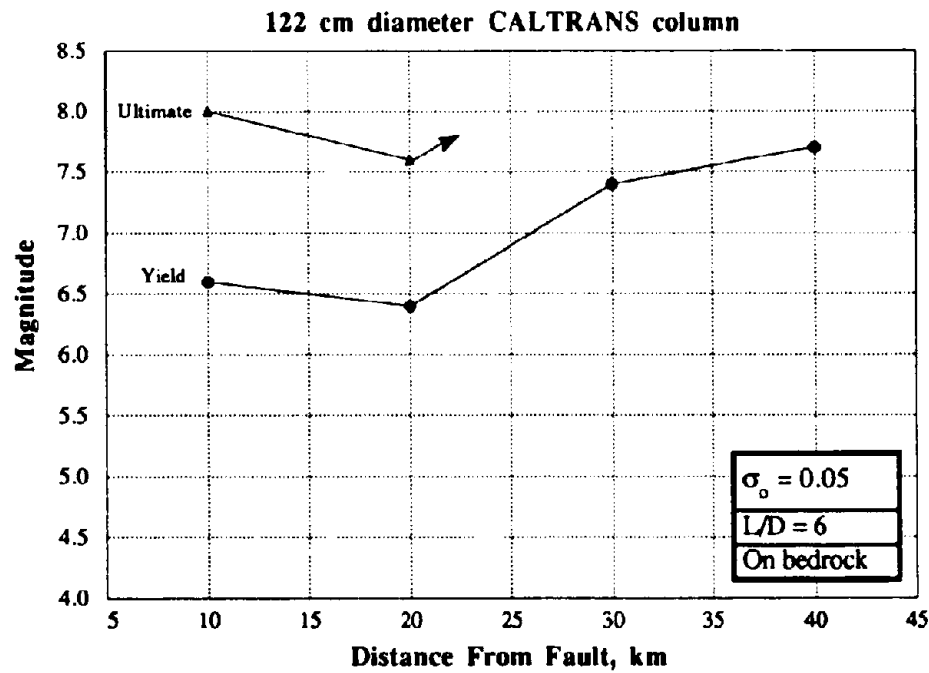
Figure 6.30. Damage states for 122 cm dia. column, $\sigma_o = 0.05$, L/D = 6, on bedrock.
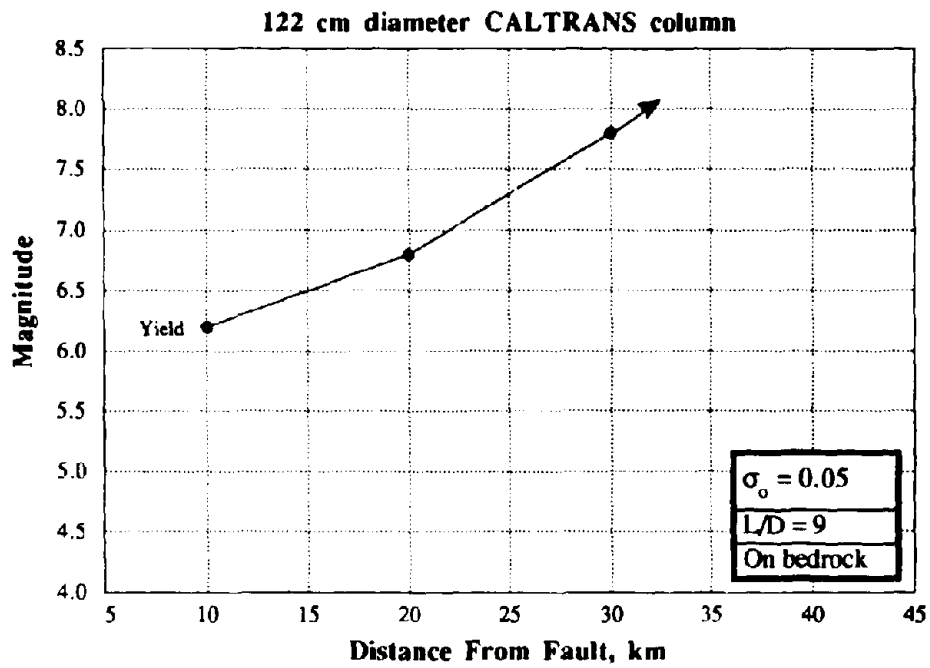
Figure 6.31. Damage states for 122 cm dia. column, σ_o = 0.05, L/D = 9, on bedrock..
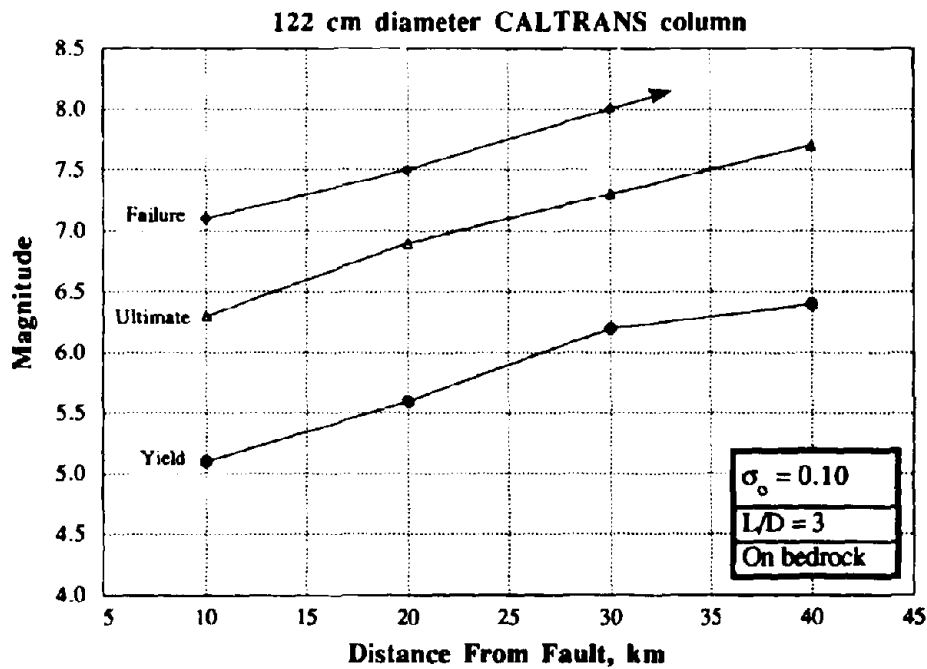
Figure 6.32. Damage states for 122 cm dia. column, σ_o = 0.10, L/D = 3, on bedrock.

122 cm diameter CALTRANS column
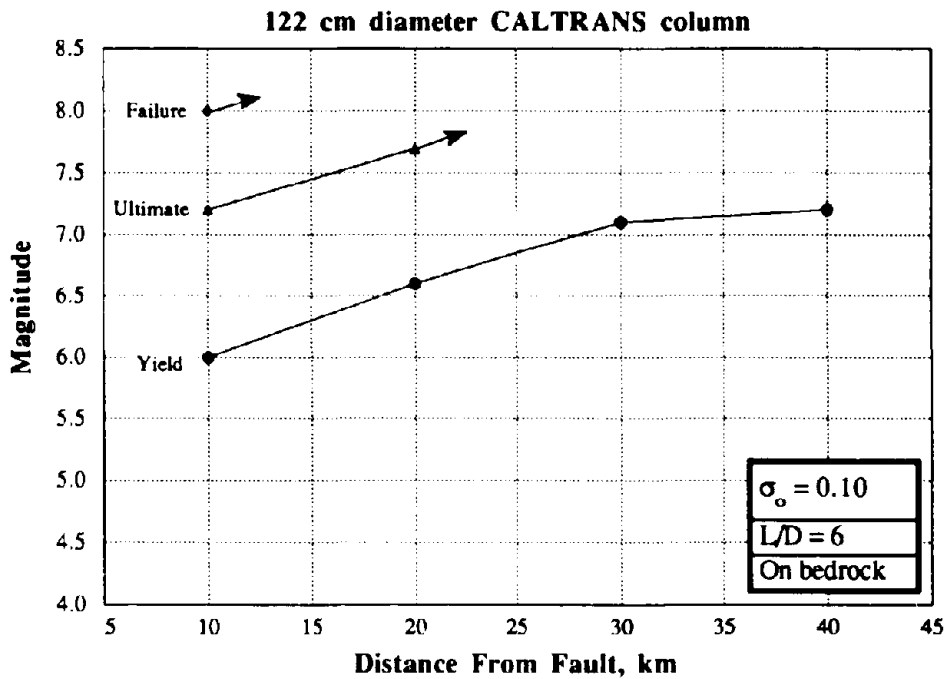
Figure 6.33. Damage states for 122 cm dia. column, σ_o = 0.10, L/D = 6, on bedrock.

122 cm diameter CALTRANS column
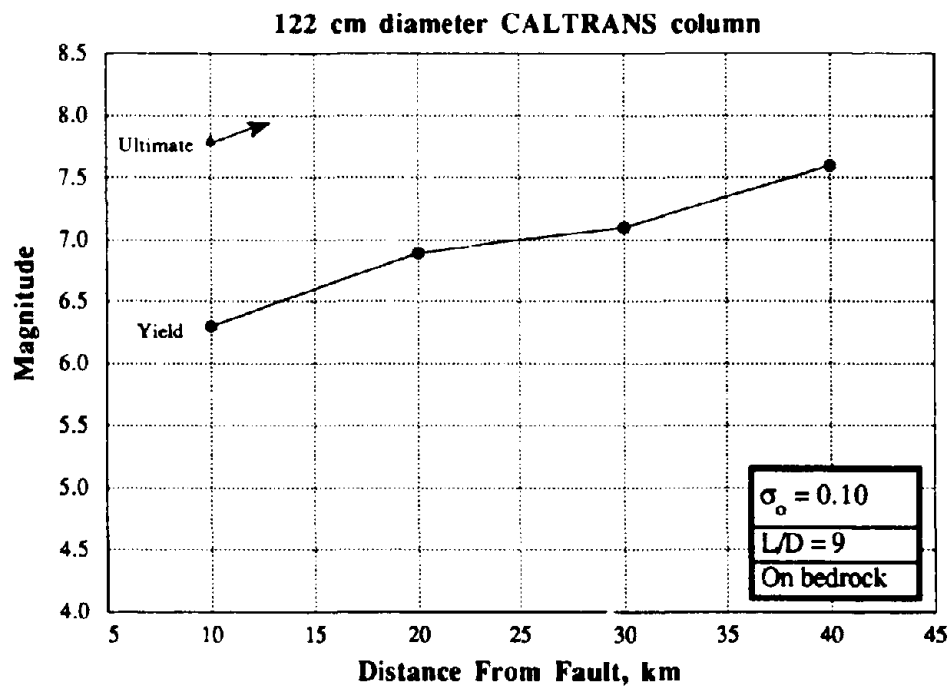
Figure 6.34. Damage states for 122 cm dia. column, σ_o = 0.10, L/D = 9, on bedrock.

122 cm diameter CALTRANS column

Failure

Ultimate

Yield

$\sigma_o = 0.15$
$L/D = 3$
On bedrock

Distance From Fault, km
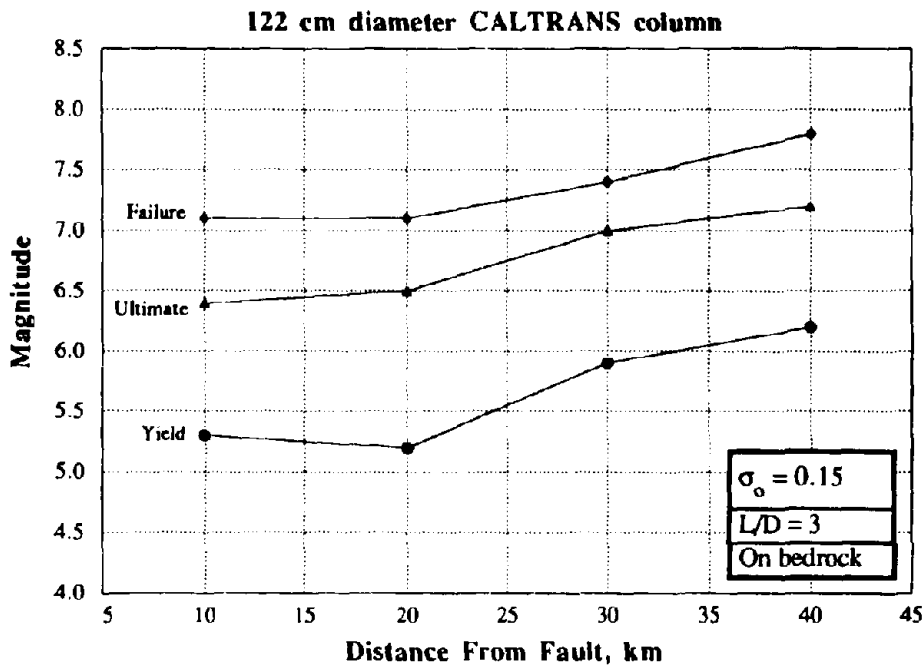
Figure 6.35. Damage states for 122 cm dia. column, $\sigma_o = 0.15$, $L/D = 3$, on bedrock.

122 cm diameter CALTRANS column

Ultimate

Yield

$\sigma_o = 0.15$
$L/D = 6$
On bedrock

Distance From Fault, km
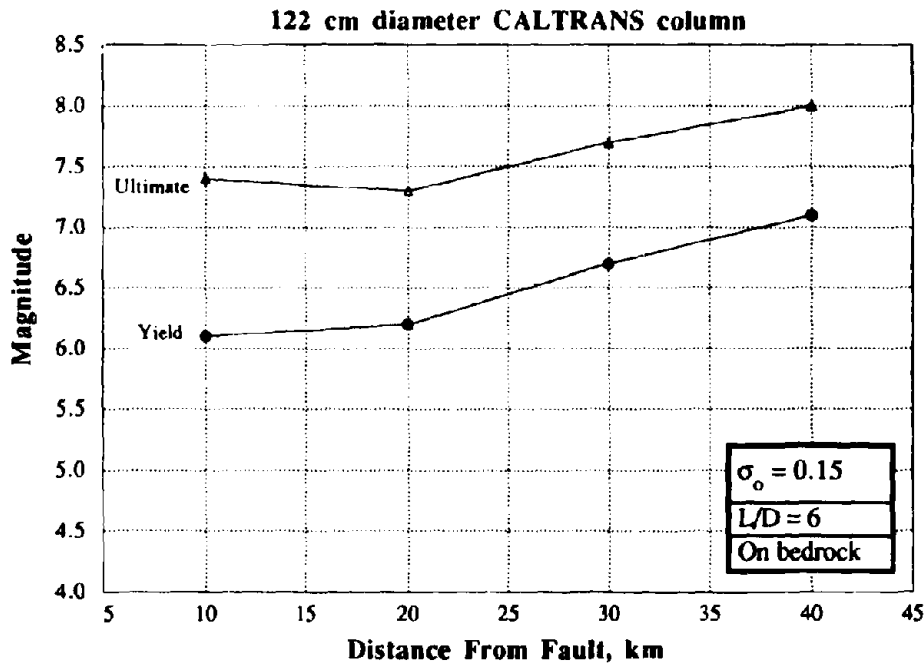
Figure 6.36. Damage states for 122 cm dia. column, $\sigma_o = 0.15$, $L/D = 6$, on bedrock.

122 cm diameter CALTRANS column
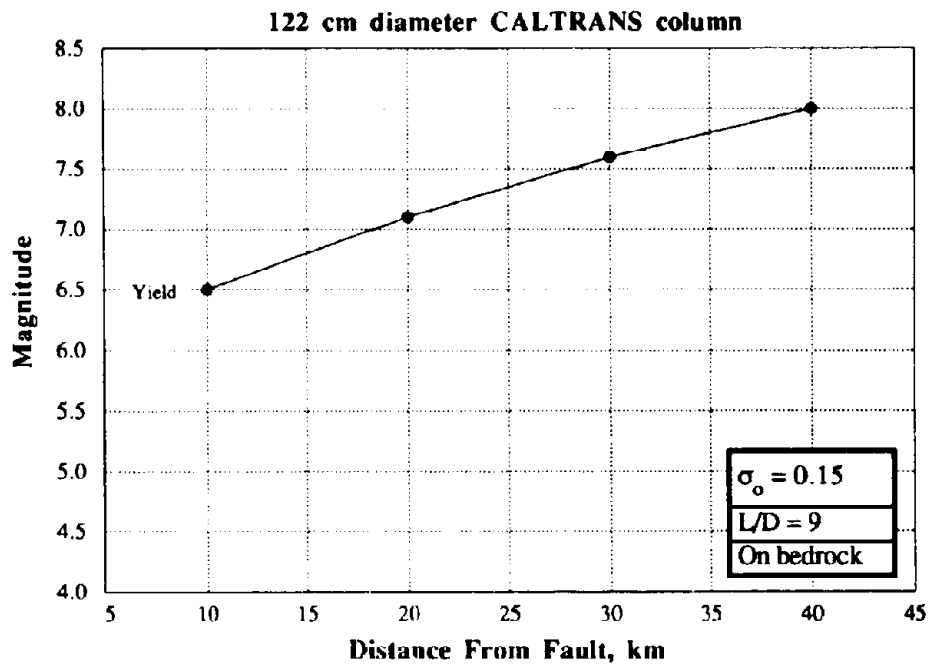
Figure 6.37.   Damage states for 122 cm dia. column, σ_o = 0.15, L/D = 9, on bedrock.

122 cm diameter CALTRANS column
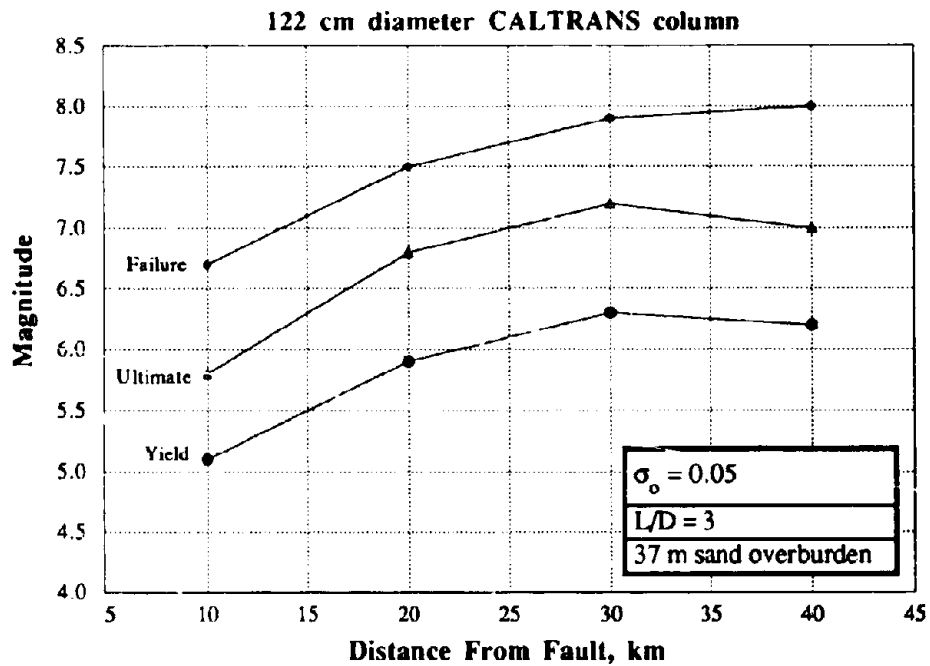
Figure 6.38.   Damage states for 122 cm dia. column, σ_o = 0.05, L/D = 3, on 37 m sand.
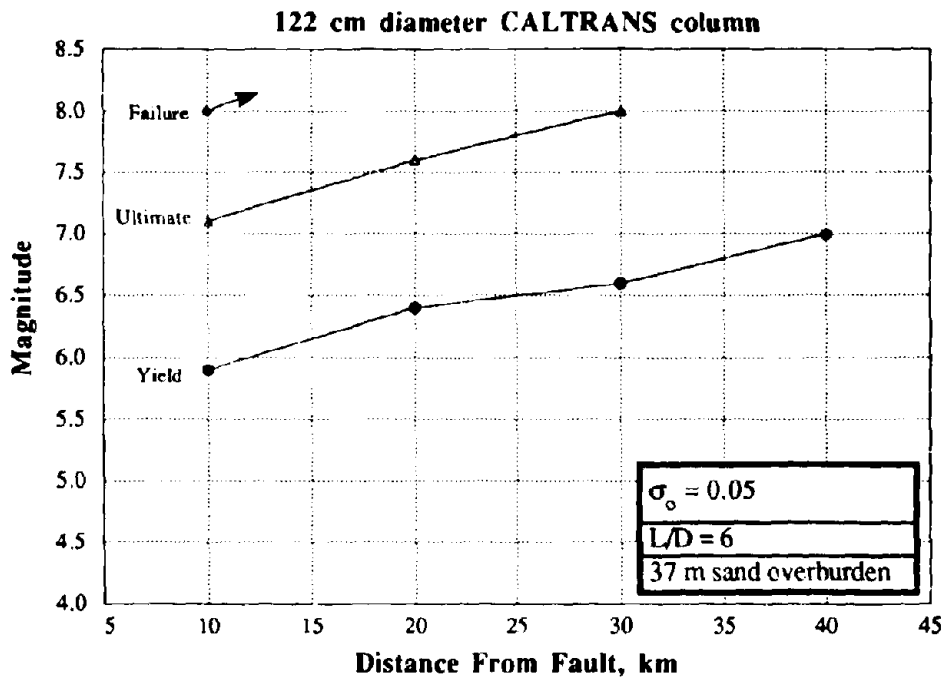
Figure 6.39. Damage states for 122 cm dia. column, σ_o = 0.05, L/D = 6, on 37 m sand.
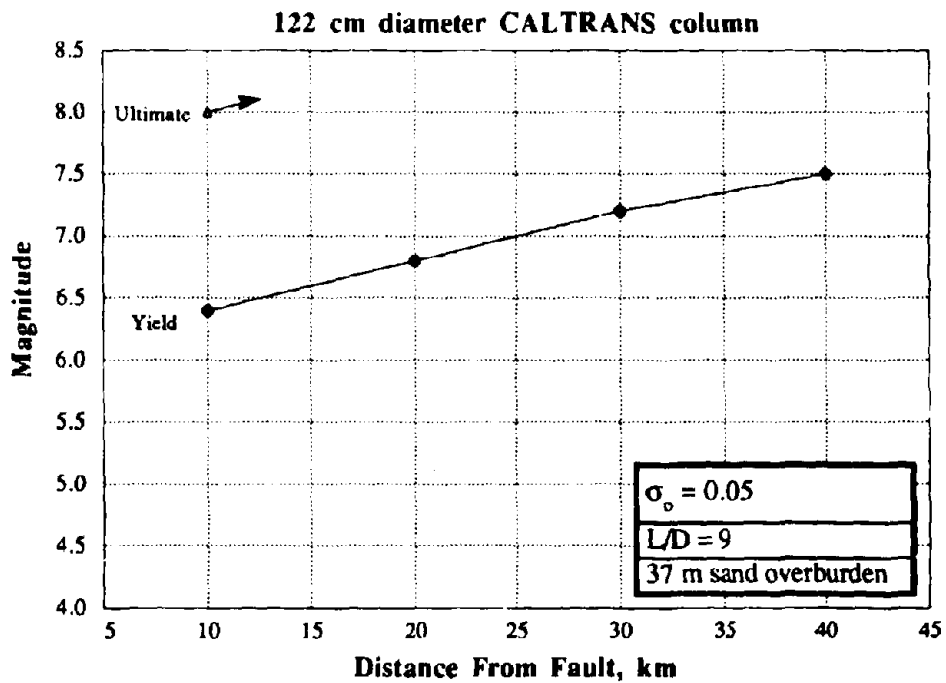
Figure 6.40. Damage states for 122 cm dia. column, σ_o = 0.05, L/D = 9, on 37 m sand.
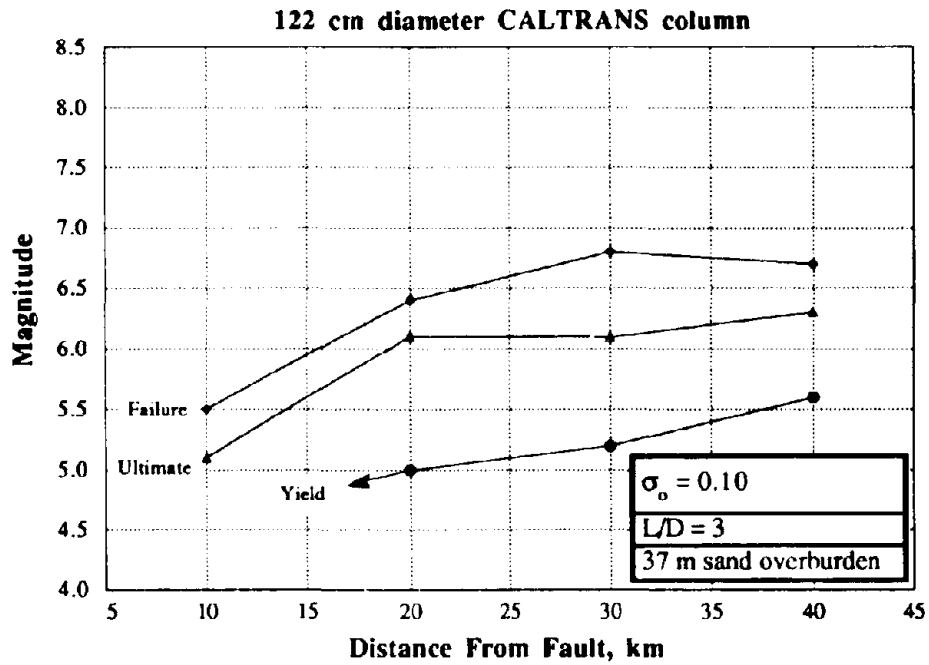
Figure 6.41. Damage states for 122 cm dia. column, σ_o = 0.10, L/D = 3, on 37 m sand.
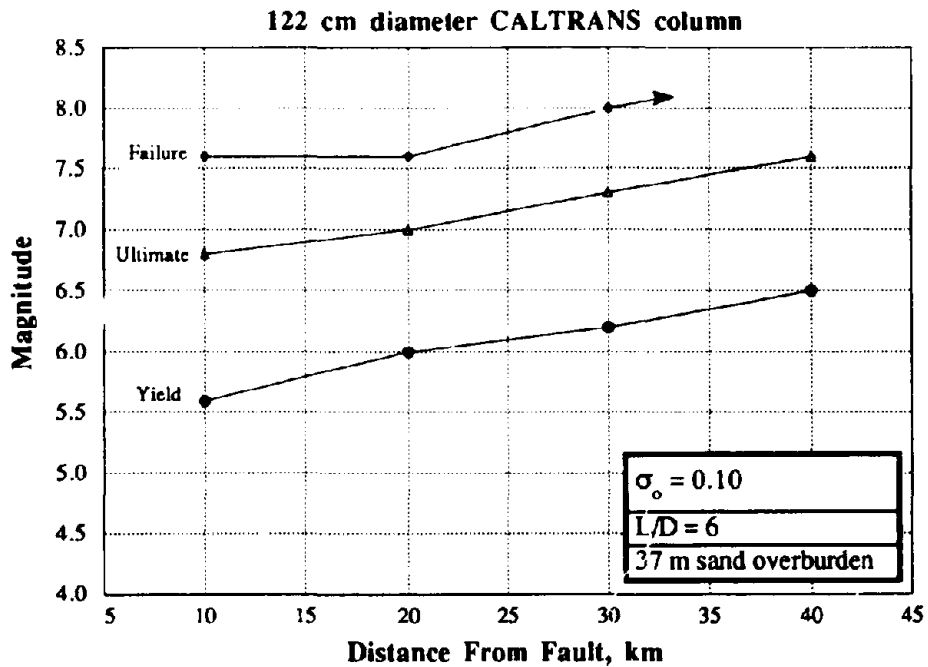
Figure 6.42. Damage states for 122 cm dia. column, σ_o = 0.10, L/D = 6, on 37 m sand.

122 cm diameter CALTRANS column
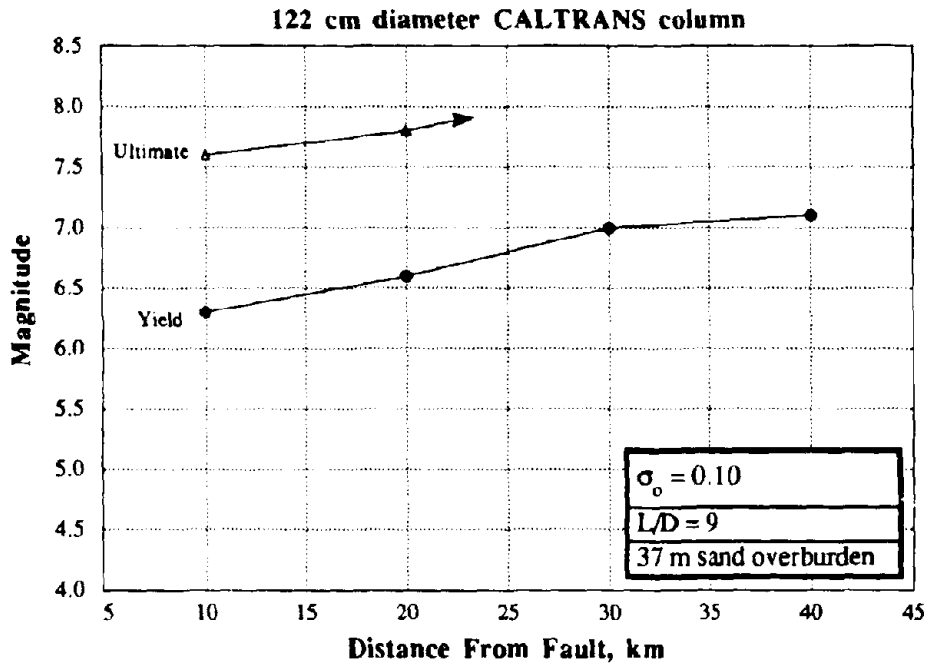
Figure 6.43. Damage states for 122 cm dia. column, σ_o = 0.10, L/D = 9, on 37 m sand.

122 cm diameter CALTRANS column
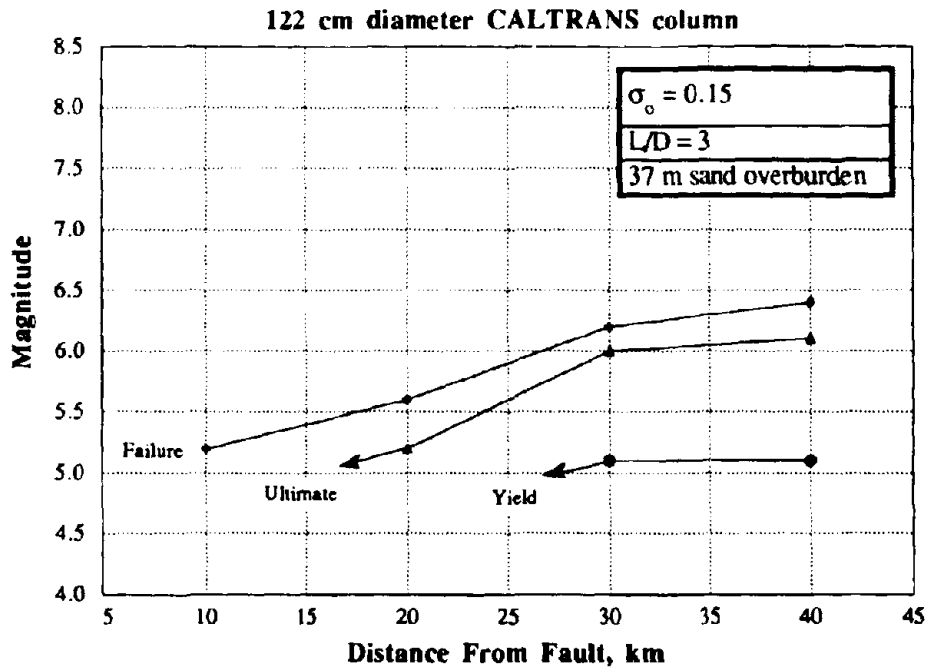
Figure 6.44. Damage states for 122 cm dia. column, σ_o = 0.15, L/D = 3, on 37 m sand.

122 cm diameter CALTRANS column
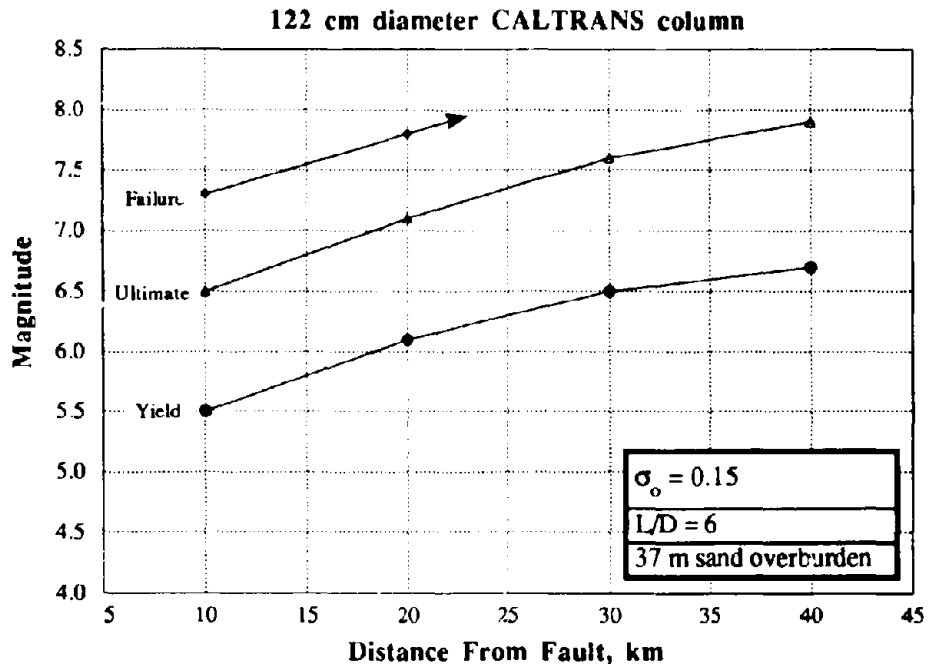
Figure 6.45. Damage states for 122 cm dia. column, $\sigma_o = 0.15$, L/D = 6, on 37 m sand.

122 cm diameter CALTRANS column
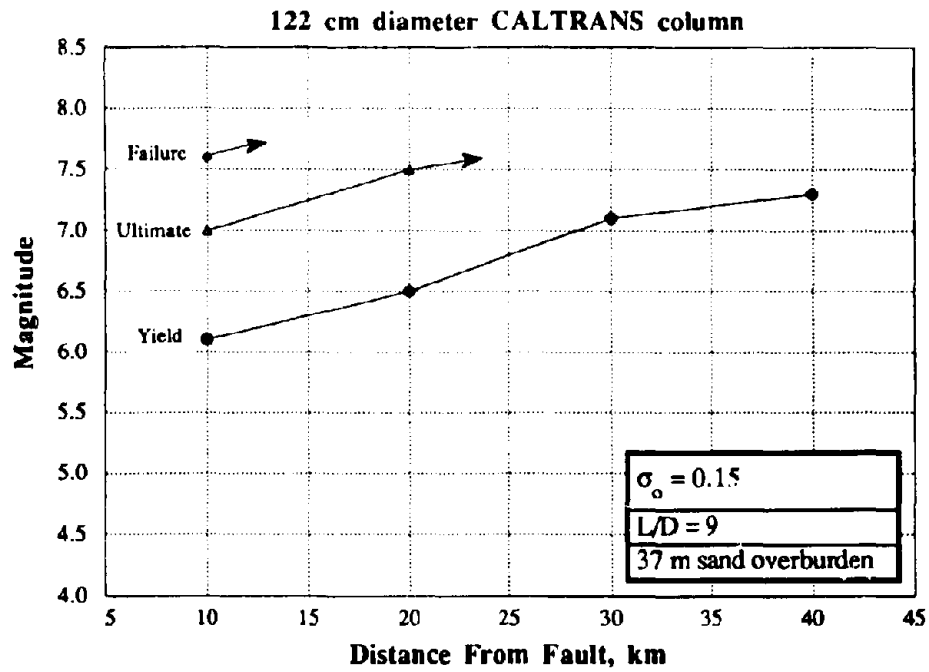
Figure 6.46. Damage states for 122 cm dia. column, $\sigma_o = 0.15$, L/D = 9, on 37 m sand.

7.0 Retrofit Analysis

7.1 Introduction

According to a recent Federal Highway Administration memorandum [Cooper, 1992],

> "There are more than 7 million kilometers of roads and highways in the United States of America and approximately 575,000 bridges, ranging from 7 m in length to 40 km. The bridge inventory varies from single, simple-span structures to multispan suspension bridges. About one-half are State-owned and 47,000 are on the Interstate System. Approximately 72 percent of the bridges in the U.S. were constructed prior to 1935 with little or no consideration given to seismic resistance."

> "Historically, bridges have proven to be vulnerable to earthquakes, sustaining damage to substructures and foundations and in some cases being destroyed as substructures fail or superstructures are unseated from their supporting elements. In 1971 the San Fernando earthquake damaged more than 60 bridges on the Golden State Freeway in California. This 1971 earthquake is estimated to have cost the State approximately $100 million to repair these bridges, including the indirect costs due to bridge closures. In 1989, the Loma Prieta earthquake in Northern California damaged more than 80 bridges in a five-county region, and caused the deaths of more than 40 people in bridge-related collapses alone. The cost of the earthquake to the transportation system was $1.8 billion of which the damage to State-owned viaducts was about $200 million and to other State owned bridges about $100 million."

Given the above statistics there is a clear need for the development of improved vulnerability assessment techniques, as well as retrofit procedures which can be used to improve the seismic resistance of older bridges. During the 1970's, particularly in the State of California, emphasis was placed on the development of improved design procedures for new bridges, with particular attention paid to reinforcement requirements for new columns. The focus shifted in the 1980's towards implementation of a multi-phase retrofitting program. This effort was largely concerned with improving connections between bridge elements. Cable restrainers and other motion-limiting devices were installed to prevent unseating of spans during an earthquake. Two useful reports, "Seismic Design and Retrofit Manual for Highway Bridges" (FHWA, 1987) and "Seismic Retrofitting Guidelines for Highway Bridges" (FHWA, 1983) contain in-depth

discussion of these procedures. Most engineers familiar with retrofit restrainers point to their use in California as one of the little-recognized success stories of the Loma Prieta earthquake; without them the damage toll would likely have been far greater.

Nonetheless, much work remains to be done on seismic retrofitting of existing bridges. Only a few retrofitting schemes (as described above) have actually been used in practice and given the present state of knowledge, retrofitting is still an art requiring a considerable amount of engineering judgment. While it is beyond the scope of this report to address all aspects of bridge retrofitting (see FHWA 1987 for a global perspective on the complexity of the problem) the specific problem of vulnerability assessment and retrofit design for RC column substructures is highly amenable to solution using the ISDP procedure described in this report. In the remainder of this chapter ISDP first will be employed to investigate the performance of an existing RC column when subjected to a range of earthquake intensities. These responses will then be compared to the design standard proposed in Chapter 6, and the effectiveness of a common retrofit strategy will be analyzed.

7.2 Retrofit Procedure

Figure 7.1 depicts a box girder bridge cross section at a single column bent, as might be typically employed at an elevated interchange. The column is circular with a diameter of 122 cm and a height of 732 cm giving an aspect ratio of L/D = 6. Hence flexural effects are expected to dominate the behavior of the column. Axial reinforcement consists of 18 #10 bars ($d_a = 3.2$ cm). Confining reinforcement is provided by 1.6 cm diameter bars at a pitch of 12.1 cm. The yield stress for both types of reinforcement is 414 MPa. The nominal concrete cylinder strength is 27.6 MPa. The axial load is 3220 kN, producing a normalized axial stress level, σ_0, of 0.10. Concrete cover is presumed to be 5.1 cm to the centerline of the confining steel. The structure is situated 20 km from a known fault (i.e., the most likely source of a future earthquake that would be of sufficient energy to damage the bridge). The bridge is considered a critical lifeline structure which must remain fully operational following a severe earthquake.

Column Specification:

f'c = 27.6 MPa
fy = 414 MPa
fu = 725 MPa
Pe = 3220 kN
D = 122 cm
cover = 5.1 cm
ds, spiral bar dia. = 1.6 cm
s, spiral pitch = 12.1 cm
L = 732 cm
da, long. bar dia. = 3.2 cm
long. bars = 18 (#10)
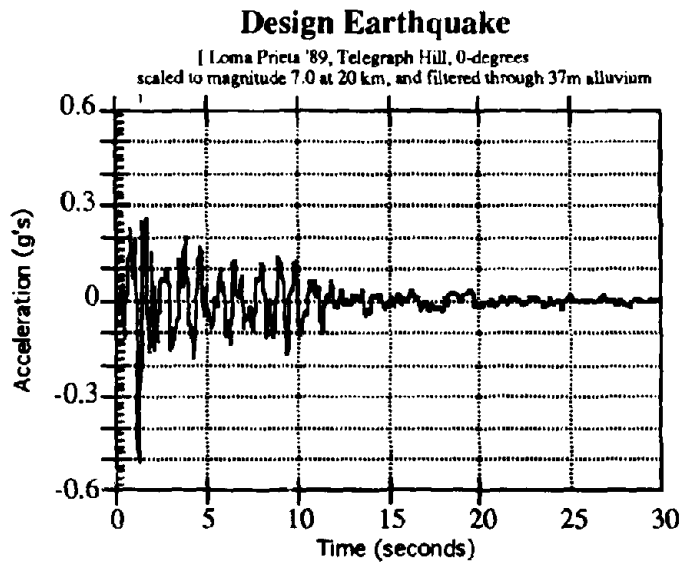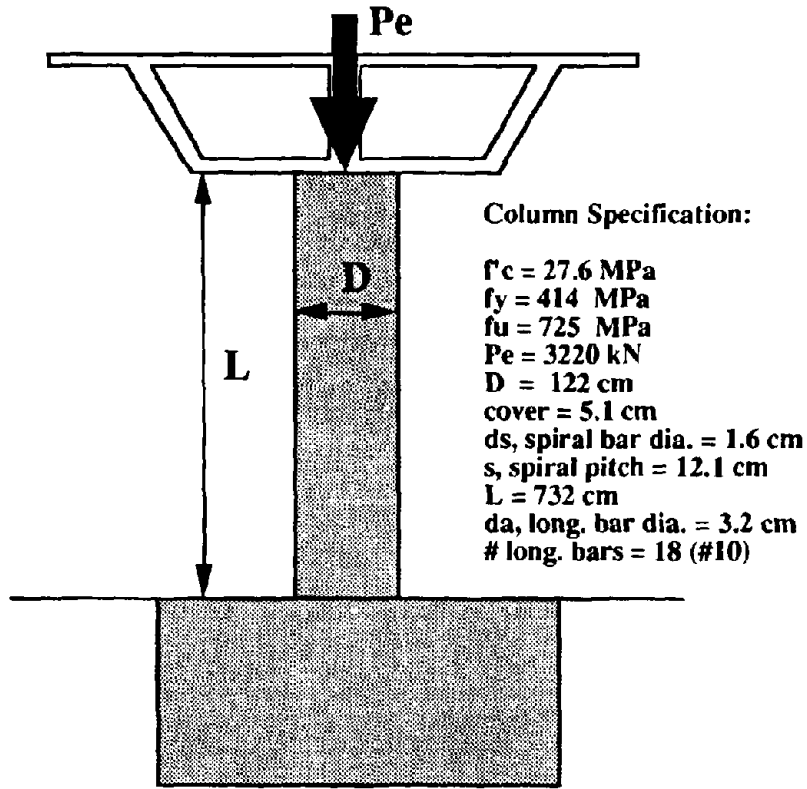
Figure 7.1. Retrofit design example – initial conditions and design earthquake.

The column described above was designed in accordance with current CALTRANS seismic design procedures [CALTRANS 1990] for a structure founded on 37 m of alluvium. As was demonstrated in Chapter 6, it is possible using ISDP to generate continuous curves representing the damage sustained by the column when subjected to earthquakes of increasing energy content (increasing magnitude). For the purposes of retrofit analysis it will be useful to initially look at the response of the column to a specific earthquake, and then to expand the parametric analysis to examine various levels of retrofit.

Figure 7.2 shows the response of the column to a magnitude 7.0 earthquake (shown at the bottom of fig. 7.1). The acceleration-time history shown in figure 7.1 was obtained by first scaling the Loma Prieta Telegraph Hill 0-degree record to magnitude 7.0 (as outlined in Chapter 3) and then filtering the record through 37 m of alluvium using SHAKE91, which was embedded as a subroutine in ISDP. In a general retrofit analysis each magnitude level will be accompanied by a suite of time histories, selected in accordance with the principles set out in Chapter 3. The record shown in figure 7.1 was shown through analysis to produce the greatest damage of the four-record suite generated for that magnitude. The damage response shown in figure 7.2 indicates that, at a final damage index value of approximately 0.34, the column, subjected to this particular earthquake, would have sustained loading approaching its ultimate capacity but would remain standing and could possibly sustain emergency traffic. At a damage level of 0.34 substantial yielding will have taken place as well as extensive spalling but none of the confining steel would have fractured. Below the trace of the damage-time history in figure 7.2 is a shaded area indicating the zone of acceptable damage for important lifeline structures, in accordance with the principles presented in Chapter 6. This indicates that the damage sustained by the column in this particular event is nearly double the desired maximum for important structures. The worst-case response for all time-history suites for all magnitudes is plotted in figure 7.6. It can be seen that the as-built column fails to meet the maximum allowable damage design criteria for important structures, as detailed in Chapter 6, at all earthquake magnitudes. Thus, some form of column retrofit is required.
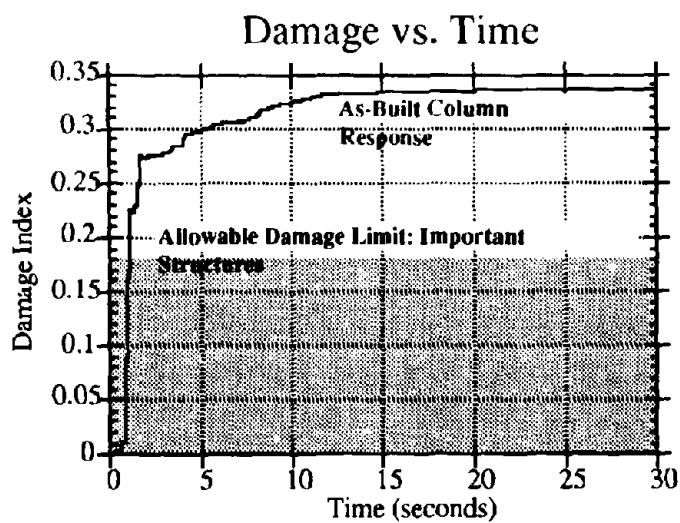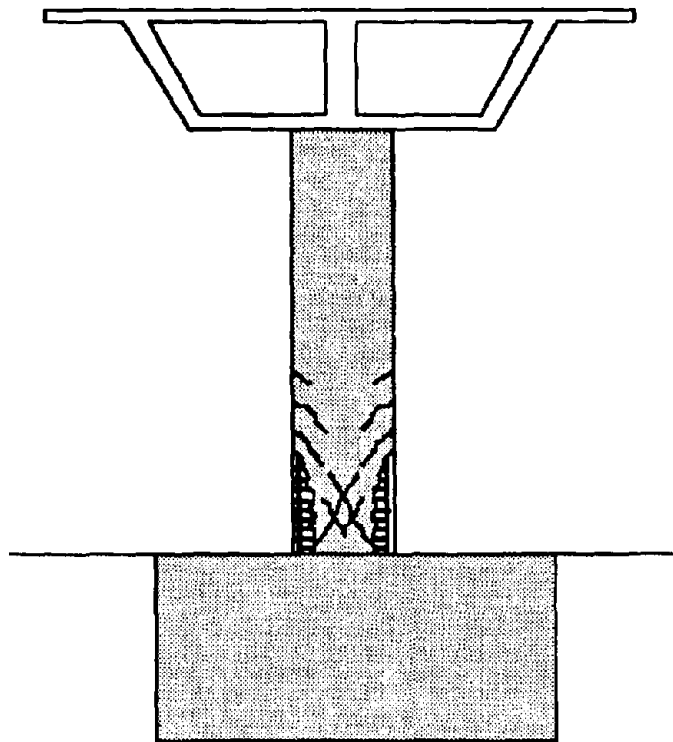
Figure 7.2. Retrofit design example - predicted response of the as-built column
to the design earthquake shown in figure 7.1.

For the specific class of columns investigated in this report (single circular column, cantilevered construction, stiff box girder superstructure) failure occurs in the plastic hinge region at the base of the column. In this type of construction the foundations are generally designed with significant conservatism. It is thus assumed in the following discussion that failure is constrained to occur in the column and will not be permitted to migrate into the foundation. Since any retrofit to the column will necessarily increase the loading on the foundation, a follow up study would be required to determine if subsequent strengthening is required of the foundation.

A number of bridge column retrofit schemes have been investigated in recent years, including cast-in-place concrete jackets; welded or bolted cylindrical steel plate jackets; wrapped epoxy-fiberglass jackets; and tension-wound prestressed confining steel. A useful report on the merits of these various techniques is presented by Priestley and Seible [1991]. The latter two approaches listed above must still be considered experimental as only a few laboratory tests have been conducted. The first two techniques have seen limited application in the United States, Japan, and elsewhere. Of these, steel jacketing appears to be the most effective technique and will be used in this report as the basis for parametric retrofit analyses. It should be noted that, with appropriate constitutive modeling, all of the aforementioned retrofitting schemes could be incorporated into ISDP, both for the purposes of routine design and for automated parameter sensitivity studies.

Figure 7.3 summarizes the retrofit approach used for the present example. This procedure maintains the as-built column diameter and adds successively thicker cylindrical jacketing plates to the zone of high predicted damage. These plates are presumed to be rolled to form a close match to the column surface and are welded in place in the field. A narrow gap of a few millimeters is permitted between the shell and column to allow for cement-based pressure grouting to ensure integrity with the column. Generally, the height of the jacket should extend a significant distance above the plastic hinge region, to a height of approximately 2D or greater to ensure that a localized hinge is not simply translated to the top of the jacket. In the retrofit analysis described below the participation of the existing spiral reinforcement is included together with the enhancement provided by the jacket. The jacket is presumed to be effective in providing confinement only and not to act as additional longitudinal reinforcement.
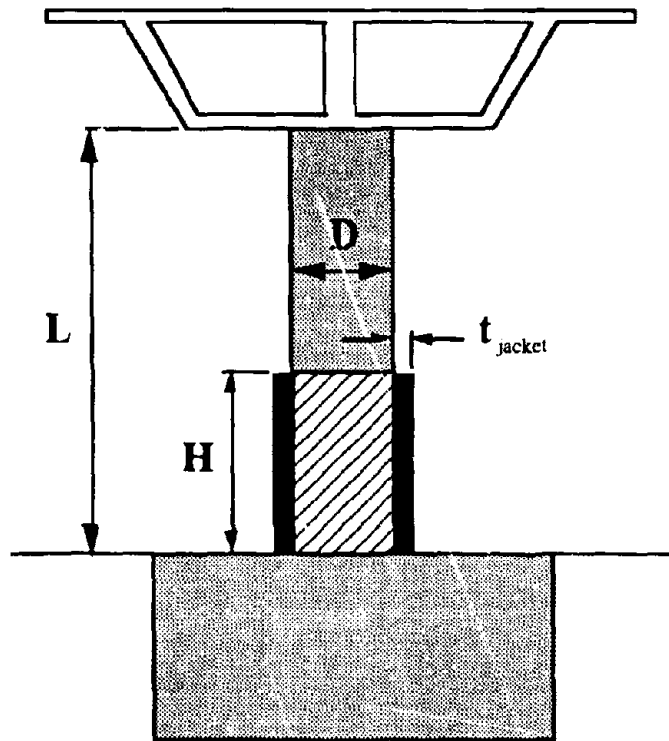
Retrofit Procedure :

1: Maintain D
2: Vary (increase) jacket
   plate thickness, t.
3: L remains a fixed parameter.
4: H > 2D

Figure 7.3. Retrofit design example - steel jacket retrofit configuration.

It is assumed in the above procedure that the column height is a fixed parameter and that, for reasons of economy, complete replacement of the column or a reduction in the diameter of the column is not feasible. Depending on the likely frequency content of the earthquakes in a given region it may actually be desirable to increase the fundamental period of the structure by making the column more flexible. This could only be achieved through complete replacement of the column (to achieve an increase in the L/D ratio) or possibly by removal of selected longitudinal reinforcement. These techniques are both rather extreme, and would only be warranted where critical structures could not be retrofitted by more conventional methods.

7.3 Results of Steel Jacket Retrofit Analyses

Figure 7.4 shows a series of damage index versus time plots for various thickness jackets in response to the magnitude 7.0 earthquake shown in figures 7.1 and 7.4. As can be seen, the addition of even a relatively thin steel casing significantly improves the survivability of the column.

There is, apparently, a point of diminishing returns, beyond which there is no significant decrease in damage index for an increase in shell thickness. Figure 7.5 shows the response of the retrofitted column to all 16 design earthquakes (a four-record suite for each of four earthquake magnitudes) as a function of the shell thickness. This clearly indicates that the maximum benefit afforded by this type retrofit approach is achieved by the time the jacket shell has reached about 5 mm. Indeed, auxiliary analyses indicated that for very thick shells (greater than 10 mm) there may in fact be a loss of performance. This is because the increase in concrete strain capacity afforded by the thicker shell is ultimately offset by tensile fracture of the longitudinal reinforcement. This phenomenon is accounted for in the fiber model employed in IDARC, which presently forms the analysis core of ISDP.

Damage vs. Time

Acceleration Record

[Loma Prieta '89, Telegraph Hill, 0-degrees
scaled to magnitude 7.0 at 20 km, and filtered through 37m alluvium]
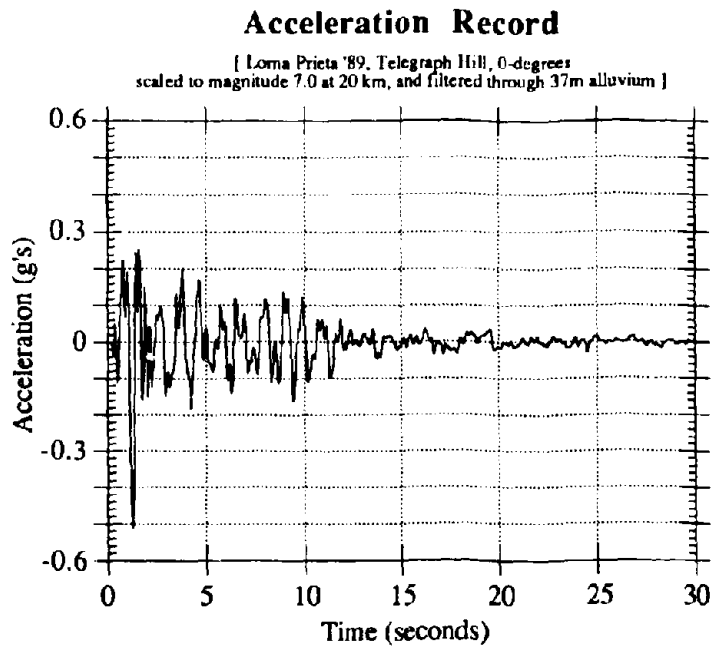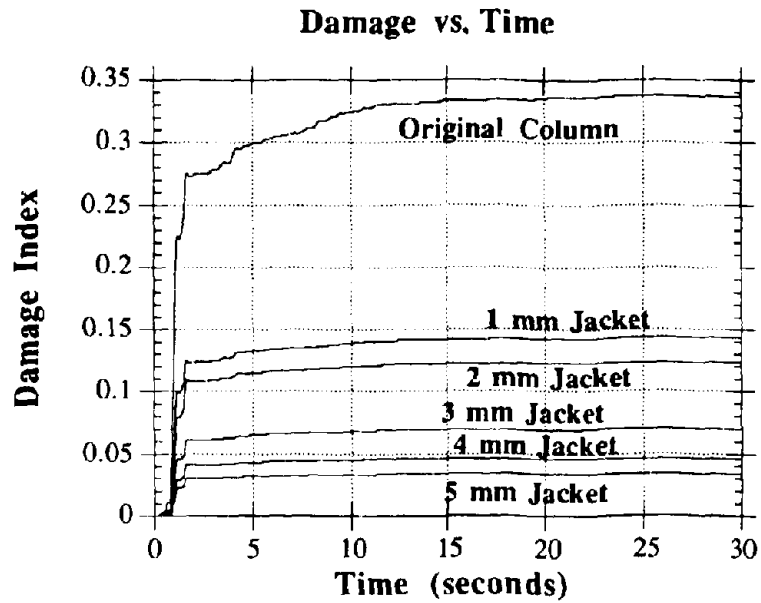
Figure 7.4. Damage accumulation for various steel jacket thicknesses.
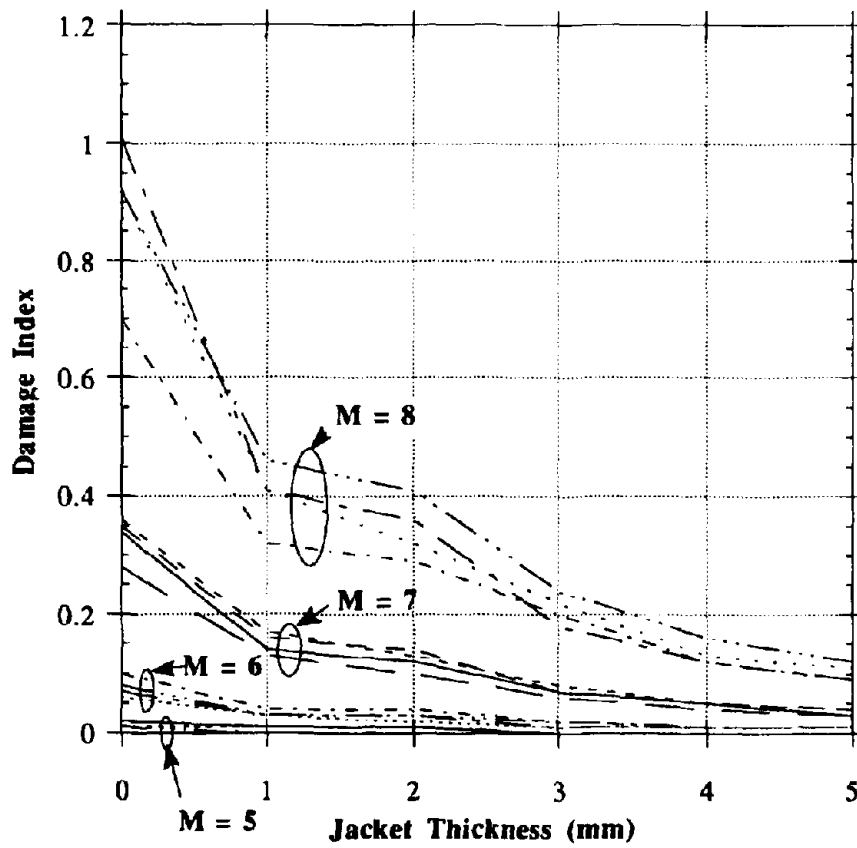
Figure 7.5. Cumulative damage vs. retrofit jacket thickness for example column.

7.4 Discussion

Figures 7.6 and 7.7 summarize the retrofit analyses described in this chapter. Given the as-built specifications and material properties for any column it is possible using ISDP to predict the damage-vs.-time response of the column to any acceleration-time history. By compiling the worst-case response of the column to suites of design records appropriate for a particular construction site, it is possible to construct a damage profile for the column as a function of earthquake energy content (as expressed by magnitude at a particular distance from the likely source of the earthquake). In cases where there are many possible sources for earthquakes at a certain construction site, similar damage response analysis sets should be performed for each likely source distance, to ensure that all possible scenarios are reasonably accounted for. Although this may sound complex, using ISDP it is a straightforward matter to analyze a wide range of design cases.

Retrofit of 122 cm dia. CALTRANS column, 10% axial load
20km from fault, 37 m sand overburdern
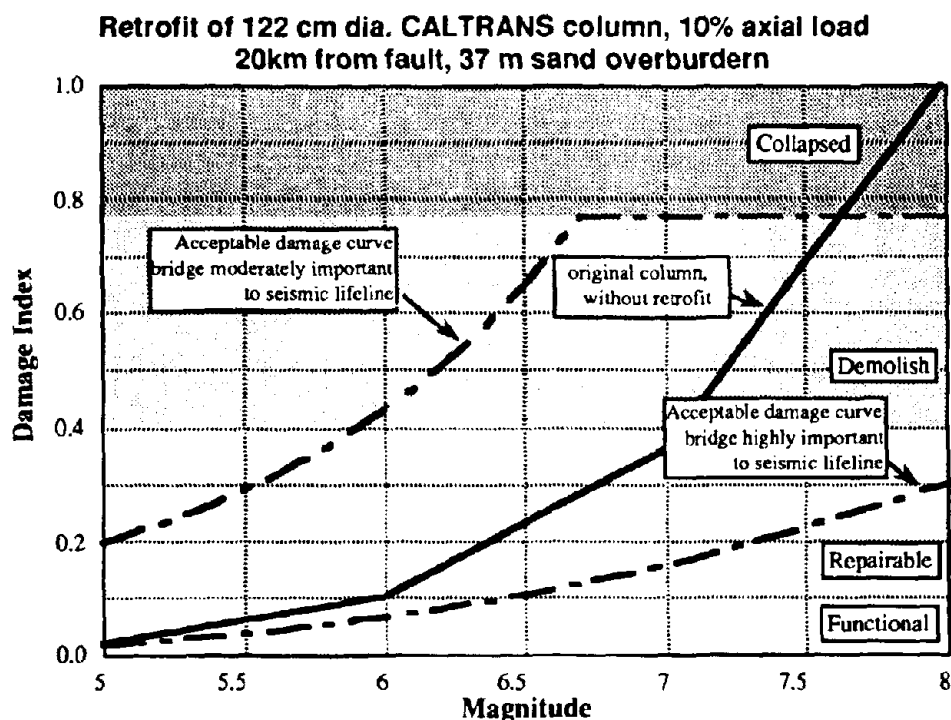
Figure 7.6. Original state of example CALTRANS column before addition of external steel jacket.

Retrofit of CALTRANS column, 10% axi.l load
20km from fault, 37 m sand overburdern
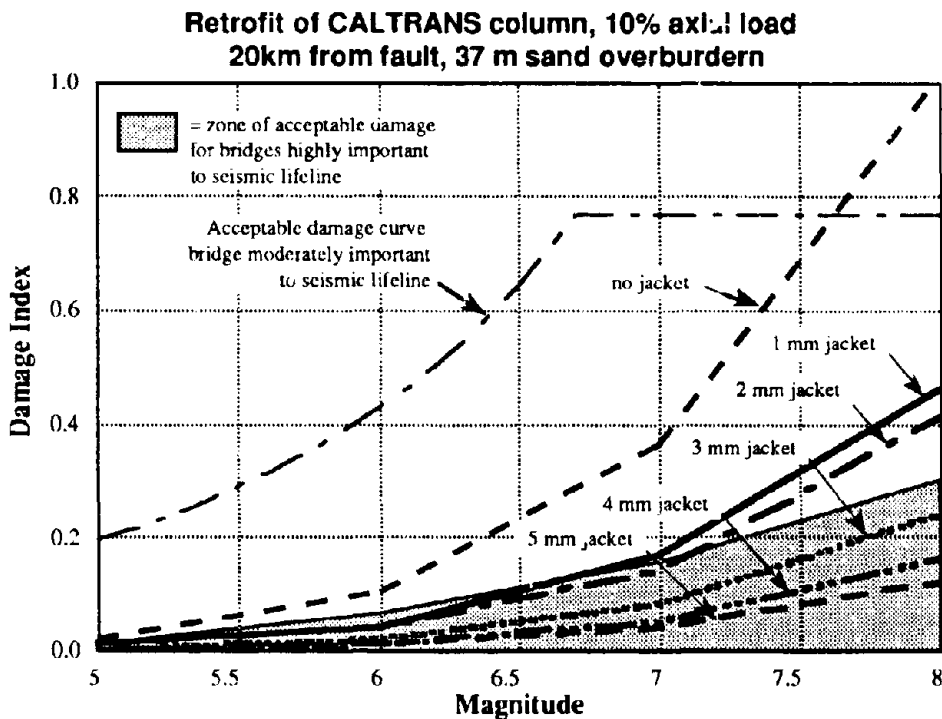
Figure 7.7. Effect of external jackets on example CALTRANS column.

In figure 7.6 the overall response for the as-built column is shown as a function of earthquake magnitude together with the two limiting design criteria set forth in Chapter 6 for highly important and moderately important structures. Since the initial criteria for this particular retrofit problem was that the bridge must be serviceable under even the most severe event, the lower criteria corresponding to important structures is the one of interest. From this perspective it is clear that the as-built column does not satisfy the criteria for any magnitude.

In contrast, figure 7.7 shows the effectiveness of the steel jacket retrofit. It is evident from this graph that a jacket thickness of 3 mm will be sufficient to bring the column up to specification. However, it is also important to recognize the issue of constructability. Bridge columns of the type described in this report will generally vary in diameter from 100 to 300 cm. Retrofitting of such columns using steel jackets means handling relatively large thin shell structures at the job site. These shells may, if abused, be subject to buckling during

transport and placement, which could compromise the ability of the shell to provide the necessary column confinement. It may be more reasonable in such cases to use a slightly thicker shell, for example using the 5 mm jacket in the present example instead of the 3 mm jacket, to avoid problems in the field. Furthermore, although there is presently no known experimental or field data to support it, there is the possibility of localized tearing of particularly thin jacket plates during an earthquake, at such locations as weld lines or bolt holes. Such tearing would appear to be less likely for thicker plates. For these reasons a 4 mm or 5 mm thick jacket would be the recommended retrofit for the column used in this example.

As was mentioned above, the present analysis was limited to retrofitting procedures which employ a steel jacket. Further research is required to develop appropriate constitutive models for other retrofit strategies and substructure configurations. In this way ISDP could be become a design tool capable of assessing the relative merits of a number of retrofit techniques for both single- and multiple-column bridge bents.

8.0 Conclusions

8.1 Integrated Seismic Design Procedure

The authors have proposed an alternative procedure for the seismic design of reinforced concrete bridge columns, which is in their opinion more rational than the codified techniques presently in use in seismically active regions of the United States. The approach, referred to as the Integrated Seismic Design Procedure (ISDP), is in essence a unification of many disparate aspects of advanced seismic design which heretofore have existed separately within the various fields of seismology, geotechnical engineering, structural design, and structural engineering research. It has been shown that the data and techniques utilized in these fields (e.g., reinforced concrete test results; earthquake time histories both at bedrock and at the top of soil overburden; soil boring records; site geographic location; and the like) can be included either in computer codes or in knowledge databases. Using these computer codes and knowledge databases it is possible to approach the seismic analysis problem in rational stages, arriving ultimately at specific columns designs (cross section geometry, L/D ratio, material properties and reinforcement contents) which meet specific levels of performance for specific seismic events.

The implementation of ISDP necessarily involves the use of a very high performance computer with fast, sophisticated graphics capabilities. The reasons for this are obvious when one considers, first, that database manipulation requires processing of hundreds of earthquake time histories (each of which generally consists of some 10,000 data points); hundreds of experimental test records (which also may consist of several thousand data points) and second the computational burdens of wave propagation analyses and full non-linear transient dynamic analyses associated with each trial case in a parametric column design (of which there may easily be hundreds or thousands of runs involved in the design matrix of variables of interest). Until recently, with the advent of RISC-based desktop workstations which are both compact and affordable to the average design office, such a large, computationally intensive program as ISDP would have been intractable, except on a few supercomputers operating at industry or government laboratories.

That such an integration of all the various pieces necessary for advanced seismic design is feasible was demonstrated through the results of the ISDP analyses presented in Chapters 6 and 7. At the inception of the research described in this report three necessary components of the ISDP did not exist in any form. These were a) a set of closed-form equations which, given material

and geometric properties for a prospective column design, could be used to calculate an appropriate set of hysteretic failure model parameters for subsequent use in the non-linear time history analysis module; b) a realistic damage assessment model that could relate an intangible (but analytically tractable) damage index to a specified level of observed damage in laboratory tests of a wide variety of bridge columns; and c) an acceptable damage-based design criteria which preferably could be reduced to a set of closed form equations relating allowable damage to earthquake energy content and the importance of the structure. The first two of these components were based on extensive system identification analyses of empirical test results, including full-scale column tests, and are believed to be relatively accurate over the range of parameters within which the models were developed. The third element was based on a systematic study of damage states, and could serve as a model for future development of damage-based performance criteria.

8.2 Acceptable Damage Limits

The acceptable damage model developed in Chapter 6 presents an initial attempt by the authors to address the complex, socio-economic-technological topic that is summarized by the question: "What cost are we willing to pay in order for a particular bridge to survive a given earthquake?" The authors have proposed a non-linear scale which relates allowable damage level to earthquake intensity and structural importance. The criteria were developed, somewhat subjectively, by considering limiting cases in a three-dimensional space defined by allowable damage, distance from the earthquake epicenter, and earthquake magnitude. From these discrete values parametric equations were developed to model the three-dimensional surfaces of acceptable damage. Equations for two classes of bridges were presented: bridges deemed moderately important to seismic lifelines, and bridges deemed highly important to seismic lifelines. This was largely done in an effort to maintain consistency with existing design procedures, which also recognize two levels of importance.

Refinement of the acceptable damage models beyond the ones presented by the authors will necessarily involve probabilistic analyses on the likelihood of a particular earthquake occurring during the useful lifetime of a bridge, as well as the estimation of the cost to society of repair/retrofit/replacement of the bridge following a particular earthquake. While these tasks are well-defined, they are beyond the scope of the present study. The important distinctions between this approach and the approach presently employed by the model code agencies are that a) the concept of acceptable damage, as a calculable quantity, replaces ambiguous safety factors and base shear coefficients and b) the acceptable

performance is tied specifically to two engineering quantities: the earthquake magnitude and the distance of the construction site from the earthquake source.

8.3 Deficiencies in Current CALTRANS/AASHTO Designs

Using the ISDP and the aforementioned acceptable damage criteria a large number of parametric analyses were conducted to investigate the performance of a certain class of circular, spirally-reinforced concrete bridge columns such as would be designed in accordance with current CALTRANS specifications and procedures. The parameters investigated included column aspect ratio (L/D), normalized axial load (σ_0), the type of subsoil deposit (either bedrock or 37 m of alluvium), the earthquake magnitude (M), and the distance of the bridge from the causative fault (d).

The detailed results of these analyses were presented in Chapter 6. However, several notable points are worth summarizing here:

For columns founded on bedrock:

a) At axial load levels of 5% of ultimate, all columns analyzed performed acceptably, regardless of aspect ratio and distance from the causative fault.

b) At axial load levels greater than 10% but less than 15%, columns with aspect ratios of three or less can be expected to suffer total failure under a magnitude 7.0 earthquake at 10 km from the epicenter and for a magnitude 8.0 earthquake at 30 km from the epicenter.

For columns founded on 37m of alluvium:

c) At axial load levels as low as 5%, total failure of columns with aspect ratios of less than 3 is indicated for a magnitude 6.6 event at 10 km and for a magnitude 8.0 event at 40 km.

d) At axial load levels of 10%, total failure of columns with aspect ratios of less than 3 is predicted for a magnitude 5.5 event at 10 km and for a magnitude 6.7 event at 40 km. Failure of columns with L/D ratios of 6 are indicated at magnitude 7.5 and distances less than 20 km.

e) At axial load levels of 15%, failure of columns with aspect ratios of less than 3 is indicated for a magnitude 5.3 event at 10 km and for a magnitude 6.4 event at 40 km. Failure of columns with $L/D = 6$ is indicated for a magnitude 7.2 earthquake at 10 km.

It may be concluded from the above summary that short, stubby CALTRANS-designed columns as well as columns carrying high axial loads are particularly

susceptible to failure, in spite of what is currently considered to be a significant amount of confining reinforcement (as compared with, for example, pre-1971 design standards).

In most cases only columns with axial loads of less than 10% and L/D ratios of at least 9 met the acceptable damage criteria for important structures presented in Chapter 6. Presuming such an acceptable damage criteria were to become part of a future AASHTO Code it is fortunate that steel jacketing procedures, as discussed in Chapter 7. appear to be particularly effective at improving the behavior of columns to acceptable levels.

8.4 Retrofit Procedures Based on ISDP

For existing columns that have been identified (through analyses such as ISDP) as being highly susceptible to seismic damage, there are a number of methods which can be used for retrofitting. These include a) complete replacement; b) jacketing; c) base isolation; d) use of energy dissipaters (e.g., lead extruders) and e) active damping. Of these techniques jacketing will almost always be the most cost-effective provided it can be demonstrated that the necessary increase in performance can be achieved using this technique.

Within the jacketing subset there are four approaches presently under consideration by the seismic design community: cast-in-place concrete jacket; steel plate jacket; fiberglass-epoxy jacket; and prestressed, wire-wound jacket. Steel plate jacketing was investigated in Chapter 7. The analyses assumed that the steel jacket was rolled to form a co-axial split cylinder that effectively matched the radius of the column in the field, plus a few millimeters to permit high pressure grout placement to insure integrity with the column. Field installation was assumed to have been either by welding or bolting of the split cylinder. A parametric investigation revealed that even a relatively thin steel jacket can have a pronounced effect on the seismic behavior of a circular bridge column. There is, however, a point of diminishing returns, beyond which increased plate thickness will not yield improved performance. For the 122 cm diameter column investigated in the Chapter 7 retrofit study it was found that this point of diminishing returns was reached at a jacket thickness of approximately 5 mm. However, the application of that 5 mm jacket reduced the predicted column damage by about 75%.

These results clearly indicate the beneficial effects of steel jacketing. However certain precautionary notes are in order. First, while steel jacketing can significantly improve the seismic performance of a circular column, retrofitting

of columns may simply divert damage to other elements of the bridge, such as the foundation or superstructure. Second, it is possible that thin steel jackets may be susceptible to tearing when subjected to high internal pressures and cyclic lateral loads. Along these same lines, the methods of installing thin steel jackets (e.g., welding or bolting) should be adequate to maintain the integrity of the jacket under these severe conditions. Further studies of the toughness and durability of thin steel jackets subjected to seismic loads may be required before they then can be used with complete confidence.

9.0 References

AASHTO (1989), "Standard Specifications for Highway Bridges, 14th Edition," The American Association of State Highway and Transportation Officials (AASHTO), Washington, D.C., 1989.

Allahabadi, Rakesh (1987), "Drain-2DX, Seismic Response and Damage Assessment for 2D Structures," doctoral dissertation, Department of Civil Engineering, University of California, Berkeley, March 1987.

Ang Beng Ghee; Priestley, M. J. N.; and Park, R. (1981), "Ductility of Reinforced Concrete Bridge Piers Under Seismic Loading," Report 81-3, Department of Civil Engineering, University of Canterbury, Christchurch, New Zealand, February 1981.

Ang Beng Ghee; Priestley, M. J. N.; and Paulay, T. (1985), "Seismic Shear Strength of Circular Bridge Piers," Report 85-5, Department of Civil Engineering, University of Canterbury, Christchurch, New Zealand, July 1985.

Ang Beng Ghee; Priestley, M. J. N.; and Paulay, T. (1989), "Seismic Shear Strength of Circular Reinforced Concrete Columns," ACI Structural Journal, January-February 1989, pp 45-59.

CALTRANS (1990), "Bridge Design Specifications," State of California, Department of Transportation (CALTRANS), Office of Structure Design, Sacramento, California, August 1986 (with revisions up to June 1990).

Campbell, K.W. (1981), "Near Source Attenuation of Peak Horizontal Acceleration," *Bulletin of the Seismological Society of America*, Vol. 71, No. 6, 1981, pp 2039-2070.

Cheok, G.S.; and Stone, W.C. (1990), "Behavior of 1/6-Scale Model Bridge Columns Subjected to Inelastic Cyclic Loading," ACI Structural Journal, Nov.-Dec. 1990, Vol. 87, No. 6, American Concrete Institute, Detroit, Michigan, pp 630-638.

Cooper, James (1992), "High Priority National Program Area: Seismic Protection," Structures Division, HNR-10, Research Plan 1992-1996, Federal Highway Administration, Turner-Fairbank Highway, McLean, Virginia, July 1992.

Davey, B.E. (1975), "Reinforced Concrete Bridge Piers Under Seismic Loading," Master of Engineering Report, Civil Engineering Department, University of Canterbury, Christchurch, New Zealand, February 1975.

Diaconis, Persi; and Efron, Bradley (1983), "Computer-Intensive Methods in Statistics," *Scientific American*, Vol. 248, No. 5, May 1983, pp 116-130.

Efron, Bradley; and Gong, Gail (1983), "A Leisurely Look at the Bootstrap, the Jackknife, and Cross-Validation," *The American Statistician*, Vol. 37, No. 1, February 1983, pp 36-48.

Efron, Bradley; and Tibshirani, R. (1986), "Bootstrap Methods for Standard Errors, Confidence Intervals, and Other Measures of Statistical Accuracy," *Statistical Science*, Vol. 1, No. 1, 1986, pp 54-77.

El-Borgi, S.; White, R.N.; and Gergely, P. (1991), "Analytical Modeling of Pinching and Degrading Hysteretic Systems and System Identification of Parameters: Progress Report to NIST," Department of Structural Engineering, School of Civil Engineering, Cornell University, Ithaca, New York, 14853, January 1991, NIST Contract #50SBNB1C6543.

FHWA (1983), "Seismic Retrofitting Guidelines for Highway Bridges," report FHWA/RD-83/007, Office of Research and Development, Federal Highway Administration, U.S. Department of Transportation, Washington, D.C., 20590, December 1983.

FHWA (1987), "Seismic Design and Retrofit Manual for Highway Bridges," report FHWA-IP-87-6, Office of Implementation, HRT-10, Federal Highway Administration, 6400 Georgetown Pike, McLean, Virginia, 22101, May 1987.

Idriss, I.M. (1985), "Evaluating Seismic Risk in Engineering Practice," *Proceedings*, XIth International Conference on Soil Mechanics and Foundation Engineering, San Francisco, California, August 1985, pp. 255-320.

Joyner, W.B.; and Boore, D.M. (1988), "Measurement, Characterization, and Prediction of Strong Ground Motion," *Earthquake Engineering and Soil Dynamics II - Recent Advances in Ground-Motion Evaluation*, Proceedings of the specialty conference sponsored by the Geotechnical Engineering Division of the American Society of Civil Engineers, Park City, Utah, 1988, pp 43-102.

Kenchiku Kenkyu Siryo (1975), "Aseismic Analysis of Building Structural Members: A List of Experimental Results on Deformation Ability of

Reinforced Concrete Columns under Large Deflection (No.2)," Building Research Institute, Ministry of Construction, Japan, March 1975.

Kenchiku Kenkyu Siryo No.21 (1978), "Aseismic Analysis of Building Structural Members: A List of Experimental Results on Deformation Ability of Reinforced Concrete Columns Under Large Deflection (No.3)," Building Research Institute, Ministry of Construction, Japan, February 1978.

Lew, H.S. (ed.) (1990), "Performance of Structures During the Loma Prieta Earthquake of October 17, 1989," NIST Special Publication 778, Center for Building Technology, National Engineering Laboratory, National Institute of Standards and Technology, Gaithersburg, MD, 20899, January 1990.

Lim, Kuang Y.; and McLean, David I., (1991), "Scale Model Studies of Moment-Reducing Hinge Details in Bridge Columns," ACI Structural Journal, Vol. 88, No. 4, July-August 1991, pp 465-474.

McLean, David I.; and Lim, Kuang Y. (1990), "Moment-Reducing Hinge Details for the Bases of Bridge Columns," Report No. WA-RD 220.1, Washington State Department of Transportation, Planning, Research and Public Transportation Division, October 1990.

Mander, J.B. (1984), "Seismic Design of Bridge Piers," Research Report #84-2, Department of Civil Engineering, University of Canterbury, Christchurch, New Zealand, February 1984.

Maroney, Brian (1990), "CALTRANS' Seismic Risk Algorithm for Bridge Structures", Seismic and Structural Analysis, Division of Structures, California Department of Transportation, Sacramento, California, 94274-0001, June 30, 1990, 23 pages.

Munro, I. R. M.; Park, R.; and Priestley, M. J. N. (1976), "Seismic Behaviour of Reinforced Concrete Bridge Piers," Report 76-9, Department of Civil Engineering, University of Canterbury, Christchurch New Zealand, February 1976.

Ng Kit Heng; Priestley, M. J. N.; and Park, R. (1978), "Seismic Behaviour of Circular Reinforced Concrete Bridge Piers," Report 78-14, Department of Civil Engineering, University of Canterbury, Christchurch, New Zealand, February 1978.

Otani, S. (1974), "SAKE, a Computer Program for Inelastic Response of R/C Frames Subject to Earthquakes," Civil Engineering Studies, SRS No. 413, University of Illinois, Urbana, November 1974.

Park, Y.J.; Ang, A. H-S.; and Wen, Y.K. (1984), "Seismic Damage Analysis and Damage-Limiting Design of R.C. Buildings," Civil Engineering Studies, SRS No. 516, University of Illinois, Urbana, October 1984.

Park, Y.J.; Reinhorn, A.M.; and Kunnath, S.K. (1987), "IDARC: Inelastic Damage Analysis of Reinforced Concrete Frame-Shearwall Structures, (1987)" Department of Civil Engineering. State University of New York at Buffalo. Buffalo, New York, 14260, Technical Report NCEER-87-0008, July 20, 1987.

Petrovski, J.; and Ristic, D. (1984), "Reversed Cyclic Loading Test of Bridge Column Models," Institute of Earthquake Engineering and Engineering Seismology, University "Kiril and Metodij," Skopje, Yugoslavia. Report # IZIIS 84-164, September 1984.

Priestley, M. J. N.; and Park, R. (1984), "Strength and Ductility of Bridge Substructures," Report 84-20, Department of Civil Engineering, University of Canterbury, Christchurch, New Zealand, December 1984.

Priestley, M. J. N.; and Seible, F. Eds. (1991), "Seismic Assessment and Retrofit of Bridges," Report SSRP-91/03, Department of Applied Mechanics and Engineering Sciences, University of California, San Diego, San Diego, California, July 1991. 416 pp.

Rodriguez-Gomez, S.; Chung, Y.S.; and Meyer, C. (1990), "SARCF-II User's Guide: Seismic Analysis of Reinforced Concrete Frames," Technical Report NCEER-90-0027, National Center for Earthquake Engineering Research, State University of New York at Buffalo, September, 1990.

SAS/STAT (1987), "SAS/STAT Guide for Personal Computers," Version 6 Ed., SAS Institute, Inc., Cary, North Carolina, 1987, pp. 773-876.

SHAKE91 (1992), "User's Manual for SHAKE91, a Computer Program for Conducting Equivalent Linear Response Analysis of Horizontally Layered Soil Deposits," I.M. Idriss, Joseph I. Sun, and Peter Dirrim, Department of Civil Engineering, University of California, Davis, California, March 1992.

Stone, W.C.; and Cheok, G.C. (1989), "Inelastic Behavior of Full-Scale Bridge Columns Subjected to Cyclic Loading," NIST Building Science Series

166, National Institute of Standards and Technology, Gaithersburg, Maryland, 20899, January 1989.

Stone, W.C.; and Taylor, A.W. (1991), "System Identification of Spirally Reinforced Circular Bridge Columns Subjected to Cyclic Lateral Loading," Wind and Seismic Effects; Proceedings of the 23rd Joint Meeting UJNR, NIST SP 820, National Institute of Standards and Technology, September 1991.

Watson, Soesianawati (1989), "Design of Reinforced Concrete Frames of Limited Ductility," Report 89-4, Department of Civil Engineering, University of Canterbury, Christchurch, New Zealand, January 1989.

Wong, Yuk Lung; Paulay, T.; and Priestley, M. J. N. (1990), "Squat Circular Bridge Piers Under Multi-Directional Seismic Attack," Report 90-4, Department of Civil Engineering, University of Canterbury, Christchurch, New Zealand, October 1990.

Youngs, R.R.; Day, S.M.; and Stevens, J.L. (1988), "Near Field Ground Motions on Rock for Large Subduction Earthquakes," *Earthquake Engineering and Soil Dynamics II - Recent Advances in Ground-Motion Evaluation*, Proceedings of the specialty conference sponsored by the Geotechnical Engineering Division of the American Society of Civil Engineers, Park City, Utah, 1988, pp 445-462.

Zahn, F. A.; Park, R.; and Priestley, M. J. N. (1986), "Design of Reinforced Concrete Bridge Columns for Strength and Ductility," Report 86-7, Department of Civil Engineering, University of Canterbury, Christchurch, New Zealand, March 1986.

10.0 Appendix A: Table of Available Digital Test Records

Table A.1 (part 1 of 2). Spiral column database used in this study, data group 1

Test Name	f'c MPa	fy MPa	Column OD mm	Cover mm	C-to-C long. bars mm	No. of long. bars	Diameter long.bars mm	Diameter hoop bars mm
mun76no1	40.0	305	500	20	434	20	18	8
ng78no2	35.1	305	250	11	211	10	13	4
ng78no2	33.0	294	250	10	213	10	12	4
pot79no1	28.4	303	600	25	516	16	24	10
pot79no3	26.6	303	600	25	516	16	24	10
pot79no4	32.9	303	600	25	516	16	24	10
pot79no5a	32.5	307	600	28	504	16	24	16
pot79no5b	32.5	307	600	28	504	16	24	16
ang81unit1	26.0	308	400	16	346	16	16	6
ang81unit2	28.5	308	400	18	338	16	16	10
zahn86unit5	32.3	337	400	18	338	16	16	10
zahn86unit6	27.0	337	400	18	338	16	16	10
modeln1	24.1	393	250	10	220	25	7	3
modeln2	23.1	393	250	10	220	25	7	3
modeln3	25.4	393	250	10	221	25	7	3
modeln4	24.4	393	250	10	220	25	7	3
modeln5	24.3	393	250	10	220	25	7	3
modeln6	23.2	393	250	10	221	25	7	3
flexnew	35.8	475	1520	59	1344	25	43	16
shearnew	34.3	475	1520	60	1337	25	43	19
arakawa1	28.8	366	275	20	213	12	16	6
arakawa2	29.3	366	275	20	213	12	16	6
arakawa4	29.8	366	275	20	213	12	16	6
arakawa6	28.6	366	275	20	213	12	16	6
arakawa8	31.4	366	275	20	213	12	16	6
arakawa9	30.5	366	275	20	213	16	16	6
arakawa10	30.2	366	275	20	213	8	16	6
arakawa11	28.7	366	275	20	213	12	16	0
arakawa12	27.8	366	275	20	213	12	16	6
arakawa13	30.5	366	275	20	213	12	16	6
arakawa14	31.3	366	275	20	213	12	16	6
arakawa15	32.0	363	275	20	213	12	16	6
arakawa16	31.3	363	275	20	213	12	16	6
arakawa17	31.3	363	275	20	213	12	16	6
arakawa18	31.1	363	275	20	213	12	16	0
arakawa19	31.2	363	275	20	213	12	16	6
arakawa20	29.3	363	275	20	213	12	16	6
arakawa21	30.5	363	275	20	213	12	16	6
arakawa22	20.5	363	275	20	213	12	16	6
arakawa23	42.2	363	275	20	213	12	16	6
arakawa24	31.1	363	275	20	213	12	16	0
arakawa25	29.7	363	275	20	213	12	16	6
arakawa26	30.9	363	275	20	213	12	16	6
arakawa27	18.9	363	275	20	213	12	16	6
arakawa28	41.3	363	275	20	213	12	16	6

Table A.1 (part 2 of 2). Spiral column database used in this study, data group I

Test Name	fc MPa	fy MPa	Column OD mm	Cover mm	C-to-C long. bars mm	No. of long. bars	Diameter long.bars mm	Diameter hoop bars mm
ang85unit2	37.2	296	400	18	342	20	16	6
ang85unit4	30.6	436	400	20	334	20	16	10
ang85unit6	30.1	436	400	18	342	20	16	6
ang85unit7	29.5	448	400	18	342	20	16	6
ang85unit9	29.9	448	400	18	342	20	16	6
ang85unit10	31.2	448	400	21	330	20	16	12
ang85unit13	36.2	436	400	18	342	20	16	6
ang85unit14	33.7	424	400	18	334	9	24	6
ang85unit15	34.8	436	400	18	342	12	16	6
ang85unit16	33.4	436	400	18	342	20	16	6
ang85unit17	34.3	436	400	18	342	20	16	6
ang85unit18	35.0	436	400	18	342	20	16	6
ang85unit19	34.4	436	400	18	342	20	16	6
ang85unit20	36.7	482	400	18	342	20	16	6
ang85unit22	30.9	436	400	20	334	20	16	10
ang85unit23	32.3	436	400	21	330	20	16	12
ang85unit24	33.1	436	400	20	334	20	16	10
ang85unit25	32.8	296	400	18	342	20	16	0
davey75unit1	33.2	373	500	20	435	20	18	7
davey75unit2	34.8	371	500	20	435	20	18	7
davey75unit3	33.8	373	500	20	435	20	18	7
wong90unit1	38.0	423	400	20	334	20	16	10
wong90unit2	37.0	475	400	18	342	20	16	6
wong90unit3	37.0	475	400	20	334	20	16	10
watson10	40.0	474	400	17	342	12	16	8
watson11	39.0	474	400	18	338	12	16	10
petrovm1c1	38.8	240	307	36	217	12	12	6
petrovm1c2	36.2	240	307	36	217	12	12	6
petrovm2c1	38.8	240	307	36	217	12	12	6
petrovm2c2	36.2	240	307	36	217	12	12	6
mc1shift	34.5	448	152	10	115	8	13	4
mc2shift	34.5	448	152	10	115	8	13	4
mc3shift	34.5	448	152	10	115	8	13	4
bri2spbaa1	26.5	399	250	40	151	4	10	9
bri3ws21bs	26.5	375	250	40	151	8	10	9
bri3ws22bs	31.6	375	250	38	158	8	10	6
bri3ws25bs	26.5	381	250	40	148	8	13	9
bri3ws26bs	31.6	381	250	37	159	8	13	4
bri3ws27bs	31.6	345	250	40	145	8	16	9

Table A.2 (part 1 of 2). Spiral column database used in this study, data group II, and measured hysteretic model parameters

Test Name	Hoop Spacing mm	Axial Load kN	Column Height mm	Measured alpha	Measured beta	Measured gamma	Post-Yield Stiffness Reduction Ratio
mun76no1	34	26.4	2730	14.00	0.001	1.00	0.0500
ng78no2	14	16.9	1340	14.00	0.001	1.00	0.0988
ng78no2	10	550	930	5.00	0.120	0.95	0.0271
pot79no1	75	1920	1200	8.75	0.100	1.00	0.0329
pot79no3	50	4300	1200	13.00	0.030	1.00	0.0411
pot79no4	70	3785	1200	10.50	0.240	1.00	0.0320
pot79no5a	55	3385	1200	5.00	0.310	1.00	0.0511
pot79no5b	55	6770	1200	14.00	0.001	1.00	0.1283
ang81unit1	40	680	1600	8.00	0.080	1.00	0.0256
ang81unit2	55	2111	1600	14.00	0.001	1.00	0.0800
zahn86unit5	135	555	1600	10.50	0.250	1.00	0.0563
zahn86unit6	75	2080	1600	14.00	0.001	1.00	0.0834
modeln1	9	120	750	12.01	0.005	1.00	0.0110
modeln2	9	239	750	10.50	0.320	1.00	0.0402
modeln3	15	120	1500	10.50	0.170	1.00	0.0489
modeln4	9	120	750	12.01	0.230	1.00	0.0463
modeln5	9	239	750	10.50	0.280	1.00	0.0452
modeln6	15	120	1500	14.00	0.180	1.00	0.0724
flexnew	89	4450	9140	7.50	0.065	1.00	0.0326
shearnew	54	4450	4570	10.50	0.250	1.00	0.0311
arakawa1	100	0	600	2.00	0.850	0.30	0.0850
arakawa2	50	0	600	2.00	0.600	0.25	0.0562
arakawa4	100	215	600	3.50	1.200	0.85	0.0572
arakawa6	50	215	600	4.00	0.980	0.26	0.0708
arakawa8	35	215	600	3.00	0.900	0.40	0.0741
arakawa9	50	215	600	3.32	1.100	0.60	0.1020
arakawa10	50	215	600	2.87	0.850	0.42	0.0925
arakawa11	N/A	430	600	4.53	2.400	0.93	0.0813
arakawa12	100	430	600	2.60	1.100	0.65	0.0274
arakawa13	50	430	600	2.55	0.980	0.65	0.0482
arakawa14	35	430	600	3.20	0.900	0.65	0.0722
arakawa15	75	0	900	1.90	0.470	0.20	0.0467
arakawa16	35	0	900	6.00	0.260	0.98	0.0856
arakawa17	75	215	600	2.80	1.000	0.26	0.0974
arakawa18	N/A	215	900	3.00	2.000	0.60	0.0968
arakawa19	75	215	900	1.90	0.700	0.50	0.0870
arakawa20	35	215	900	2.50	0.120	0.65	0.0507
arakawa21	75	215	1200	2.25	0.120	0.75	0.0245
arakawa22	75	215	900	1.90	0.750	0.18	0.0753
arakawa23	75	215	900	1.52	0.520	0.30	0.0736
arakawa24	N/A	430	600	2.95	0.820	0.40	0.0818
arakawa25	75	430	900	1.60	0.640	0.36	0.0718
arakawa26	75	430	1200	1.80	0.200	1.00	0.0665
arakawa27	75	430	900	2.30	0.700	0.25	0.0632
arakawa28	75	430	900	2.00	0.950	0.20	0.0792

Table A.2 (part 2 of 2). Spiral column database used in this study, data group II, and measured hysteretic model parameters

Test Name	Hoop Spacing mm	Axial Load kN	Column Height mm	Measured alpha	Measured beta	Measured gamma	Post-Yield Stiffness Reduction Ratio
ang85unit2	60	0	800	25.00	0.030	1.00	0.0246
ang85unit4	165	0	800	6.00	0.290	0.51	0.1068
ang85unit6	60	0	600	20.00	0.728	0.92	0.3175
ang85unit7	80	0	800	12.50	0.490	0.45	0.4421
ang85unit9	30	751	1000	18.00	0.070	1.00	0.0483
ang85unit10	120	784	800	30.00	0.002	1.00	0.1164
ang85unit13	30	455	800	5.00	0.090	0.70	0.0385
ang85unit14	60	0	800	4.50	0.160	0.50	0.0384
ang85unit15	60	0	800	9.00	0.140	0.72	0.0442
ang85unit16	60	420	800	1.40	0.350	0.90	0.0960
ang85unit17	60	431	1000	2.25	0.220	0.70	0.1193
ang85unit18	60	440	600	2.90	0.300	0.98	0.0743
ang85unit19	80	432	600	12.50	0.400	0.60	0.3047
ang85unit20	80	807	700	12.50	0.380	0.98	0.1385
ang85unit22	220	0	800	2.50	0.380	0.76	0.1962
ang85unit23	160	0	800	5.20	0.240	0.60	0.0180
ang85unit24	110	0	800	5.00	0.080	0.44	0.0152
ang85unit25	N/A	0	600	5.00	0.380	0.70	0.0886
davey75unit1	65	380	2750	12.50	0.375	1.00	0.0442
davey75unit2	65	380	1750	7.03	0.250	1.00	0.0705
davey75unit3	65	380	3250	12.50	0.780	1.00	0.0780
wong90unit1	60	907	800	5.00	0.100	1.00	0.0361
wong90unit2	65	1813	800	0.38	0.120	1.00	0.0907
wong90unit3	60	1813	800	2.10	0.080	1.00	0.0827
watson10	84	2652	1600	9.50	0.290	1.00	0.0630
watson11	57	3620	1600	19.00	0.002	1.00	0.1595
petrovm1e1	75	145	1910	7.50	0.100	1.00	0.0730
petrovm1e2	75	254	1910	7.00	0.040	1.00	0.0595
petrovm2e1	75	145	900	12.50	0.075	0.96	0.0857
petrovm2e2	75	254	895	9.00	0.180	1.00	0.0440
mc1shift	22	151	1140	9.00	0.120	1.00	0.1827
mc2shift	22	151	570	15.50	0.005	1.00	0.1168
mc3shift	22	220	570	12.50	0.048	1.00	0.1417
bri2spbaa1	50	184	375	1.35	0.020	0.60	0.0240
bri3ws21bs	33	322	250	4.00	0.280	0.80	0.0429
bri3ws22bs	63	322	500	3.00	0.180	0.50	0.0592
bri3ws25bs	45	161	250	5.00	0.705	0.20	0.0770
bri3ws26bs	37	161	500	2.50	0.064	0.58	0.0678
bri3ws27bs	42	322	500	7.99	0.200	0.75	0.0726

11.0 Appendix B: Table of Earthquakes Selected for Analyses

Table B.1 shows the bedrock acceleration record database that was used in this study. From this data base acceleration records were selected and scaled, using EARTHGEN and the procedures outlined in Chapter 3. Table B.2 shows the suites of four records that were selected for each magnitude and distance, and the amplitude scale factor applied to each record.

Table B.1 (part 1 of 2). Database of recorded bedrock acceleration records used in this study

Record No.	Location	Orientation Deg. CW	Agency*	Event Name
1	Golden Gate Park	10	CALTECH	San Francisco, 1957
2	Golden Gate Park	100	CALTECH	
3	2011 Zonal Avenue	118	USGS	San Fernando, 1971
4	2011 Zonal Avenue	208	USGS	
5	3838 Lankershim	0	USGS	
6	3838 Lankershim	270	USGS	
7	420 South Grand Avenue	127	USGS	
8	420 South Grand Avenue	217	USGS	
9	455 South Figueroa Street	218	USGS	
10	455 South Figueroa Street	308	USGS	
11	800 West 1st Street	37	USGS	
12	800 West 1st Street	307	USGS	
13	Santa Anita Reservoir Dam abutment	3	USGS	
14	Santa Anita Reservoir Dam abutment	273	USGS	
15	Caltech Seismic Laboratory	180	USGS	
16	Caltech Seismic Laboratory	270	USGS	
17	Fairmont Reservoir Dam	56	USGS	
18	Fairmont Reservoir Dam	326	USGS	
19	Santa Felicia Dam, outlet works	172	USGS	
20	Santa Felicia Dam, outlet works	262	USGS	
21	Griffith Park Observatory	180	USGS	
22	Griffith Park Observatory	270	USGS	
23	Lake Hughes Array #4	111	USGS	
24	Lake Hughes Array #4	201	USGS	
25	Lake Hughes Array #9	21	USGS	
26	Lake Hughes Array #9	291	USGS	
27	Puddingstone Reservoir Dam abutment	55	USGS	
28	Puddingstone Reservoir Dam abutment	325	USGS	
29	Pacoima Dam Abutment	164	USGS	
30	Pacoima Dam Abutment	254	USGS	
31	Superstition Mountain	45	USGS	Imperial Valley, 1979
32	Superstition Mountain	135	USGS	

* CALTECH = California Institute of Technology; USGS = U.S. Geological Survey; CDMG = California Division of Mines and Geology

Table B.1 (part 2 of 2). Database of recorded bedrock acceleration records used in this study

Record No.	Location	Orientation Deg. CW	Agency*	Event Name
33	Castaic, Old Ridge Road	0	CDMG	Whittier, 1987
34	Castaic, Old Ridge Road	90	CDMG	
35	Leona Valley #5	0	CDMG	
36	Leona Valley #5	90	CDMG	
37	Leona Valley #6	0	CDMG	
38	Leona Valley #6	90	CDMG	
39	Mount Wilson, Caltech Seismic Station	0	CDMG	
40	Mount Wilson, Caltech Seismic Station	90	CDMG	
41	Pacoima, Kagel Canyon	0	CDMG	
42	Pacoima, Kagel Canyon	90	CDMG	
43	Cliff House, 1090 Point Lobos	0	CDMG	Loma Prieta, 1989
44	Cliff House, 1090 Point Lobos	90	CDMG	
45	Corralitos, 1473 Eureka Canyon Road	90	CDMG	
46	Corralitos, 1473 Eureka Canyon Road	360	CDMG	
47	Diamond Heights, 80 Digby Street	0	CDMG	
48	Diamond Heights, 80 Digby Street	90	CDMG	
49	Gilroy #1, Gavilan College water tank	90	CDMG	
50	Gilroy #1, Gavilan College water tank	360	CDMG	
51	Pacific Heights	270	CDMG	
52	Pacific Heights	360	CDMG	
53	Presidio	0	CDMG	
54	Presidio	90	CDMG	
55	Rincon Hill	0	CDMG	
56	Rincon Hill	90	CDMG	
57	Santa Cruz	0	CDMG	
58	Santa Cruz	90	CDMG	
59	Telegraph Hill	0	CDMG	
60	Telegraph Hill	90	CDMG	
61	Yerba Buena Island	90	CDMG	
62	Yerba Buena Island	360	CDMG	

Table B.2. Suites of design bedrock accelerations and amplitude scaling factors for magnitudes 5.0, 6.0, 7.0, and 8.0, and distances of 10 km, 20 km, 30 km, and 40 km.

	Magnitude 5.0		Magnitude 6.0		Magnitude 7.0		Magnitude 8.0	
	Record No.	Amplitude Scale Factor	Record No.	Amplitude Scale Factor	Record No.	Amplitude Scale Factor	Record No.	Amplitude Scale Factor
Distance 10 km	23	0.755	16	1.169	59	7.259	7	4.187
	37	2.488	30	0.256	30	0.518	10	4.288
	57	0.198	27	3.390	48	3.477	59	12.570
	50	0.228	5	1.627	21	2.214	48	6.117
Distance 20 km	23	0.374	16	0.636	59	4.575	7	2.960
	37	1.233	30	0.139	30	0.327	10	3.031
	57	0.098	27	1.844	48	2.191	59	8.886
	50	0.113	5	0.885	21	1.396	48	4.324
Distance 30 km	23	0.217	16	0.396	59	3.198	7	2.262
	37	0.715	30	0.087	30	0.228	10	2.316
	57	0.057	27	1.150	48	1.532	59	6.790
	50	0.066	5	0.552	21	0.975	48	3.304
Distance 40 km	23	0.139	16	0.270	59	2.387	7	1.815
	57	0.037	27	0.781	48	1.143	10	1.859
	38	0.384	31	0.405	62	3.755	59	5.450
	50	0.042	5	0.375	21	0.728	48	2.652

12.0 Appendix C: Table of Damage States for Column Tests

Table C.1 (part 1 of 6). Damage indices for test columns at critical damage states

Analysis Run:	Number of Data Points	Damage State	Deformation Damage Index	Energy Damage Index	Total Damage Index
mun76no1_1	121	yield	0.17	0.04	0.2
mun76no1_2	376	ultimate	0.69	0.56	1.25
ng78no2_1	241	yield	0.26	0.11	0.37
ng78no2_2	481	ultimate	0.53	0.51	1.04
ng78no3_1	61	yield	0.19	0.03	0.23
ng78no3_2	421	ultimate	0.85	0.56	1.41
pot79no1_1	121	yield	0.40	0.12	0.52
pot79no1_2	241	ultimate	0.88	0.40	1.28
pot79no3_1	61	yield	0.33	0.06	0.39
pot79no3_2	181	ultimate	0.70	0.25	0.96
pot79no4_1	121	yield	0.60	0.12	0.72
pot79no4_2	241	ultimate	1.18	0.44	1.63
pot79no5a_1	121	yield	0.18	0.04	0.22
pot79no5a_2	241	ultimate	0.37	0.13	0.49
pot79no5b_1	121	yield	0.46	0.20	0.66
pot79no5b_2	181	ultimate	0.69	0.38	1.07
ang81unit1_1	121	yield	0.14	0.03	0.17
ang81unit1_2	241	ultimate	0.29	0.11	0.40
ang81unit2_1	121	yield	0.17	0.03	0.19
ang81unit2_2	241	ultimate	0.39	0.12	0.51
ang81unit2_3	361	failure	0.58	0.31	0.89
zahn86no5_1	69	yield	0.23	0.04	0.26
zahn86no5_2	121	ultimate	0.48	0.12	0.60
zahn86no5_3	361	failure	1.50	0.88	2.37
zahn86no6_1	68	yield	0.15	0.02	0.17
zahn86no6_2	121	ultimate	0.38	0.07	0.46
zahn86no6_3	361	failure	1.26	0.76	2.02
modeln1_1	121	yield	0.43	0.13	0.55
modeln1_2	241	ultimate	0.97	0.44	1.42
modeln1_3	421	failure	1.50	1.30	2.80
modeln2_1	121	yield	0.34	0.09	0.42
modeln2_2	241	ultimate	0.74	0.30	1.04
modeln2_3	601	failure	2.11	1.85	3.95
modeln3_1	61	yield	0.11	0.01	0.13
modeln3_2	121	ultimate	0.38	0.10	0.48
modeln3_3	421	failure	0.80	0.66	1.46
modeln4_1	121	yield	0.21	0.06	0.26
modeln4_2	241	ultimate	0.46	0.20	0.66
modeln4_3	721	failure	1.32	1.71	3.04
modeln5_1	121	yield	0.27	0.06	0.34
modeln5_2	241	ultimate	0.57	0.23	0.80
modeln5_3	661	failure	1.52	1.69	3.21
modeln6_1	61	yield	0.09	0.01	0.10
modeln6_2	121	ultimate	0.28	0.07	0.35
modeln6_3	841	failure	0.60	1.13	1.73

Table C.1 (part 2 of 6). Damage indices for test columns at critical damage states

Analysis Run:	Number of Data Points	Damage State	Deformation Damage Index	Energy Damage Index	Total Damage Index
flexnew_1	121	yield	0.36	0.09	0.45
flexnew_2	241	ultimate	0.56	0.25	0.81
flexnew_3	1201	failure	1.18	2.47	3.65
shearnew_1	121	yield	0.25	0.09	0.33
shearnew_2	289	ultimate	0.76	0.47	1.23
shearnew_3	529	failure	1.27	1.50	2.77
arakawa1_1	121	yield	0.32	0.04	0.35
arakawa1_2	181	ultimate	0.50	0.08	0.57
arakawa1_3	421	failure	1.22	0.36	1.59
arakawa2_1	181	yield	0.52	0.08	0.60
arakawa2_2	241	ultimate	0.69	0.13	0.82
arakawa2_3	481	failure	1.50	0.48	1.97
arakawa4_1	61	yield	0.17	0.01	0.18
arakawa4_2	181	ultimate	0.57	0.12	0.69
arakawa4_3	301	failure	1.02	0.32	1.34
arakawa6_1	121	yield	0.17	0.02	0.18
arakawa6_2	181	ultimate	0.26	0.04	0.30
arakawa6_3	361	failure	0.57	0.14	0.72
arakawa8_1	61	yield	0.04	0.01	0.05
arakawa8_2	181	ultimate	0.16	0.03	0.19
arakawa8_3	421	failure	0.43	0.14	0.57
arakawa9_1	61	yield	0.08	0.01	0.08
arakawa9_2	181	ultimate	0.27	0.05	0.32
arakawa9_3	361	failure	0.60	0.19	0.79
arakawa10_1	121	yield	0.16	0.02	0.18
arakawa10_2	241	ultimate	0.34	0.07	0.41
arakawa10_3	421	failure	0.60	0.22	0.81
arakawa11_1	13	yield	0.31	0.01	0.33
arakawa11_2	61	ultimate	0.65	0.05	0.71
arakawa11_3	121	failure	1.04	0.15	1.19
arakawa12_1	61	yield	0.23	0.01	0.25
arakawa12_2	121	ultimate	0.53	0.07	0.60
arakawa12_3	181	failure	0.87	0.15	1.03
arakawa13_1	61	yield	0.11	0.01	0.11
arakawa13_2	181	ultimate	0.38	0.07	0.45
arakawa13_3	301	failure	0.69	0.19	0.88
arakawa14_1	121	yield	0.15	0.02	0.18
arakawa14_2	241	ultimate	0.34	0.08	0.43
arakawa14_3	361	failure	0.53	0.18	0.72
arakawa15_1	301	yield	0.38	0.07	0.45
arakawa15_2	421	ultimate	0.56	0.13	0.69
arakawa15_3	601	failure	0.90	0.27	1.18
arakawa16_1	241	yield	0.22	0.06	0.28
arakawa16_2	361	ultimate	0.34	0.16	0.50
arakawa17_1	121	yield	0.27	0.03	0.30
arakawa17_2	181	ultimate	0.42	0.06	0.48
arakawa17_3	361	failure	0.91	0.22	1.14

Table C.1 (part 3 of 6). Damage indices for test columns at critical damage states

Analysis Run:	Number of Data Points	Damage State	Deformation Damage Index	Energy Damage Index	Total Damage Index
arakawa18_1	73	yield	0.28	0.02	0.30
arakawa18_2	121	ultimate	0.35	0.03	0.38
arakawa18_3	181	failure	0.59	0.07	0.66
arakawa19_1	181	yield	0.18	0.02	0.20
arakawa19_2	301	ultimate	0.34	0.07	0.40
arakawa19_3	541	failure	0.64	0.22	0.86
arakawa20_1	241	yield	0.10	0.02	0.12
arakawa20_2	421	ultimate	0.18	0.07	0.25
arakawa21_1	301	yield	0.19	0.05	0.24
arakawa21_2	541	ultimate	0.35	0.17	0.53
arakawa22_1	181	yield	0.15	0.01	0.16
arakawa22_2	361	ultimate	0.34	0.06	0.40
arakawa22_3	541	failure	0.57	0.14	0.70
arakawa23_1	181	yield	0.17	0.02	0.19
arakawa23_2	361	ultimate	0.39	0.08	0.47
arakawa23_3	601	failure	0.74	0.25	0.99
arakawa24_1	61	yield	0.48	0.03	0.51
arakawa24_2	181	ultimate	1.67	0.28	1.95
arakawa24_3	301	failure	2.97	0.73	3.70
arakawa25_1	181	yield	0.27	0.03	0.29
arakawa25_2	301	ultimate	0.50	0.09	0.59
arakawa25_3	541	failure	1.02	0.30	1.33
arakawa26_1	241	yield	0.22	0.04	0.26
arakawa26_2	541	ultimate	0.51	0.24	0.75
arakawa27_1	181	yield	0.19	0.02	0.20
arakawa27_2	301	ultimate	0.37	0.06	0.42
arakawa27_3	481	failure	0.64	0.15	0.80
arakawa28_1	181	yield	0.18	0.02	0.20
arakawa28_2	301	ultimate	0.34	0.05	0.40
arakawa28_3	481	failure	0.60	0.14	0.73
ang85no2_1	361	yield	0.56	0.46	1.02
ang85no2_2	961	ultimate	1.06	1.78	2.84
ang85no2_3	1981	failure	1.87	6.44	8.31
ang85no4_1	314	yield	0.77	0.37	1.14
ang85no4_2	361	ultimate	0.88	0.42	1.30
ang85no4_3	721	failure	1.32	1.11	2.43
ang85no6_1	11	yield	0.57	0.14	0.70
ang85no6_2	61	ultimate	0.85	0.27	1.12
ang85no6_3	361	failure	1.27	1.08	2.35
ang85no7_1	13	yield	0.58	0.12	0.69
ang85no7_2	61	ultimate	0.72	0.16	0.87
ang85no7_3	361	failure	0.94	0.66	1.60
ang85no9_1	361	yield	1.03	0.85	1.88
ang85no9_2	915	ultimate	1.92	3.18	5.11
ang85no9_3	1381	failure	2.78	7.10	9.89
ang85no10_1	61	yield	1.13	0.39	1.53
ang85no10_2	361	ultimate	1.56	1.99	3.54
ang85no10_3	721	failure	2.30	5.33	7.63

Table C.1 (part 4 of 6). Damage indices for test columns at critical damage states

Analysis Run:	Number of Data Points	Damage State	Deformation Damage Index	Energy Damage Index	Total Damage Index
ang85no13_1	361	yield	0.41	0.21	0.63
ang85no13_2	961	ultimate	1.13	1.05	2.18
ang85no13_3	1201	failure	1.13	1.73	2.86
ang85no14_1	361	yield	0.90	0.39	1.29
ang85no14_2	661	ultimate	1.22	0.89	2.11
ang85no14_3	961	failure	2.31	1.80	4.11
ang85no15_1	361	yield	0.38	0.21	0.59
ang85no15_2	961	ultimate	1.02	1.01	2.03
ang85no15_3	1201	failure	1.05	1.69	2.74
ang85no16_1	314	yield	0.61	0.24	0.85
ang85no16_2	361	ultimate	0.70	0.26	0.97
ang85no16_3	721	failure	0.95	0.74	1.69
ang85no17_1	361	yield	0.51	0.19	0.70
ang85no17_2	661	ultimate	0.67	0.47	1.14
ang85no17_3	961	failure	1.02	0.88	1.90
ang85no18_1	361	yield	1.16	0.60	1.77
ang85no18_2	661	ultimate	1.70	1.47	3.17
ang85no18_3	721	failure	1.74	1.73	3.47
ang85no19_1	61	yield	0.92	0.20	1.12
ang85no19_2	361	ultimate	1.50	0.91	2.41
ang85no19_3	421	failure	1.55	1.16	2.71
ang85no20_1	314	yield	1.29	0.73	2.02
ang85no20_2	361	ultimate	1.63	0.92	2.55
ang85no20_3	421	failure	1.68	1.21	2.89
ang85no22_1	61	yield	0.57	0.08	0.64
ang85no22_2	361	ultimate	1.01	0.44	1.45
ang85no22_3	421	failure	1.01	0.57	1.58
ang85no23_1	361	yield	1.22	0.47	1.69
ang85no23_2	661	ultimate	2.42	1.34	3.76
ang85no23_3	721	failure	2.42	1.64	4.06
ang85no24_1	361	yield	1.03	0.41	1.44
ang85no24_2	661	ultimate	2.11	1.18	3.30
ang85no24_3	721	failure	2.16	1.41	3.57
ang85no25_1	61	yield	1.39	0.3	1.68
ang85no25_2	361	ultimate	2.30	1.27	3.58
ang85no25_3	421	failure	2.35	1.57	3.92
davey75no1_1	181	yield	0.20	0.03	0.23
davey75no1_2	241	ultimate	0.53	0.14	0.66
davey75no1_3	361	failure	1.04	0.37	1.41
davey75no2_1	61	yield	0.16	0.02	0.17
davey75no2_2	241	ultimate	1.18	0.44	1.62
davey75no3_1	61	yield	0.05	0.00	0.05
davey75no3_2	181	ultimate	0.23	0.03	0.27
davey75no3_3	361	failure	0.53	0.27	0.80

Table C.1 (part 5 of 6). Damage indices for test columns at critical damage states

Analysis Run:	Number of Data Points	Damage State	Deformation Damage Index	Energy Damage Index	Total Damage Index
wong90no1_1	301	yield	0.31	0.14	0.45
wong90no1_2	1199	ultimate	0.87	0.80	1.68
wong90no2_1	301	yield	0.23	0.04	0.26
wong90no2_2	1199	ultimate	3.58	1.33	4.91
wong90no2_3	1559	failure	4.70	2.15	6.84
wong90no3_1	661	yield	0.30	0.21	0.51
wong90no3_2	1261	ultimate	1.03	0.98	2.01
wong90no3_3	1621	failure	1.37	1.94	3.31
watson10_1	241	yield	0.33	0.05	0.38
watson10_2	361	ultimate	0.54	0.17	0.71
watson10_3	661	failure	0.97	0.74	1.71
watson11_1	68	yield	0.08	0.00	0.08
watson11_2	241	ultimate	0.51	0.15	0.66
watson11_3	316	failure	0.77	0.32	1.09
mc1shift_1	181	yield	0.15	0.02	0.16
mc1shift_2	421	ultimate	0.45	0.18	0.63
mc1shift_3	781	failure	0.93	0.92	1.85
mc2shift_1	181	yield	0.30	0.06	0.36
mc2shift_2	541	ultimate	1.33	1.14	2.47
mc3shift_1	301	yield	0.72	0.27	0.99
mc3shift_2	421	ultimate	1.15	0.66	1.81
mc3shift_3	856	failure	2.39	3.73	6.12
bri2spbaa1_1	121	yield	2.95	0.55	3.50
bri2spbaa1_2	2701	ultimate	22.35	34.98	57.33
bri2spbaa1_3	2761	failure	24.22	38.21	62.43
bri3ws21bs_1	121	yield	3.37	1.01	4.38
bri3ws21bs_2	781	ultimate	6.34	6.02	12.37
bri3ws21bs_3	1501	failure	9.63	18.59	28.21
bri3ws22bs_1	121	yield	1.22	0.24	1.46
bri3ws22bs_2	721	ultimate	2.50	1.47	3.98
bri3ws22bs_3	2641	failure	7.78	14.16	21.94
bri3ws25bs_1	121	yield	1.23	0.28	1.51
bri3ws25bs_2	721	ultimate	2.60	1.33	3.93
bri3ws25bs_3	1441	failure	3.67	4.81	8.48
bri3ws26bs_1	121	yield	0.39	0.08	0.47
bri3ws26bs_2	1381	ultimate	1.28	1.56	2.85
bri3ws26bs_3	2881	failure	3.48	7.26	10.74
bri3ws27bs_1	121	yield	0.64	0.19	0.82
bri3ws27bs_2	721	ultimate	1.27	1.08	2.35
bri3ws27bs_3	1561	failure	2.03	3.95	5.98

Table C.1 (part 6 of 6). Damage indices for test columns at critical damage states

Analysis Run:	Number of Data Points	Damage State	Deformation Damage Index	Energy Damage Index	Total Damage Index
pet1e1_1	420	yield	0.04	0.01	0.05
pet1e1_2	1201	ultimate	0.31	0.16	0.48
pet1e1_3	1561	failure	0.52	0.55	1.07
pet1e2_1	485	yield	0.05	0.01	0.06
pet1e2_2	1265	ultimate	0.37	0.16	0.54
pet1e2_3	1565	failure	0.56	0.51	1.07
pet2e1_1	961	yield	0.25	0.26	0.51
pet2e1_2	1201	ultimate	0.50	0.50	1.01
pet2e1_3	2041	failure	1.56	3.07	4.63
pet2e2_1	601	yield	0.23	0.15	0.39
pet2e2_2	1141	ultimate	0.86	0.88	1.74
pet2e2_3	1501	failure	2.01	2.20	4.21

119

NIST-114A (REV. 3-90)	U.S. DEPARTMENT OF COMMERCE NATIONAL INSTITUTE OF STANDARDS AND TECHNOLOGY **BIBLIOGRAPHIC DATA SHEET**	1. PUBLICATION OR REPORT NUMBER NIST/BSS-170
		2. PERFORMING ORGANIZATION REPORT NUMBER
		3. PUBLICATION DATE February 1993

4. TITLE AND SUBTITLE

SEISMIC PERFORMANCE OF CIRCULAR BRIDGE COLUMNS DESIGNED IN ACCORDANCE WITH AASHTO/CALTRANS STANDARDS

5. AUTHOR(S)

WILLIAM C. STONE AND ANDREW W. TAYLOR

6. PERFORMING ORGANIZATION (IF JOINT OR OTHER THAN NIST, SEE INSTRUCTIONS)

U.S. DEPARTMENT OF COMMERCE
NATIONAL INSTITUTE OF STANDARDS AND TECHNOLOGY
GAITHERSBURG, MD 20899

7. CONTRACT/GRANT NUMBER

8. TYPE OF REPORT AND PERIOD COVERED
Final

10. SUPPLEMENTARY NOTES

11. ABSTRACT (A 200-WORD OR LESS FACTUAL SUMMARY OF MOST SIGNIFICANT INFORMATION. IF DOCUMENT INCLUDES A SIGNIFICANT BIBLIOGRAPHY OR LITERATURE SURVEY, MENTION IT HERE.)

Limitations of present procedures for the design of bridge columns to withstand seismic loads are discussed. An integrated seismic design procedure is developed which 1) allows the automatic selection and scaling of design earthquakes given the earthquake magnitude, the distance from the site to the fault, and the type of overlying soil strata; 2) predicts the inelastic behavior of reinforced concrete bridge columns when subjected to random lateral loads up to and including failure; and 3) calculates cumulative damage which can be directly correlated to observed states of damage in laboratory tests of bridge columns. Techniques for achieving the above capabilities are described and new design criteria, based on acceptable damage indices as functions of earthquake magnitude, distance, and structural importance, are proposed. Using the proposed procedure and criteria the performance of 72 representative bridge columns designed in accordance with 1992 CALTRANS specifications is analyzed. Analysis parameters included earthquake magnitude, distance from epicenter, subsurface soil characteristics, column aspect ratio, and normalized column axial load. Design charts, based on allowable damage index versus earthquake magnitude, are developed and retrofit strategies are discussed for those designs which do not meet the proposed design criteria.

12. KEY WORDS (6 TO 12 ENTRIES; ALPHABETICAL ORDER; CAPITALIZE ONLY PROPER NAMES; AND SEPARATE KEY WORDS BY SEMICOLONS)

circular bridge columns; damage index; design; dynamic analysis; earthquakes; hysteretic damage model; inelastic modeling; reinforced concrete; seismic loads; site specific response; soil amplification; spiral reinforcement.

13. AVAILABILITY		14. NUMBER OF PRINTED PAGES
XX	UNLIMITED	129
	FOR OFFICIAL DISTRIBUTION. DO NOT RELEASE TO NATIONAL TECHNICAL INFORMATION SERVICE (NTIS).	
XX	ORDER FROM SUPERINTENDENT OF DOCUMENTS, U.S. GOVERNMENT PRINTING OFFICE, WASHINGTON, DC 20402.	15. PRICE
XX	ORDER FROM NATIONAL TECHNICAL INFORMATION SERVICE (NTIS), SPRINGFIELD, VA 22161.	

ELECTRONIC FORM

NIST Technical Publications

Periodical

Journal of Research of the National Institute of Standards and Technology—Reports NIST research and development in those disciplines of the physical and engineering sciences in which the Institute is active. These include physics, chemistry, engineering, mathematics, and computer sciences. Papers cover a broad range of subjects, with major emphasis on measurement methodology and the basic technology underlying standardization. Also included from time to time are survey articles on topics closely related to the Institute's technical and scientific programs. Issued six times a year.

Nonperiodicals

Monographs—Major contributions to the technical literature on various subjects related to the Institute's scientific and technical activities.

Handbooks—Recommended codes of engineering and industrial practice (including safety codes) developed in cooperation with interested industries, professional organizations, and regulatory bodies.

Special Publications—Include proceedings of conferences sponsored by NIST, NIST annual reports, and other special publications appropriate to this grouping such as wall charts, pocket cards, and bibliographies.

Applied Mathematics Series—Mathematical tables, manuals, and studies of special interest to physicists, engineers, chemists, biologists, mathematicians, computer programmers, and others engaged in scientific and technical work.

National Standard Reference Data Series—Provides quantitative data on the physical and chemical properties of materials, compiled from the world's literature and critically evaluated. Developed under a worldwide program coordinated by NIST under the authority of the National Standard Data Act (Public Law 90-396). NOTE: The Journal of Physical and Chemical Reference Data (JPCRD) is published bimonthly for NIST by the American Chemical Society (ACS) and the American Institute of Physics (AIP). Subscriptions, reprints, and supplements are available from ACS, 1155 Sixteenth St., NW., Washington, DC 20056.

Building Science Series—Disseminates technical information developed at the Institute on building materials, components, systems, and whole structures. The series presents research results, test methods, and performance criteria related to the structural and environmental functions and the durability and safety characteristics of building elements and systems.

Technical Notes—Studies or reports which are complete in themselves but restrictive in their treatment of a subject. Analogous to monographs but not so comprehensive in scope or definitive in treatment of the subject area. Often serve as a vehicle for final reports of work performed at NIST under the sponsorship of other government agencies.

Voluntary Product Standards—Developed under procedures published by the Department of Commerce in Part 10, Title 15, of the Code of Federal Regulations. The standards establish nationally recognized requirements for products, and provide all concerned interests with a basis for common understanding of the characteristics of the products. NIST administers this program in support of the efforts of private-sector standardizing organizations.

Consumer Information Series—Practical information, based on NIST research and experience, covering areas of interest to the consumer. Easily understandable language and illustrations provide useful background knowledge for shopping in today's technological marketplace.

Order the above NIST publications from: Superintendent of Documents, Government Printing Office, Washington, DC 20402.

Order the following NIST publications—FIPS and NISTIRs—from the National Technical Information Service, Springfield, VA 22161.

Federal Information Processing Standards Publications (FIPS PUB)—Publications in this series collectively constitute the Federal Information Processing Standards Register. The Register serves as the official source of information in the Federal Government regarding standards issued by NIST pursuant to the Federal Property and Administrative Services Act of 1949 as amended, Public Law 89-306 (79 Stat. 1127), and as implemented by Executive Order 11717 (38 FR 12315, dated May 11, 1973) and Part 6 of Title 15 CFR (Code of Federal Regulations).

NIST Interagency Reports (NISTIR)—A special series of interim or final reports on work performed by NIST for outside sponsors (both government and non-government). In general, initial distribution is handled by the sponsor; public distribution is by the National Technical Information Service, Springfield, VA 22161, in paper copy or microfiche form.